12-2015

Geochemical and Petrological Characterization of the Back Forty Volcanogenic Massive Sulfide Deposit

Anthony Robert Boxleiter

GEOCHEMICAL AND PETROLOGICAL CHARACTERIZATION OF THE BACK FORTY VOLCANOGENIC MASSIVE SULFIDE DEPOSIT

by

Anthony Robert Boxleiter

A thesis submitted to the Graduate College
in partial fulfillment of the requirements
for the degree of Master of Science
Geosciences
Western Michigan University
December 2015

Thesis Committee:

Joyashish Thakurta, Ph.D., Chair
R.V. Krishnamurthy, Ph.D.
Heather Petcovic, Ph.D.

GEOCHEMICAL AND PETROLOGICAL CHARACTERIZATION OF THE BACK FORTY VOLCANOGENIC MASSIVE SULFIDE DEPOSIT

Anthony Robert Boxleiter, M.S.

Western Michigan University, 2015

The Back Forty Zn-Au deposit is the eastern-most Volcanogenic Massive Sulfide (VMS) deposit in the Penokean Volcanic Belt (PVB). It is the only VMS deposit found in Michigan, and is located along the east side of the Menominee River in Menominee County (45°26'57.5"N, 87°49'43.2"W). The Back Forty is the most zinc-enriched, copper depleted deposit among the major VMS deposits within the PVB that include Flambeau, Crandon, Bend, and Lynne. This work constitutes the first sulfur isotope study on the Back Forty VMS deposit.

The Back Forty is characterized by massive, semi-massive, disseminated and stringer sulfide mineralization hosted within felsic-dominated volcanic rocks, consistent with the bimodal-felsic, or Kuroko-type, VMS model. The host rocks include coarse-ash and fine-ash crystal tuffs, as well as lapilli lithic tuffs. $\delta^{34}S$ values obtained from pyrite, sphalerite, chalcopyrite, galena, and bornite range from 0.76 to 5.06‰-VCDT, with an average value of 3.07 ± 1.08‰ (1σ). These values are similar to the other major deposits of the PVB and are consistent to a mantle origin with minor intermixing with surficial sulfur-rich sediments. The sulfur in the ore-forming system is interpreted to have been derived by hydrothermal leaching of seafloor volcanic rocks.

ACKNOWLEDGMENTS

There are several people I would like to acknowledge for their contribution to this research and my success toward completion of the M.S. degree. Firstly, I would like to thank my advisor and mentor Dr. Joyashish Thakurta for leading me through this project from the beginning. I would also like to thank Aquila Resources, Inc., Thomas Quigley and Eric Quigley for their industry support in providing core samples, data, and advice. I would also like to acknowledge my colleague Jonathan Haynes for assisting in core sampling at Aquila Resources, Inc. I would like to thank Benjamin Underwood and the Indiana University – Bloomington Stable Isotope Research Facility for performing the sulfur isotope measurements on the samples in this project. Preparation of sulfide samples in the first batch was performed by Katherine Dvorak, whom demonstrated the process by which I was able to prepare other samples in this project.

I would like to thank my committee members Dr. R.V. Krishnamurthy and Dr. Heather Petcovic, and others including Laurel Woodruff and Klaus Schultz (U.S. Geological Survey), James Franklin (Franklin Geosciences LTD.), George Hudak (University of Minnesota Duluth), and Dr. Prajuki Bhattacharyya (University of Wisconsin-Whitewater) for all their advice through personal and written communication.

Anthony Robert Boxleiter

TABLE OF CONTENTS

ACKNOWLEDGMENTS ii

LIST OF TABLES vi

LIST OF FIGURES vii

LIST OF EQUATIONS xii

CHAPTER

I. INTRODUCTION 1

Volcanogenic Massive Sulfide Deposits 1

Classifications 1

Tectonic Settings 3

Structure of VMS Deposits 6

Origin of VMS Deposits 7

The Back Forty VMS Deposit 9

Penokean Orogeny 14

Research Objectives 16

Research Significance 16

II. METHODS 18

Sampling 22

Petrographic Descriptions 22

Sulfur Isotope Measurements 23

Sample Preparation 23

Table of Contents – Continued

CHAPTER

Instrument Processes 27

Trace Element Analysis 31

Sample Preparation 31

Instrument Processes 31

III. RESULTS, PART A: PETROGRAPHIC DESCIRPTIONS 33

Host Rocks 34

Sulfide Mineralization 63

Minerals and Properties 63

RESULTS, PART B: GEOCHEMISTRY 88

Host Rocks 88

Mineralization 90

IV. DISCUSSION 94

Host Rocks 94

Crystal Tuffs 95

Lapilli Lithic Tuffs 98

Mineralization 99

Textural Occurrences 99

Sulfur Isotope Analysis 101

Model of Formation 104

Table of Contents – Continued

REFERENCES 107

APPENDIX A – SAMPLING LOG 116

APPENDIX B – TRACE ELMENT GEOCHEMICAL DATA..... 120

APPENDIX C – SULFUR ISOTOPE VALUES (BEND, LYNNE, AND FLAMBEAU 125

LIST OF TABLES

1: VMS host rock types based on mafic, felsic, and siliclastic volumetric proportions (classification scheme adapted after Barrie and Hannington, 1999). 2

2: VMS host rock types, common names with associated metal specific enrichments and geographic examples from major districts. 3

3: Total ore tonnage and grades of major VMS deposits in the Penokean Volcanic Belt (data provided by Aquila Resources Inc.). 11

4: Sulfide sample and standard weight ranges, based on moles of sulfur in the sulfide molecule and the molecular weight of that sulfide. 1

5: Mineral abbreviations 33

6: Batch 1 91

7: Batch 2 92

8: Values and standard deviations for each mineral measured for sulfur isotope composition. 93

9: Classification of pyroclastic rock types based on grain size. 95

LIST OF FIGURES

1: Modern tectonic settings of VMS formation and host rock types typically associated with modern geologic settings. 4

2: General structure of a VMS deposit. 6

3: Diagram of a VMS forming system. 8

4: Copper, zinc and gold solubility under pH and temperature and pH conditions for sea-floor systems (modified after Franklin et al., 2005; Hannington et al., 2005). 9

5: Location of the Penokean Volcanic Belt in Northern Wisconsin and the Michigan Upper Peninsula (modified from Thakurta and Quigley, 2013). 10

6: Locations of the five major VMS deposits of the Penokean Volcanic Belt. 12

7: Base metal ratios of the five major VMS deposits in the Penokean Volcanic Belt (modified reconstruction: Klaus Schulz, USGS; after DeMatties, 1994). 13

8: Ocean closure between the Pembine Wausau Terrane and nearing collision (modified after Schulz and Cannon, 2007). 14

9: Collision of the Superior Craton and the Pembine Wausau Terrane (modified after Schulz and Cannon, 2007). 15

10: Marshfield collision at the southern margin of the Pembine Wausau Terrane (modified after Schulz and Cannon, 2007). 15

11: Back Forty 3-D model including a south-western and north-eastern cross-sections (reconstruction, after Aquila Resources, Inc.). 18

12: Back Forty 3-D model including zones (reconstruction, after Aquila Resources, Inc.). 19

List of Figures - Continued

13: North-east cross-section of the deposit containing core from four drill holes..... 20

14: South-west cross-section of the deposit containing core from drill hole LK-127. 21

15: Sample preparation equipment. 25

16: Lab instruments..... 28

17: Reactor column packing, water filter, and gas chromatograph separation column (modified from Costech Analytical Technologies Inc.). 29

18: Hand sample, ID: LK–171– #029. 36

19: Photomicrographs, sample ID: LK–171– #029. 37

20: Hand sample, ID: LK–171– #023. 38

21: Photomicrographs, sample ID: LK–171– #023. 39

22: Hand sample, ID: LK–451– #106. 41

23: Photomicrographs, sample ID: LK–451– #106 42

24: Hand sample, ID: LK–150– #060. 43

25: Photomicrographs, sample ID: LK–150– #060. 44

26: Hand sample, ID: LK–150– #055. 45

27: Photomicrographs, sample ID: LK–150– #055 46

28: Hand sample, ID: LK–150– #058. 47

List of Figures - Continued

29: Photomicrographs, sample ID: LK–150– #058 48

30: Hand sample, ID: LK–150– #085. 50

31: Photomicrographs, sample ID: LK–150– #085. 51

32: Hand sample, ID: LK–451– #087. 53

33: Photomicrographs, sample ID: LK–451– #087. 54

34: Hand sample, ID: LK–171– #007. 55

35: Photomicrographs, sample ID: LK–171– #007.. 56

36: Hand sample, ID: LK–451– #092. 58

37: Photomicrographs, sample ID: LK–451– #092. 59

38: Hand sample, ID: LK–166– #150. 60

39: Hand sample, ID: LK–171– #038.. 61

40 : Photomicrographs, sample ID 62

41: Hand sample, ID: LK–150– #065. 67

42: Photomicrographs, sample ID: LK–150– #065 68

43: Photomicrographs, sample ID: LK–150– #065.. 69

44: Hand sample, ID: LK–150– #068. 70

List of Figures - Continued

45: Photomicrographs, sample ID: LK–150– #068 71

46: Hand sample, ID: LK–171– #016. 72

47: Photomicrographs, sample ID: LK–171– #016. 73

48: Hand sample, ID: LK–171– #035. 74

49: Photomicrographs, sample ID: LK–171– #035. 75

50: Hand sample, ID: LK–451– #103. 76

51: Photomicrographs, sample ID: LK–451– #103B. 77

52: Hand sample, ID: LK–127– #045. 78

53: Photomicrographs, sample ID: LK–127– #045. 79

54: Hand sample, ID: LK–150– #069. 80

55: Photomicrographs, sample ID: LK–150– #069. 81

56: Hand sample, ID: LK–150– #070. 82

57: Photomicrographs, sample ID: LK–150– #070. 83

58: Hand sample, ID: LK–171– #009. 84

59: Photomicrographs, sample ID: LK–171– #009B. 85

60: Hand sample, ID: LK–127– #043. 86

List of Figures - Continued

61: Photomicrographs, sample ID: LK–127– #043 87

62: Rhyolite 1 data points for Zr/Y versus Y cluster within the FII-type field and Rhyolite 3 within the FIIIa-type field, Rhyolite 2 data points for Zr/Y versus Y do not cluster within any field in the classification scheme (after Lescher et al. 1983, and Barrie et al. 1993)..... 89

63: Batch 1 92

64: Batch 2 93

65: Frequency histogram of sulfur isotope values for five primary sulfide minerals in the Back Forty deposit. 93

66: Ternary diagram used to determine rock types for tuffs based upon glass, rock fragments, and crystal relative compositions (after Pettijohn, 1975; Schmid 1981).. 94

67: Rhyolite classification based on SiO2 versus Zr/TiO2. (Thakurta and Quigley, 2013; Aquila Resources). 96

68: Frequency histogram of sulfur isotope values of the five major VMS deposits of the Penokean Volcanic Belt (Crandon Values: Lesley Myers, 1983; Bend, Lynne, and Flambeau values: Laurel Woodruff, USGS, written communication). 102

69: Relative timeline of volcanic and mineralization events. 106

LIST OF EQUATIONS

1: Seal, 2006…… 30

2: Woodruff and Shanks, 1988…… 104

3: Seal, 2006……. 104

CHAPTER I

INTRODUCTION

Volcanogenic Massive Sulfide Deposits

Volcanogenic massive sulfide (VMS) deposits are metal-bearing ore deposits. This type of ore deposit is one of the world's most valuable sources of copper, zinc, lead, silver, and gold as well as many by-products including tin, cadmium, antimony, and bismuth (Kearney, 2003). These important resources primarily occur as sulfide minerals or native metals. Common sulfide minerals in VMS deposits include pyrite (FeS_2), sphalerite ((Zn,Fe)S), chalcopyrite ($CuFeS_2$), galena (PbS), arsenopyrite (FeAsS), and bornite (Cu_5FeS_4). VMS deposits are hydrothermal in origin and form during episodes of volcanic activity. Most VMS deposits occur in clusters that are often referred to as mining camps or districts. These clusters are located along belts of volcanic and sedimentary rocks, such as the Abitibi greenstone belt in Ontario and Quebec, Canada, the Iberian Pyrite Belt in Portugal and Spain, and Penokean Volcanic Belt (PVB) extending through Northern Wisconsin and into the Upper Peninsula of Michigan.

Classifications

VMS deposits are often classified by ore grade and total tonnage. The ore grade is a numerical value representing the concentration of specific metals within the deposit. For example, base metals such as copper, zinc and lead are represented as weight percent (wt. %), while precious metals gold and silver are more commonly expressed in grams per tonne (g/t) or parts per million (ppm). Total tonnage is the overall weight of the

deposit, including the metals and host rock. Another way in which VMS deposits are classified is by the composition of the host rocks. Host rock types include: mafic, bimodal-mafic, mafic-siliciclastic, bimodal-felsic, and bimodal-siliciclastic. Bi-modal deposits represent the occurrence of both mafic and felsic volcanic rocks occurring within the same regional setting and are temporally related. These various types of host rocks are based on the volumetric proportions of volcanic (mafic and felsic) and siliciclastic rock (Table 1).

Table 1: VMS host rock types based on mafic, felsic, and siliclastic volumetric proportions (classification scheme adapted after Barrie and Hannington, 1999).

Rock Type	**% Felsic**	**% Mafic**	**% Siliciclastic**
Mafic	< 1%	> 75%	< 10%
Bi-modal mafic	> 3%	> 50%	< 47%
Mafic-siliciclastic	< Mafic %	> Felsic %	≈ Volcanic %
Bimodal-Felsic	> 50%	< 50%	< 15%
Bimodal-Siliciclastic	> Mafic %	< Felsic %	≈ Volcanic %

Deposits are also classified by commonly used names and associated metal specific enrichments. For example, mafic-hosted deposits are also known as Cyprus-type, based on the occurrence mafic hosted deposits at the island of Cyprus in the Eastern Mediterranean Sea, and are enriched in copper with respect to zinc (Table 2).

Table 2: VMS host rock types, common names with associated metal specific enrichments and geographic examples from major districts.

Rock Type (Barrie and Hannington, 1999)	**Common Name** (Barrie, 2007; Kearney, 2003)	**Metal Contents** (Kearney, 2003; Taylor et al., 1995)	**Examples**
Mafic	Cyprus-type	Cu±Zn	Island of Cyprus
Bi-modal mafic	Noranda-type	Cu-Zn	Noranda Caldera; Quebec, Canada
Mafic-siliciclastic	Besshi-type	Cu	Besshi district, Japan
Bimodal-Felsic	Kuroko-type	Zn-Pb-Cu	Hokuroko, Japan
Bimodal-Siliciclastic	Mattabi-type	Zn-Cu-Ag	Mattabi Mine; NW Ontario, Canada

Tectonic Settings

Modern tectonic settings of VMS formation include: back-arc basins, island arcs, mid-ocean ridges, oceanic intraplate volcanoes, continental margin arc, and continental rift/back arc basins (Figure 1) (Shanks et al., 2010). Often, the geologic and tectonic settings associated with VMS formation are related to host rock compositions. For example, mafic type deposits are associated with ocean ridges. Mafic hosted deposits are fewer in number, smaller in size (i.e. total tonnage) and copper-rich, lead-poor in comparison to all other types of deposits (Barrie and Hannington, 1999). The mafic, basaltic host rocks are dominantly tholeiitic. Tholeiitic volcanic rocks formed from a

reducing magma, where magnesium-rich, iron-poor silicate minerals (i.e. olivine and pyroxene) were preferentially crystallized and iron-content increased in the residual magma.

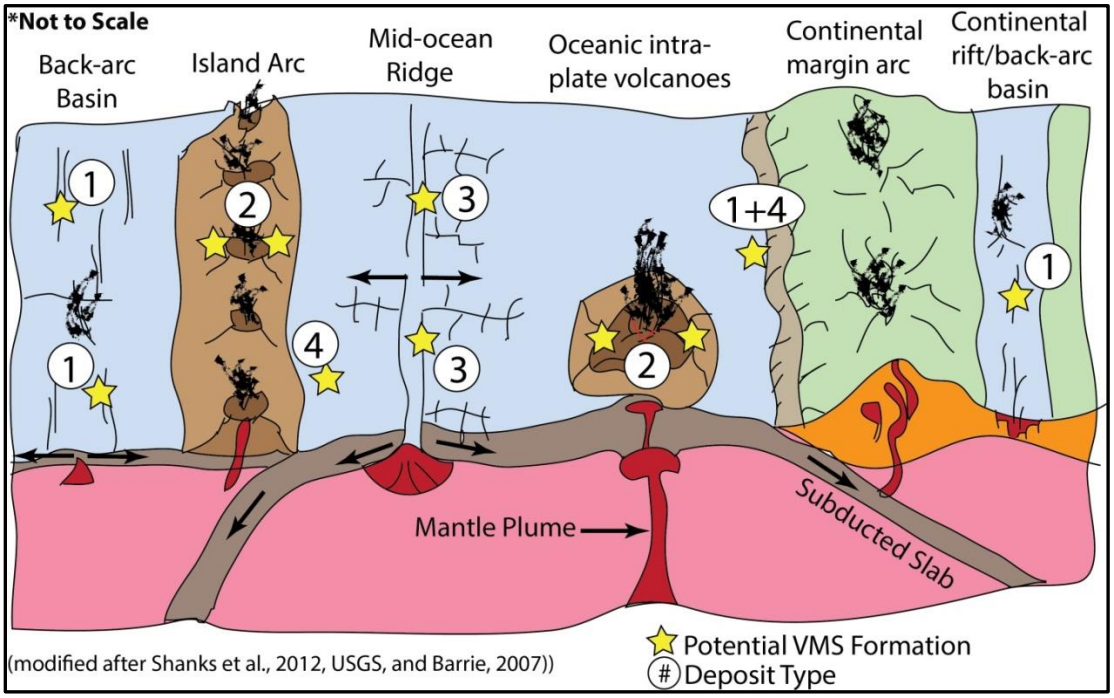

Figure 1: Modern tectonic settings of VMS formation and host rock types typically associated with modern geologic settings. [1]: Bimodal-siliciclastic type deposits, [2]: Bimodal-felsic/mafic type deposits, [3]: Mafic type deposits, and [4]: Mafic-siliciclastic.

Bimodal-mafic host rocks are associated with volcanic island arc and rifted island arc tectonic settings. Most have a ratio of mafic to felsic volcanic rock of 3 to 1 or greater, respectively (Barrie and Hannington, 1999). Mafic rocks are generally tholeiitic in composition, with felsic rocks presenting more calc-alkaline affinities. Calc-alkaline volcanic rocks represent where the parental magma was oxygenated and crystallized iron-rich minerals at a more steady/even rate with magnesium-rich minerals when compared

to tholeiitic magmas. Bimodal-mafic VMS are the most common of the VMS types, having higher cooper content than all types except the mafic VMS type (Barrie and Hannington, 1999).

Mafic-siliciclastic deposits contain little felsic material, but high amounts of turbidite siliciclastics (clastic sediment gravity flow in deep ocean water) and volcanic intrusive rock. These deposits are found in rifted continental margins and rifted, sedimented oceanic crust. Mafic-siliciclastic hosted deposits are less numerous than other types, but represent the second largest average total tonnage to bimodal-siliciclastic hosted deposits (Barrie and Hannington, 1999).

Bimodal-felsic hosted deposits occur within volcanic island arc or rifted island arc tectonic settings. The felsic rocks are dominantly calc-alkaline, with mafic rocks also generally calc-alkaline. Bi-modal-felsic deposits are the second-most numerous and on average contain the most zinc and silver when compared to other deposit types (Barrie and Hannington, 1999).

Bimodal-siliciclastic type deposits contain approximately equal portions of volcanic and sedimentary rocks, with felsic rocks in higher abundance than mafic. Felsic host rocks are dominantly calc-alkaline and suggested to have been derived from partial melting of crustal sources, consistent with a continental arc or rifted continental arc setting (Barrie and Hannington, 1999). These deposits represent the largest tonnage, highest lead content, and lowest copper content of all deposit types.

Structure of VMS Deposits

VMS deposits consist of two major parts: a massive sulfide ore-body which forms at the crest of the VMS system, and a network of vein-like structures, consisting of sulfide minerals, directly underneath the massive ore-body. Vein-like structures of sulfide minerals are often referred to as stringer-sulfides (Figure 2). Massive sulfide deposits consist of at least 50%, and commonly >80%, sulfides by volume (Kearney, 2003).

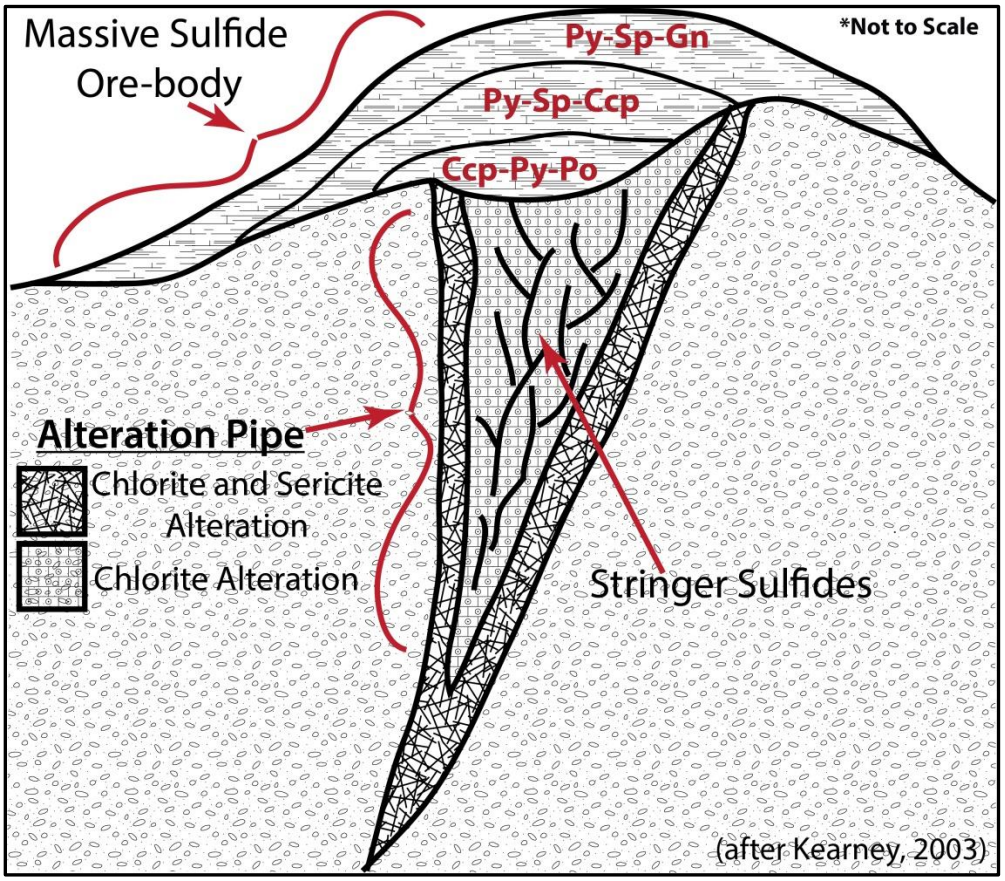

Figure 2: General structure of a VMS deposit.

Massive ore bodies are often characterized by internal zones consisting of sulfide minerals in higher abundances relative to adjacent zones. Metal specific enrichment

generally decreases upward and/or outward in a Cu/(Cu+Zn+Pb) ratio in deposits, above their stringer zones, as a result of these sulfide-specific internal zones (Kearney, 2003). For example, copper-bearing chalcopyrite typically occurs at the lower zones of the ore-body, while zinc-bearing sphalerite and lead-bearing galena occur in the outer zones of the ore-body (Figure 4).

The alteration zone (i.e. "alteration pipe") beneath deposits typically contains differences in the types of minerals formed during alteration due to the intensity and style of hydrothermal activity. The primary alteration minerals in VMS deposits are sericite, chlorite, and muscovite. For example, Noranda-type deposits are generally characterized by an inner zone of chlorite dominated alteration and a sericite-chlorite outer zone, whereas the inner zones beneath Kuroko-type deposits are often sericite dominated and dominated by chlorite in outer zones (Figure 2)(Kearney, 2003).

Origin of VMS Deposits

Seawater is able to circulate through the permeable rock at the seafloor recharge zone, directed by faulted or fractured rock and driven by the heat of an underlying magma chamber or mantle plume. The sum of reactions in the recharge zone results in a fluid that is slightly acidic, anoxic, alkali-rich and Mg-poor relative to the starting seawater (Tivey, 2007). This fluid increases in temperature, reaching the reaction zone, where sulfur and metals (e.g. Cu, Fe, Zn, and Pb) are leached or dissolved from the rock and mobilized within the ore-forming fluid. The reaction zone may also be referred to as the hydrothermal reservoir. Upper mantle (mafic) rock constitutes the composition of the reservoir and supplies heat, metals (e.g. Cu, Zn, Pb) and sulfur (e.g. SO_2 and H_2S) to the

system. The hydrothermal ore-forming fluid rises upward through the system due to buoyancy, toward the seafloor venting zone (Figure 3).

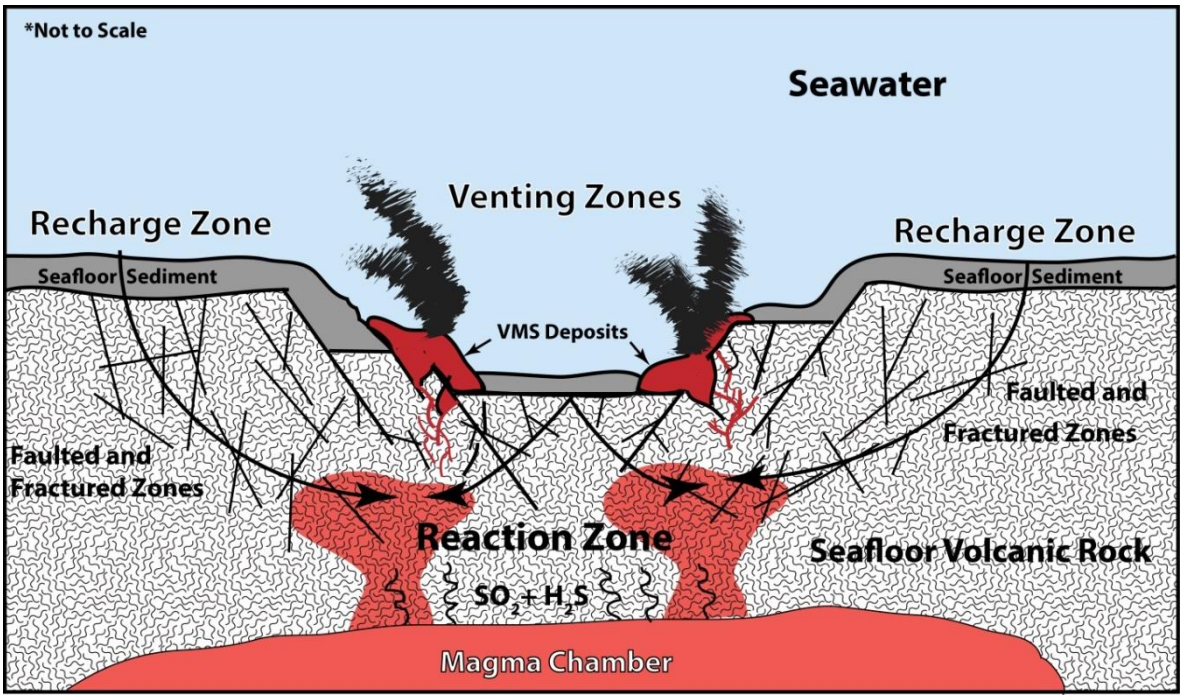

Figure 3: Diagram of a VMS forming system.

The pH of fluid ranges from less than 1 to 5, with temperature ranging between approximately 275 and 405 ^{0} C (Tivey, 2007). The temperature and pH of the fluid are important constraints on metal solubility. For example, copper solubility is primarily driven by temperature, whereas zinc content primarily driven by pH (Franklin et al., 2005). Another example is the solubility of gold in ore-forming fluids as dependent on the transporting agent, HS^- or Cl^-. The solubility of gold as a chloride complex is primarily a factor of temperature, while the solubility of gold as a hydrogen sulfide complex is primarily a factor of pH (Figure 4, Franklin et al., 2005).

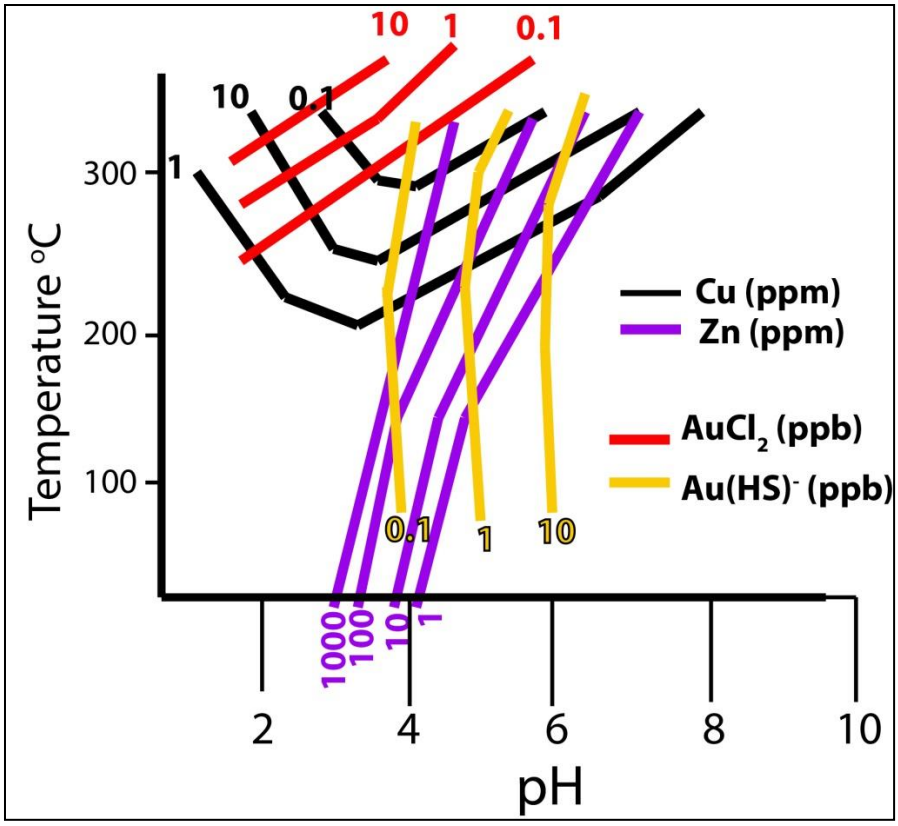

Figure 4: Copper, zinc and gold solubility under pH and temperature and pH conditions for sea-floor systems (modified after Franklin et al., 2005; Hannington et al., 2005).

Sulfide mineralization is driven primarily by mixing with seawater at or near the venting zone. Mixing of cold, neutral pH seawater with hot, low pH ore-forming fluid decreases the solubility of sulfide minerals and results in the crystallization of sulfide minerals at the seafloor.

The Back Forty VMS Deposit

The Back Forty Volcanogenic Massive Sulfide (VMS) deposit is located in Menominee County, Michigan, along the east side of the Menominee River which separates the states of Michigan and Wisconsin (45°26'57.5"N, 87°49'43.2"W). The Back

Forty is a poly-metallic ore deposit which formed during the Penokean Orogeny and is part of a major group of VMS deposits, including Crandon and Flambeau, located in the Penokean Volcanic Belt. Several VMS deposits can be found trending along this belt extending in an east-west orientation through northern Wisconsin and the Michigan Upper Peninsula (Figure 5). This belt is primarily composed of island arc volcanic and intrusive rocks (Schulz and Cannon, 2007).

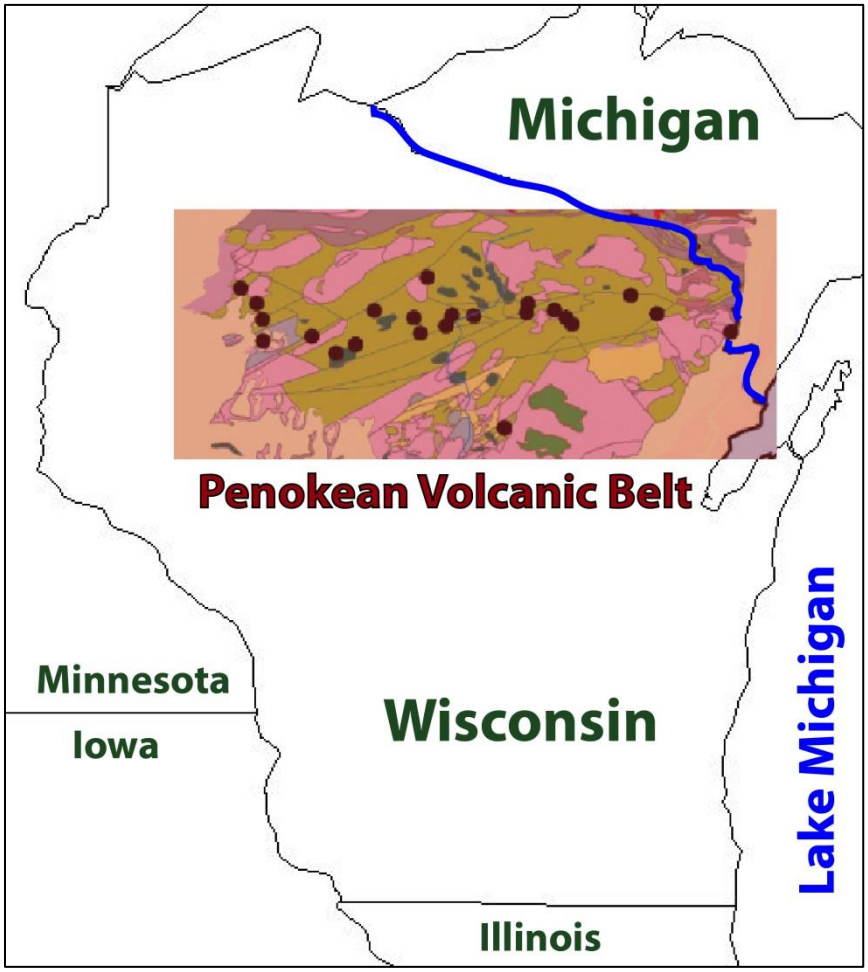

Figure 5: Location of the Penokean Volcanic Belt in Northern Wisconsin and the Michigan Upper Peninsula (modified from Thakurta and Quigley, 2013).

As part of the Penokean Volcanic Belt, the Back Forty is the eastern most known VMS deposit in the belt and is the only VMS deposit found in Michigan. The Back Forty formed during the Paleoproterozoic era approximately 1874 ± 4 million years ago. The Back Forty is characterized by felsic-dominated host rocks and metal specific enrichment that is consistent with the bimodal-felsic, or Kuroko-type, VMS deposit model (Table2). The host rocks and intrusions through the Back Forty deposit contain zircons that have yielded uranium/lead age dating of 1,874 ± 4 Ma (Schulz et al. 2007).

It has been measured that there are 15.13 million tonnes of ore, with grades of 2.03 ppm Au, 24.48 ppm Ag, 3.06% Zn, 0.33% Cu and 0.22% Pb contained within the Back Forty deposit (Aquila Resources, Inc, 2013). The deposit is unique because it contains low amounts of copper and high amounts of zinc when compared to other VMS deposits associated with the Penokean Volcanic Belt, such as Bend and Flambeau (Table 3).

Table 3: Total ore tonnage and grades of major VMS deposits in the Penokean Volcanic Belt (data provided by Aquila Resources Inc.).

Deposit	**Tonnage (million tonnes)**	**Zn (wt. %)**	**Cu (wt. %)**	**Au (g/t)**	**Ag (g/t)**
Crandon	67	5.6	1.04	1.1	39
Lynne	5.6	9.27	0.47	0.7	74
Flambeau	5.8	-	4.0	1.7	31
Flambeau	1.9	-	0.5	3.4	69
Bend	3.5	-	1.9	2.8	12
Back Forty	15.1	3.0	0.3	2.0	24

The Bend and Flambeau deposits are found in the western part of the Penokean Volcanic Belt and contain the higher copper, lower zinc concentrations when compared to deposits in the central to eastern Penokean Volcanic Belt such as Lynne, Crandon and Back Forty. The Lynne, Crandon, and Back Forty deposits contain the high zinc and low copper concentrations, with the Lynne deposit containing the highest lead content and northern-most position within the belt (Table 3). There is a distinct gradation from copper-rich to zinc-rich deposits along the east-west trend of the Penokean Volcanic Belt, based upon base metal ratios (Figure 6 and 7).

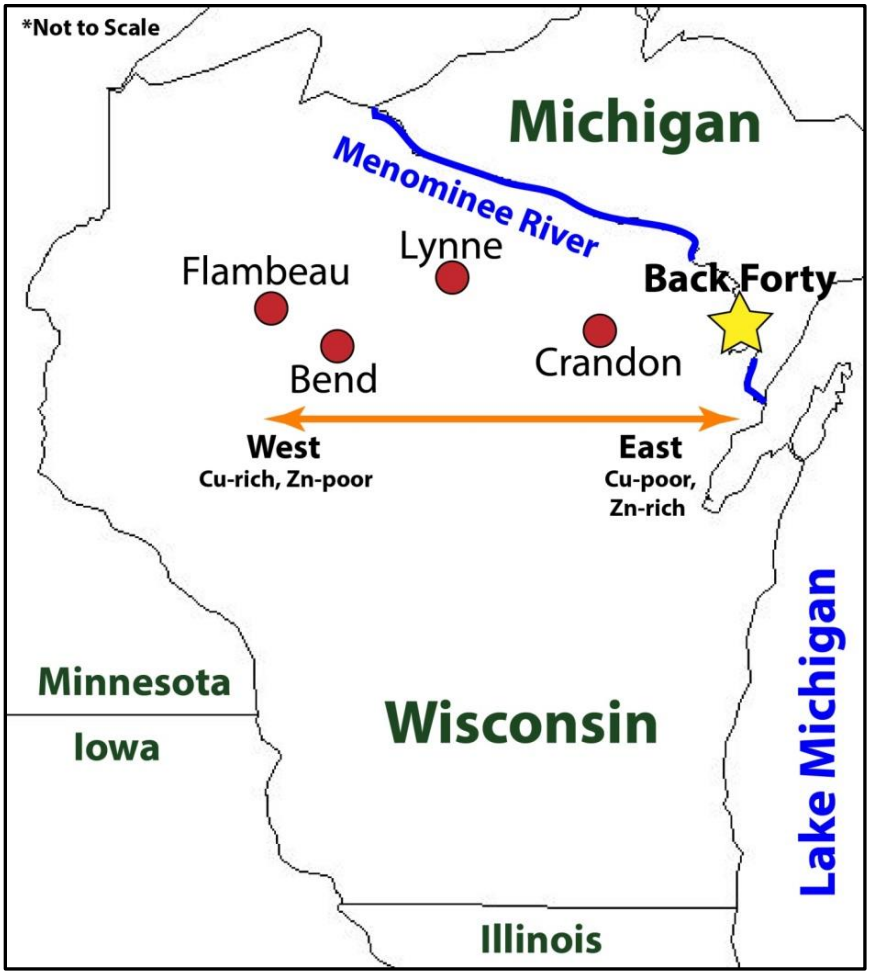

Figure 6: Locations of the five major VMS deposits of the Penokean Volcanic Belt.

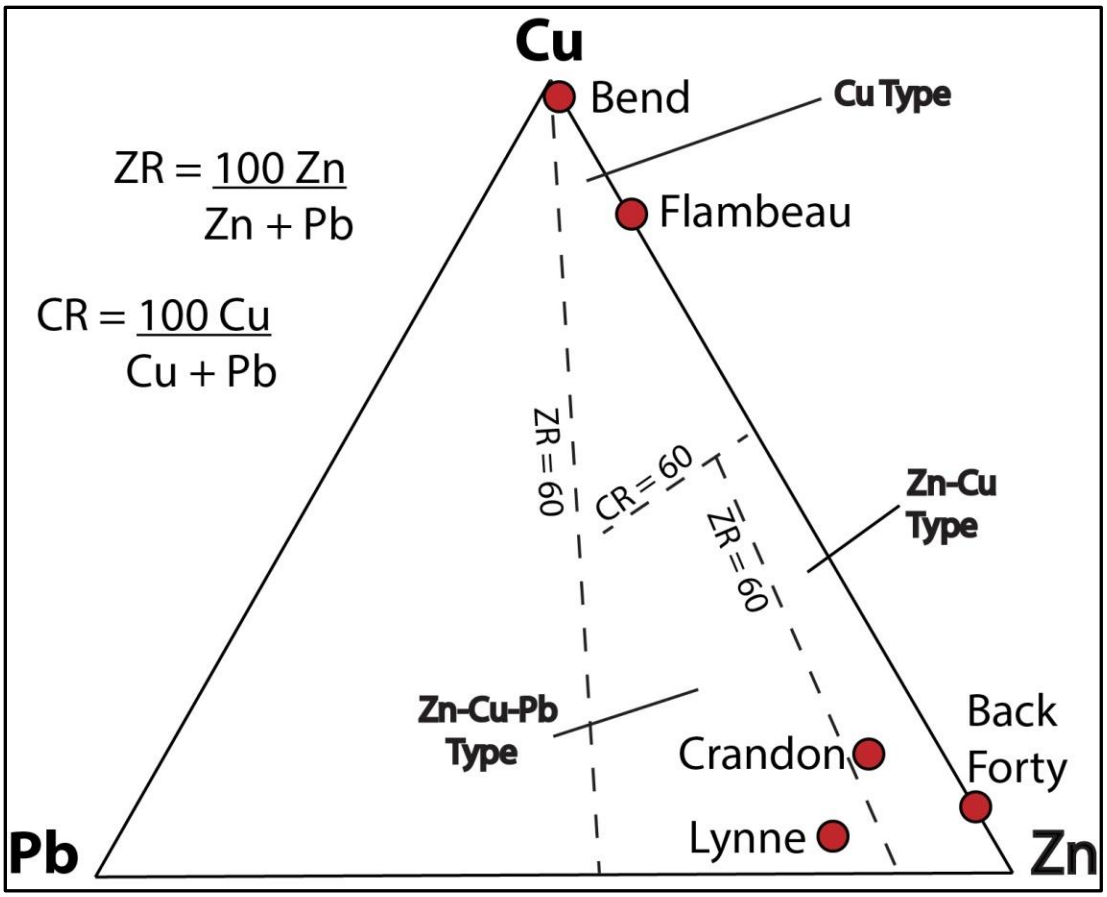

Figure 7: Base metal ratios of the five major VMS deposits in the Penokean Volcanic Belt (modified reconstruction: Klaus Schulz, USGS; after DeMatties, 1994).

Penokean Orogeny

The Penokean Orogeny in the Lake Superior region began approximately 1890 million years ago when a volcanic island arc (Pembine-Wausau Terrane) approached and collided with the Superior Craton during a period of south-directed subduction (Figure 8).

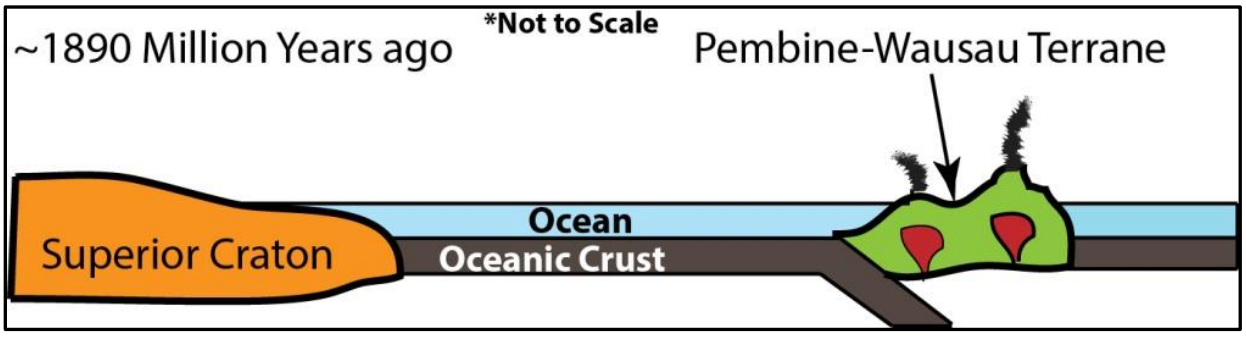

Figure 8: Ocean closure between the Pembine Wausau Terrane and nearing collision (modified after Schulz and Cannon, 2007).

Around 1875 million years ago, the Pembine Wausau Terrane collided with the southern margin of the Archean Superior Craton (Figure 9) (Schulz and Cannon, 2007). Strain in subducting thick continental lithosphere halted further subduction. This strain produced a southward redirection in subduction to a position south of the oceanic arc and followed by a reversal in the direction of subduction. North-directed subduction facilitated back-arc extension and thinning of the crust. Within the intra-arc rifting, bimodal calc-alkaline volcanic eruptions were accompanied by convective circulation of hydrothermal, VMS forming fluids. This sequence of events leads to the development of the Penokean Volcanic Belt and numerous VMS occurrences.

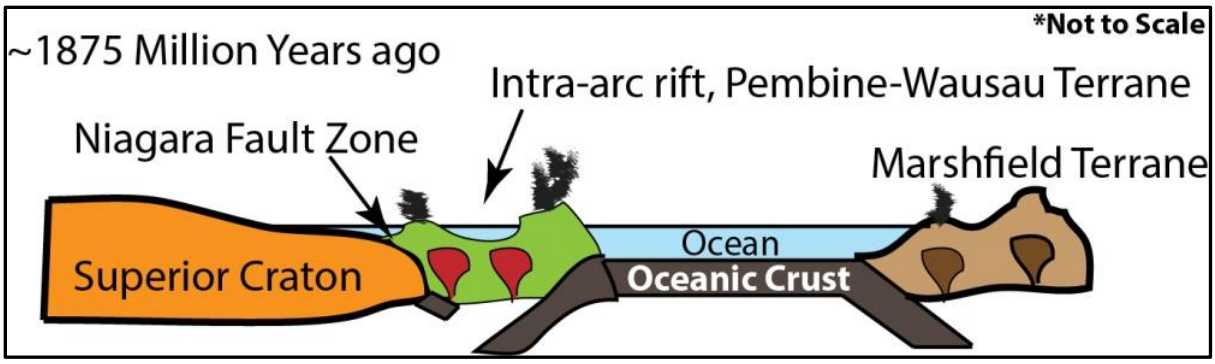

Figure 9: Collision of the Superior Craton and the Pembine Wausau Terrane (modified after Schulz and Cannon, 2007).

The Pembine Wausau Terrane is bounded on the north by the Niagara Fault Zone and on the south by the Eau Pleine Shear Zone. The Eau Pleine Shear Zone developed during the collision and accretion of the Marshfield Terrane to the south approximately 1850 million years ago (Figure 10)(Schulz and Cannon, 2007).

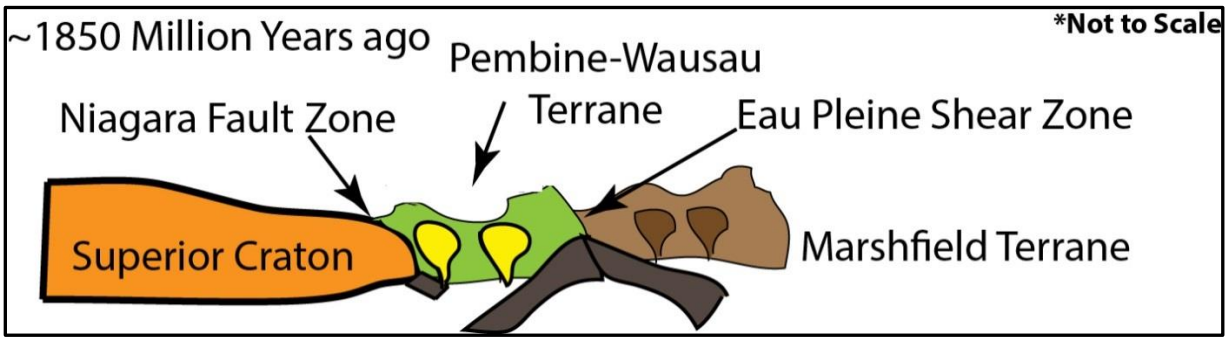

Figure 10: Marshfield collision at the southern margin of the Pembine Wausau Terrane (modified after Schulz and Cannon, 2007).

Research Objectives

The primary objective of this study is to characterize the Back Forty VMS deposits with respect to its host rocks and mineralization. Utilizing hand sample and thin-section descriptions, the relationship between sulfide ore mineral occurrence and textural characteristics within the host rock have been established. These textural characteristics and established occurrences of sulfide minerals were used to provide a relative timeline of volcanism and mineralization/hydrothermal infiltration events. A relative timeline was established based on the characterization of primary igneous textures and secondary, hydrothermal alteration and crystallization of sulfide minerals. Another objective of the study was to acquire sulfur isotope ($\delta^{34}S$) values from sulfide minerals in each of the five major zones of the Back Forty deposit containing sulfide mineralization. These values were be used to determine the source of sulfur and to compare the Back Forty with other deposits in the Penokean Volcanic Belt previously sampled for sulfur isotope values. Lastly, trace element analysis was used to classify the host rocks of sulfide mineralization.

Research Significance

This research explores the use sulfur isotope analysis and petrographic descriptions of host rocks and mineralization textures to characterize the Back Forty VMS deposit. Sulfur isotope values have been measured four other major VMS deposits in the Penokean Volcanic Belt (e.g. Lynne, Bend, Crandon, and Flambeau), as well as from many other sulfide deposits around the world, but had not been measured from the

Back Forty deposit. For example, a similar study was conducted by the U.S. Geological Survey and U.S. Department of Interior on the Greens Creek VMS deposit located in Admiralty Island, Southeastern Alaska. Sulfur isotope analysis on the Greens Creek VMS produced $\delta^{34}S$ values of -11 to -16‰. This was interpreted by Taylor et al. (2010) as indicative of local source of sulfur from the organic reduction of seawater sulfate to H_2S.

The five major deposits located within the Penokean Volcanic Belt present an east-west trending enrichment in base metal concentrations. High copper content is found in the western deposits (i.e. Flambeau and Bend) while high zinc content is found in the central to eastern deposits (i.e. Lynne, Crandon and Back Forty) (Figures 6 and 7). The Back Forty deposit is the most zinc-rich, copper depleted deposit when compared to all these other deposits.

Host rock textures and the mode of occurrence of sulfide minerals have provided clues to the relative timeline of the Back Forty formation. Sulfur isotope values obtained from the Back Forty were compared with sulfur isotope values from the other four major deposits, with known metal grades and sulfur isotope values. If the values at Back Forty differ from the other deposits, this geochemical work may also be a useful tool to model the origins of other VMS deposits in the Penokean Volcanic Belt, and to explore for new VMS deposits associated with the Penokean Volcanic Belt based upon sulfur isotope signatures.

CHAPTER II

METHODS

Core from five drill holes was sampled from an Aquila Resources Inc. owned core shed in Menominee County, Michigan, in October of 2013. Core from each drill hole was sampled for sulfide mineralization and host rocks occurring within five major zones of deposit. These zones include: the Main Zone, Deep Zone, Stringer Zone, Pinwheel Zone, and Tuff Zone. Drills holes LK-127, LK-150, LK-166, LK-171, and LK-451 were selected because they contain core from all of these zones (Figures 11 – 14). Of the three rhyolite units identified by Aquila Resources Inc., the upper-most unit, designated as Rhyolite 3, does not host massive sulfide ore and was not sampled in this study.

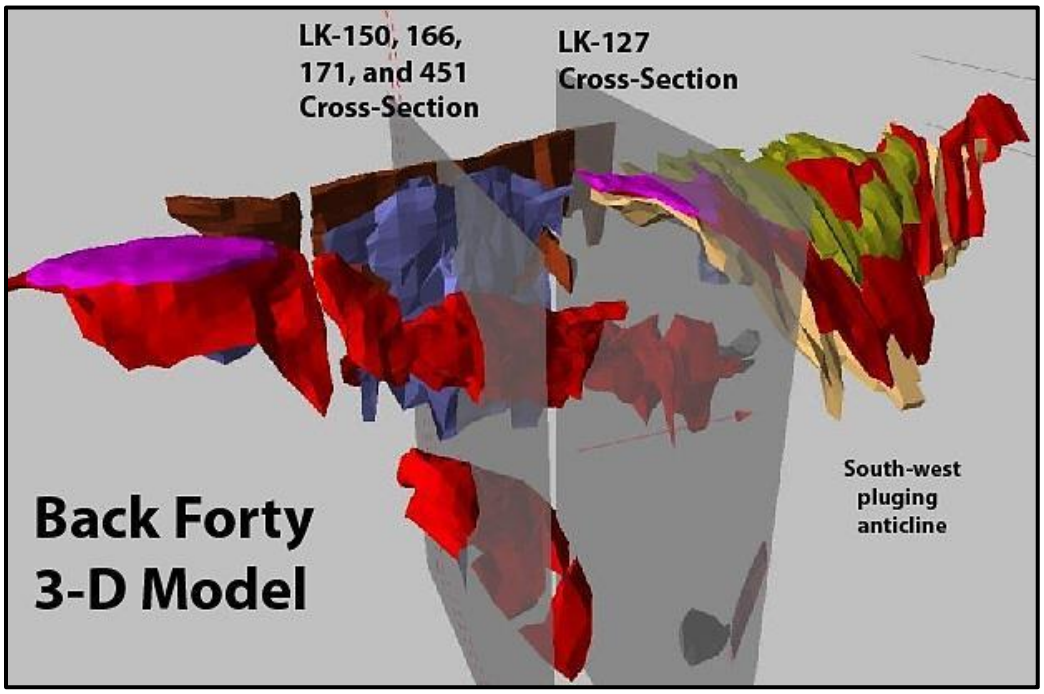

Figure 11: Back Forty 3-D model including a south-western and north-eastern cross-sections (reconstruction, after Aquila Resources, Inc.).

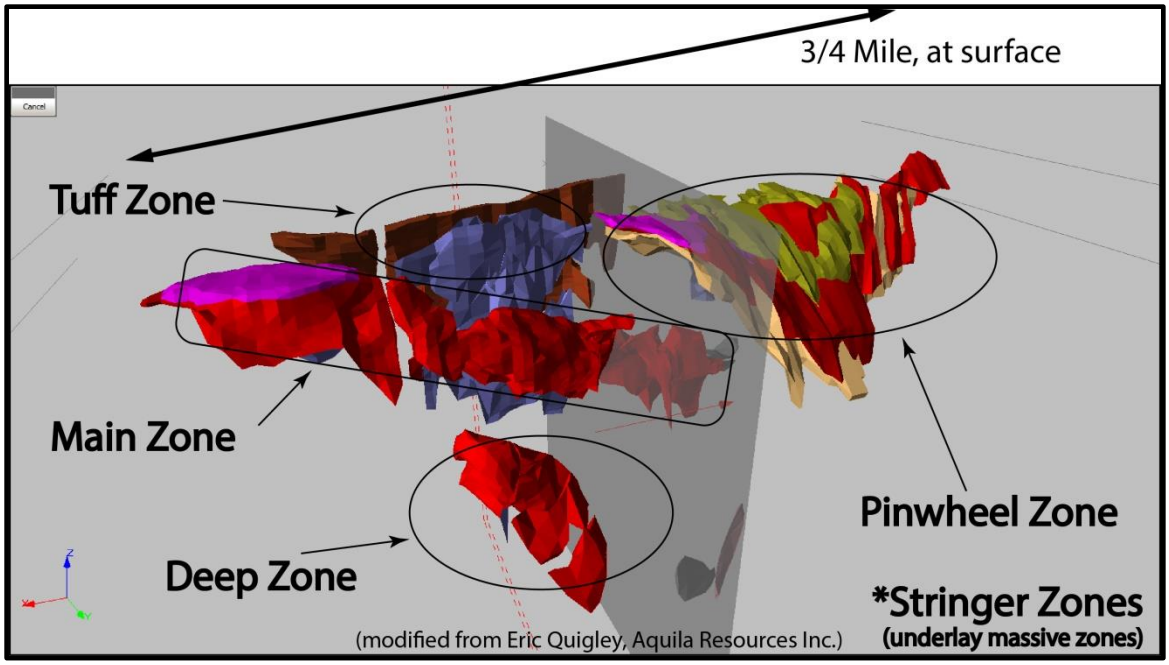

Figure 12: Back Forty 3-D model including zones (reconstruction, after Aquila Resources, Inc.).

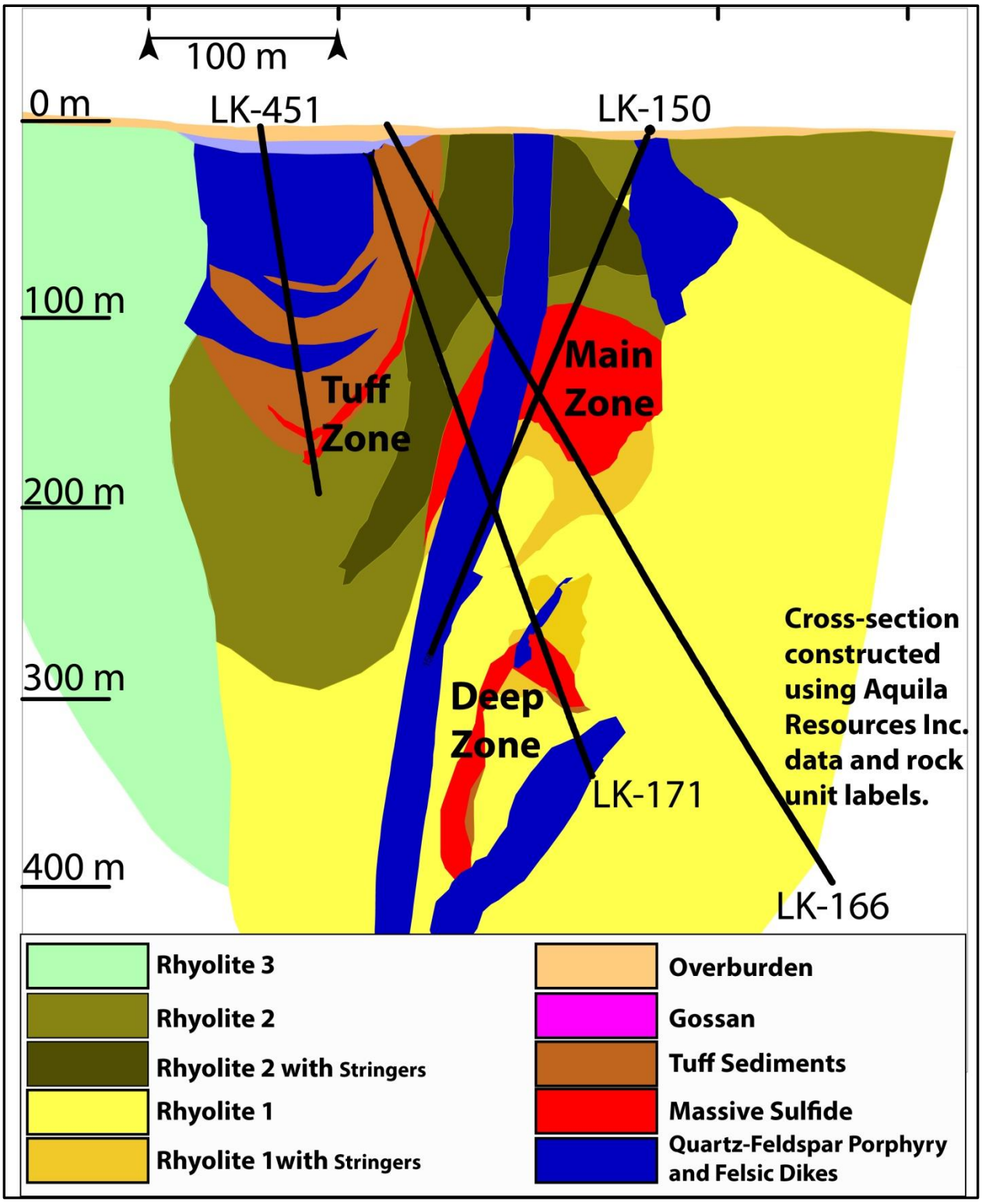

Figure 13: North-east cross-section of the deposit containing core from four drill holes.

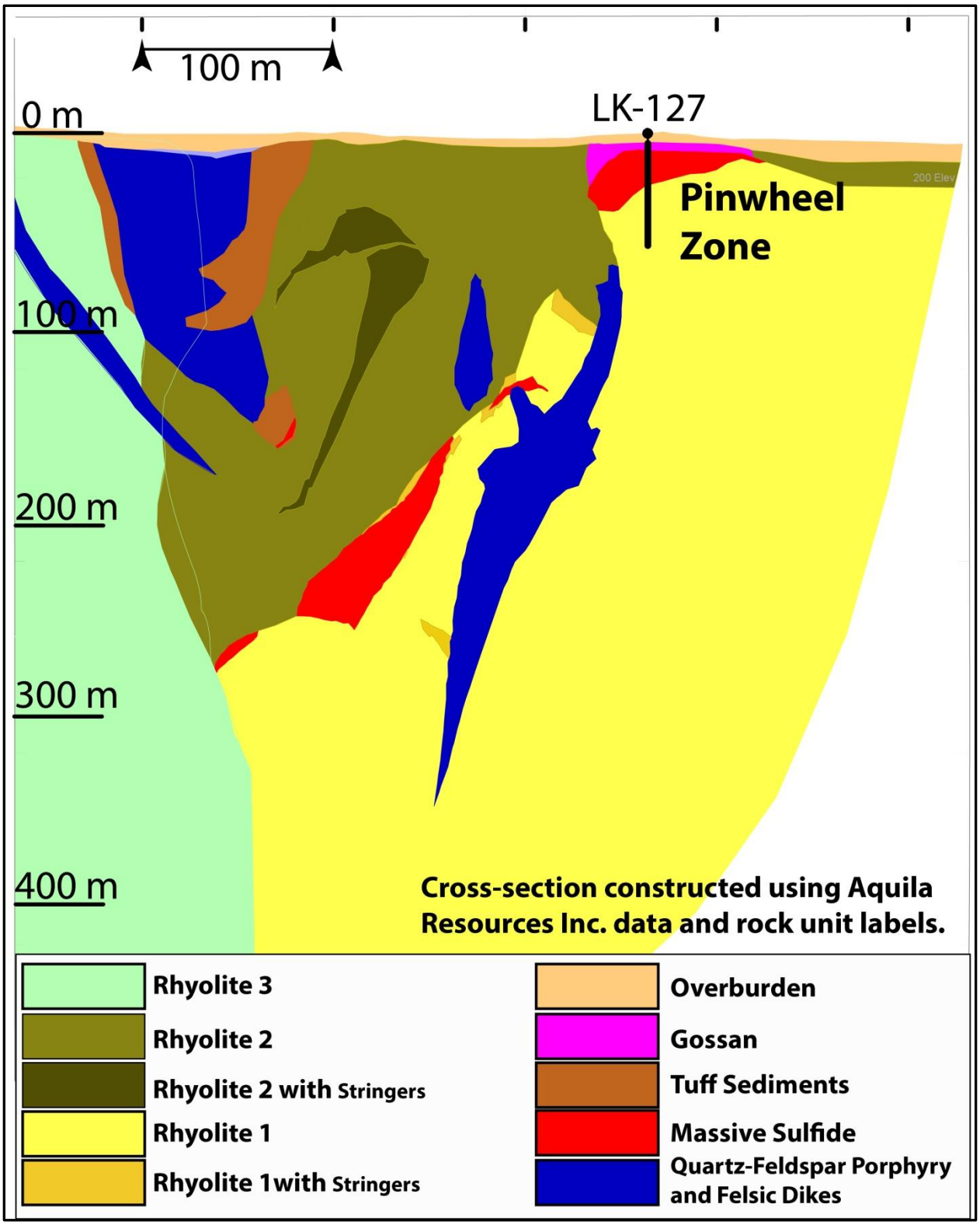

Figure 14: South-west cross-section of the deposit containing core from drill hole LK-127.

Sampling

In total, 146 core samples have been obtained from the five drills holes (Appendix I: Sampling Log). 26 of these samples were prepared as thin-sections by Spectrum Petrographics Inc. with a 0.5 µm diamond polish. For sampling purposes, core samples were cataloged using Aquila Resources identified rock unit labels. These rock units will be re-evaluated in Chapter 4. 36 samples (4 thin-sections prepared) were acquired from Rhyolite 1 (including stingers), 19 samples (3 thin-sections prepared) from Rhyolite 2 (including stringers), 35 samples (4 thin-sections prepared) from the Quartz-Feldspar Porphyry/Felsic Dikes, 22 samples (4 thin-sections prepared) from Tuff Sediments/Rhyolite Ash-tuff, 27 samples (9 thin-sections prepared) from Massive Sulfide, 3 samples (1 thin-section prepared) from Semi-Massive Sulfides/disseminated sulfide, 2 samples (1 thin-section prepared) from Pinwheel Zone Gossan, and 2 samples from Sandstone.

Petrographic Descriptions

Petrographic descriptions were carried out in two ways: hand sample and thin-sections descriptions. Hand sample descriptions were used to establish the occurrence of minerals and host rock textures. Thin-section descriptions were used to identify minerals, textural characteristics, and volumetric abundance of sulfide minerals within the host rocks. Transmitted light was used for identifying silicate minerals in thin-section, while reflected light was used to identify opaque sulfide minerals. Photomicrographs of thin-sections have been used to record representative images of minerals and textures

observed under the microscope. Leica's LAS EZ Application Suite was used produce photomicrographs.

Sulfur Isotope Measurements

A Delta V Isotope Ratio Mass Spectrometer was used to obtain sulfur isotope values ($\delta^{34}S$) from sulfide minerals prepared as a powder from core samples and thin-section billets. Sulfur isotope measurements used in this work were carried out at the Indiana University – Bloomington Isotope Lab by Benjamin Underwood while an identical instrument was being set up at Western Michigan – Stable Isotope Geochemistry/Economic Geology Laboratory. While ^{32}S is the most abundant form of sulfur, ^{34}S is the second most abundant stable isotope of sulfur, accounting for approximately 4.21% relative abundance on earth; other stable isotopes of sulfur include less abundant ^{36}S (0.02 %) and ^{33}S (0.75%) (Macnamara and Thode 1950). Sulfur isotope analyses are commonly used to investigate sources of sulfur (Hannington et al., 2006).

Sample Preparation

Preparation of sulfide samples in the first batch was performed by Katherine Dvorak (Western Michigan University) at the Indiana University – Bloomington Isotope Lab, whom demonstrated the process by which I was able to prepare my other samples in this study. Powdered samples of sulfide minerals were obtained by using a micro Dremel tool equipped with diamond-tipped rotary drill bits (Figure 15). Sulfides were drilled from billets corresponding to the prepared thin-sections, as well as core samples. Powder samples of sulfides and internal lab standards were weighed out into tin capsules (3x5

mm) within specified weight ranges for each sulfide, including an equal amount of vanadium pentoxide as a combustion agent (Table 4).

Internal lab standards are calibrated to International Atomic Energy Agency (IAES) standards. The internationally accepted reference for sulfur isotopes is Vienna Canyon Diablo Troilite (VCDT) with $\delta^{34}S = 0‰$ by definition, which is currently defined relative to the silver sulfide reference material IAES-S-1that holds an assigned value of -0.3‰ because the supply of the Canyon Diablo Troilite reference material has been exhausted (Krouse and Coplen, 1997; Seal, 2006). The reference material was originally defined on the isotopic composition of troilite (FeS) from the Canyon Diablo meteorite (Seal, 2006). The use of a meteoritic sulfide mineral as the reference for sulfur is accepted because meteoritic sulfide is thought to represent the primordial sulfur isotopic composition of the earth (Nielsen et al., 1991).

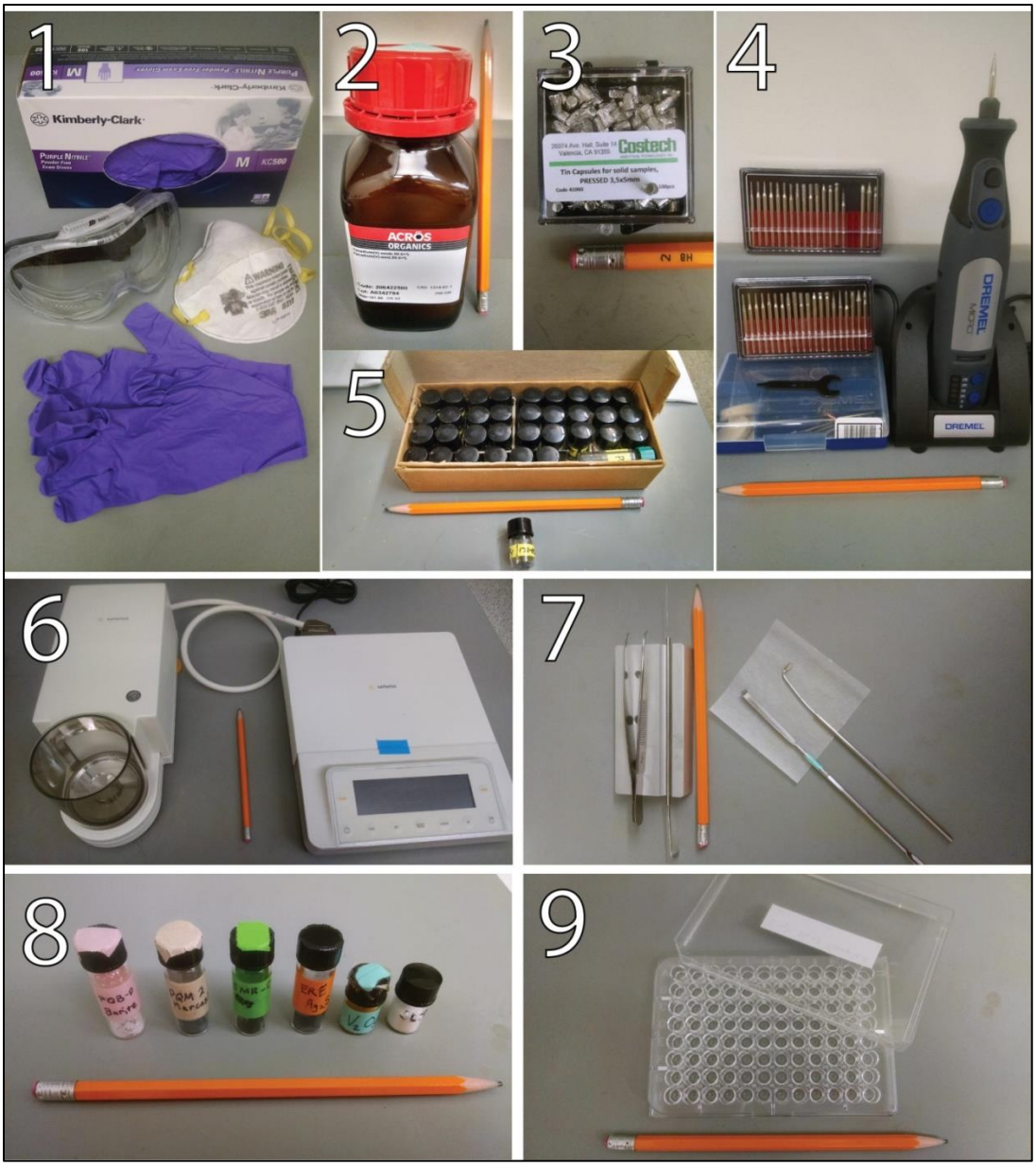

Figure 15: Sample preparation equipment. [1] safety gear, [2] vanadium pentoxide, [3] tin capsules, [4] rotary drill tool and drill bits, [5] sulfide powder sample vials, [6] weight balance, [7] spatulas and tweezers, [8] standards, and [9] sample tray.

Table 4: Sulfide sample and standard weight ranges, based on moles of sulfur in the sulfide molecule and the molecular weight of that sulfide.

Suggested micrograms (50 – 60) and micromoles of Sulfur (1.56 – 1.88) with weight ranges for sulfides(bolded)													
Molecular Weight	20	30	40	**50**	**60**	70	80	90	**wt. % S**	**Mols of S**	**Chemical Formula**	**Mineral Sample**	**Lab Standard**
	0.63	0.94	1.25	**1.56**	**1.88**	2.19	2.5	2.81					
239.26	0.15	0.22	0.30	**0.37**	**0.45**	0.52	0.60	0.67	13.40%	1	PbS	Gn	-
97.45	0.06	0.09	0.12	**0.15**	**0.18**	0.21	0.24	0.27	32.90%	1	ZnS	Sp	-
501.88	0.08	0.12	0.16	**0.20**	**0.24**	0.27	0.31	0.35	25.55%	4	Cu_5FeS_4	Bn	-
183.51	0.06	0.09	0.11	**0.14**	**0.17**	0.20	0.23	0.26	34.94%	2	$CuFeS_2$	Ccp	Ccp (EMR-Cp)
119.97	0.04	0.06	0.07	**0.09**	**0.11**	0.13	0.15	0.17	53.45%	2	FeS_2	Py/Mrc	Py/Mrc (PQM2)
247.8	0.16	0.23	0.31	**0.39**	**0.47**	0.54	0.62	0.70	12.94%	1	Ag_2S	-	(ERE-Ag_2S)
233.39	0.15	0.22	0.29	**0.36**	**0.44**	0.51	0.58	0.66	13.74%	1	$BaSO_4$	-	Barite (PQB2)
172.21	0.11	0.16	0.22	**0.27**	**0.32**	0.38	0.43	0.48	18.62%	1	$H_2NC_6H_4SO_2NH$	-	Sulfanilamide (SLJ)

Instrument Processes

Samples were loaded into a sample carousel (autosampler) that sits directly atop the reactor column housed within the elemental analyzer (Figure 16). Samples are automatically dropped from the carousel into the reactor column where the sample is combusted at 980°C. This gas contains an unknown ratio of $^{34}S/^{32}S$. Prior to combustion, oxygen is circulated into the reactor column to promote combustion. Helium gas is used to carry oxygen into the reactor column, as well as carry combustion gasses (i.e. SO_2 and H_2O) through the gas chromatograph (GC) separation column. Prior to reaching the GC separation column, water is removed by a filter (magnesium anhydrous percolate) after leaving the reactor column (Figure 17).

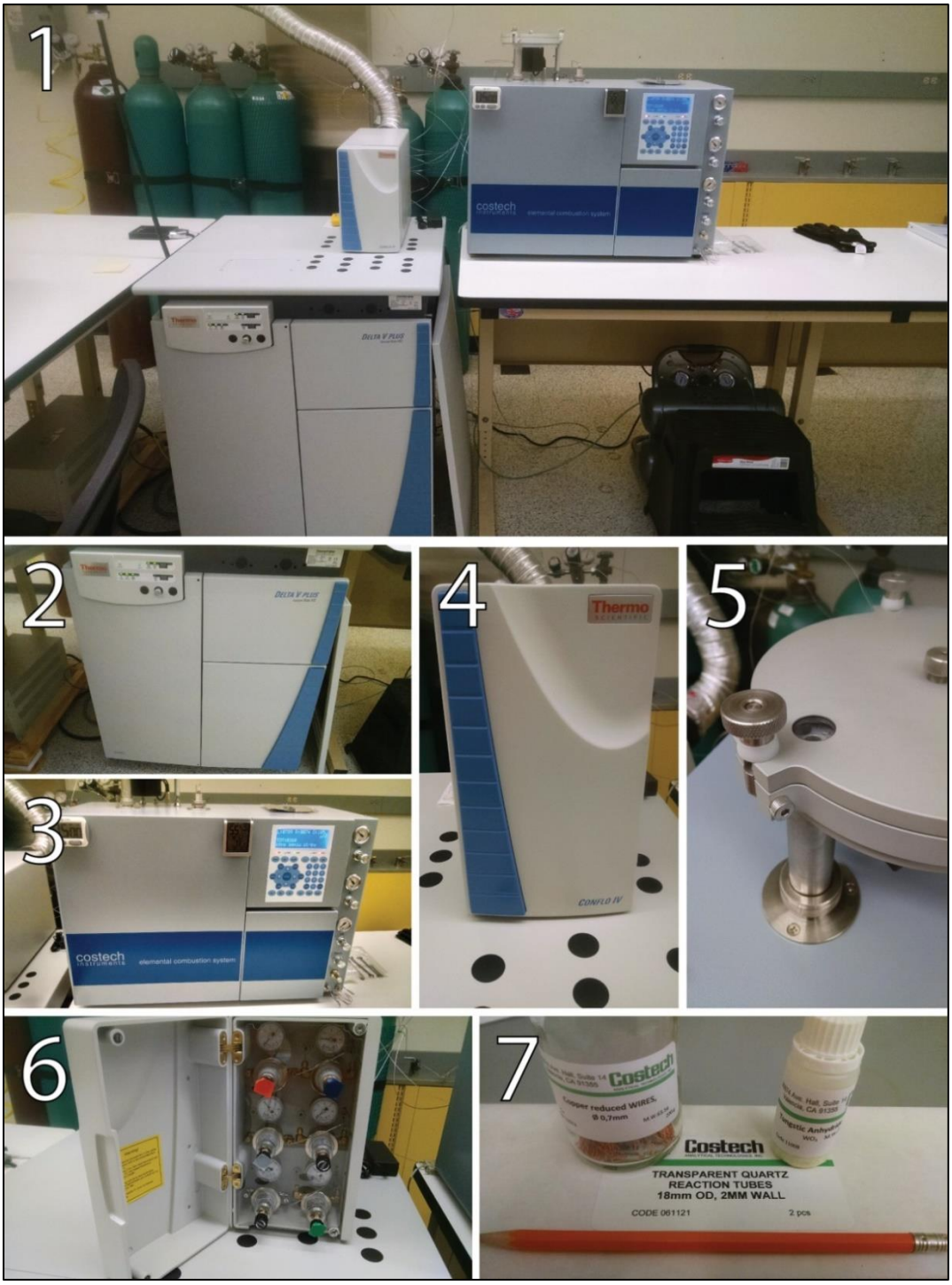

Figure 16: Lab instruments; [1] instrument assembly, [2] Delta V Mass Spectrometer, [3] Elemental Analyzer, [4] Conflo, [5] sample carousel (autosampler), [6] Conflo interior, and [7] packing components of reactor column.

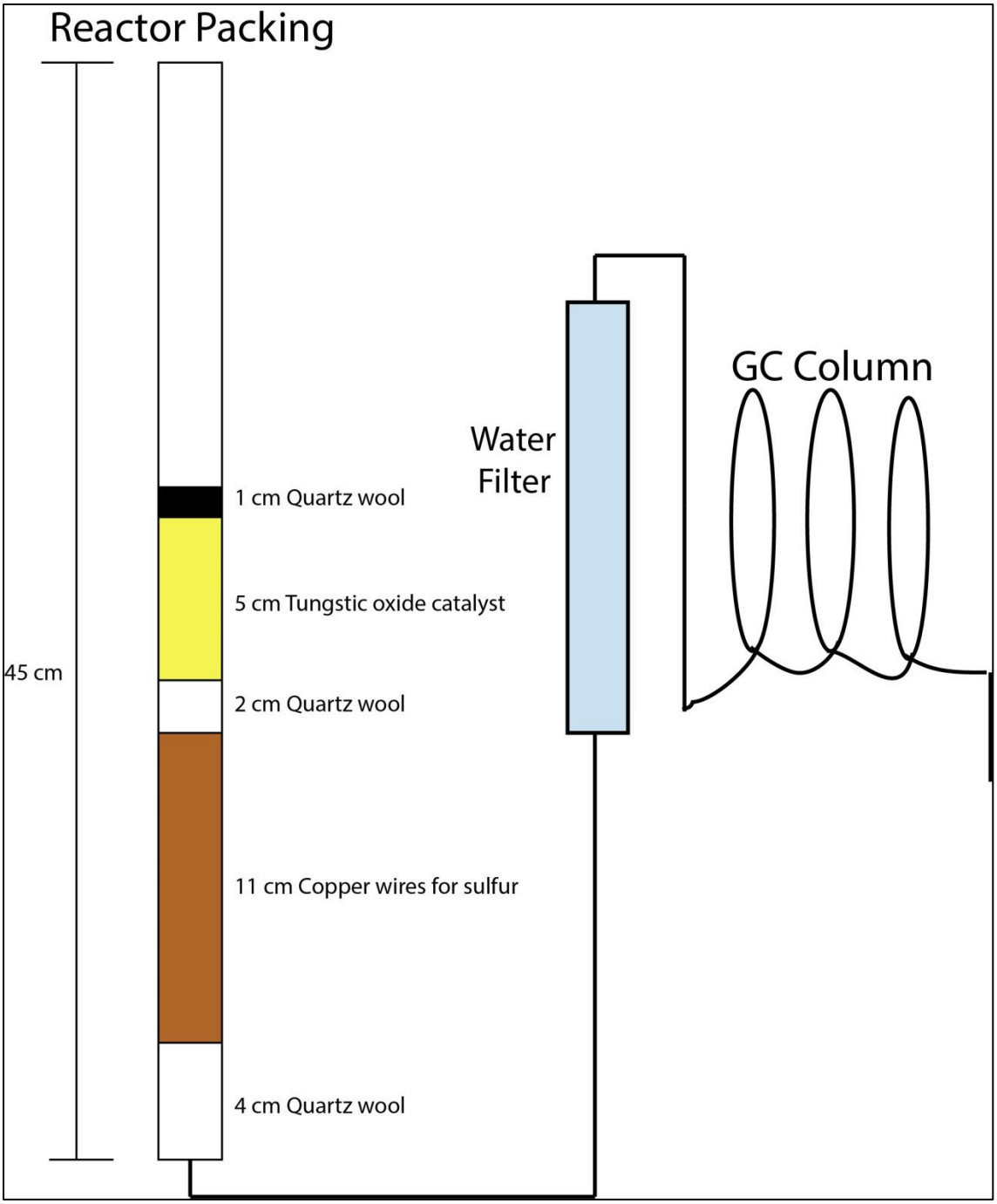

Figure 17: Reactor column packing, water filter, and gas chromatograph separation column (modified from Costech Analytical Technologies Inc.).

Leaving the GC separation column, the sulfur dioxide enters the Conflo which regulates the pulses of combustion gases and lab sulfur dioxide into the mass spectrometer. Sulfur dioxide gas is then ionized before entering the isotope ratio mass spectrometer. The gas must be ionized in order to be deflected by the magnet toward collection plates. Ionized gas will be separated by the atomic mass of the sulfur dioxide gas (e.g. $^{32}SO_2$ and $^{34}SO_2$) as ions exit the magnetic field. Collection plates (Faraday Cups) record the current generated by the ions (sulfur dioxide gas molecules).

The ratio measured for the sample gas is compared with the ratio for the lab sulfur dioxide tank gas, measured in two separate pulses prior to the measurement of the sample combustion gas. Raw $\delta^{34}S_{Sample}$ values are obtained by the calculated difference in the ratio of ^{34}S to ^{32}S for the sample to the ratio of ^{34}S to ^{32}S in the lab tank gas as the reference (Equation 1: Seal, 2006).

$$\delta^{34}S_{Sample} = \left(\frac{\frac{^{34}S}{^{32}S}sample - \frac{^{34}S}{^{32}S}reference}{\frac{^{34}S}{^{32}S}reference} \right) x\ 1000 \qquad \textbf{(1)}$$

The raw values must then be calibrated to the known values of the internal lab standards. The internal lab standards used in this study are listed in Table 4. Calculating values relative to VCDT will be described in Chapter 3: Results, Part B: Geochemistry: Mineralization.

Trace Element Analysis

Geochemical datasets of trace element concentrations were provided by Aquila Resources Inc. and utilized in this study. Aquila Resources obtained geochemical data through several laboratories that included ALS Minerals (formerly MLS Chemex), Accurassay, SGS, Actlabs, Inspectorate, and Neutron Activation Labs (Tetra Tech, 2014). These laboratories performed analyses such as Inductively Coupled Plasma – Atomic Emission Spectrometry (ICP – AES) and Inductively Coupled Plasma – Mass Spectrometry (ICP – MS). Of these labs, the general procedure for these methods performed by ALS Minerals is described below.

Sample Preparation

Samples for both ICP-AES and ICP – MS involved a multi-acid digestion composed of a mixture of four acids: perchloric, nitric, hydrofluoric and hydrochloric acids. This process is designed to dissolve most silicate phases of rock samples. The solution that is produced by this process is then vaporized into a gas by the processes involving the instrument.

Instrument Processes

In both methods, the solution produced during sample preparation was vaporized. For ICP – AES, the vapor was carried in a stream of argon gas, entering into a spectrometer. Thermally excited electrons in the outer shell of the atom release photons of light when returning to their ground state. Elements are identified by the wavelength of light emitted, and the concentration determined by the intensity of light emitted. For ICP

– MS, the vaporized solution was ionized to produce a stream of positively charged gaseous atoms that enter a mass spectrometer. The mass spectrometer is designed to separate atoms based on atomic mass. Both ICP methods were used to obtain concentration of trace elements used in this research, as provided by Aquila Resources (Chapter 3: Results, Part B: Geochemistry: Host Rocks)

\

CHAPTER III

RESULTS, PART A:

PETROGRAPHIC DESCRIPTIONS

Table 5: Mineral abbreviations

(Whitney and Evans, 2010)

Symbol	Mineral Name
Anh	Anhydrite
Asp	Arsenopyrite
Bn	Bornite
Cal	Calcite
Ccp	Chalcopyrite
Chl	Chlorite
Dol	Dolomite
Fsp	Feldspar
Gn	Galena
Gth	Goethite
Hem	Hematite
Mrc	Marcasite
Ms	Muscovite
Po	Pyrrhotite
Py	Pyrite
Qz	Quartz
Ser	Sericite
Sp	Sphalerite

Symbol	Extras
RF	Rock Fragment
Sulf	Sulfide Mineral

Host Rocks

146 hand samples and 26 thin-sections were used to build petrographic descriptions of host rock and sulfide mineralized zones. Grain sizes of minerals, volumetric/modal abundances of minerals, groundmass compositions, and xenocryst compositions were used as a mineralogical, petrological basis to classify the host rocks. Textural characteristics and the mode of occurrence of minerals were used as basis to identify primary igneous textures from secondary, hydrothermal mineralization textures. Samples are organized in Chapter 3 based on Aquila Resources rock unit labels, and will be revaluated by this study in Chapter 4.

Sample ID: LK–171– #029
Zone: Rhyolite 1 Crystal Tuff, Main Zone/Stinger Zone
Depth: 261.34 – 261.50 meters

Sample #029 is characterized by an altered rhyolite crystal tuff groundmass composed of quartz (~50%), alkali-feldspar (~45%) and plagioclase feldspar (~5%). Quartz within the groundmass is identified by equant grains and indistinct grain boundaries, < 0.1 mm average grain size, first-order white to black interference colors in cross-polarized light, and low relief with a clear color in plane-polarized light. Alkali-feldspar is identified by complete alteration to sericite: a cloudy yellow-orange color in plane-polarized with high relief, fourth-order pink to blue interference colors in crossed-polarized light, and fine-grained. Plagioclase feldspars are low in volumetric/modal abundance with a lath-like and fine-grained habit, first-order white to black interference colors with albite twinning when viewed under cross-polarized light, and a clear-white color in plane-polarized light with low relief. Quartz eye-shaped xenocrysts (0.5 mm to 1

mm in diameter) are present throughout and exhibit variable extinction patterns in first-order white to yellow-orange interference colors when viewed under crossed-polarized light, and low relief with a clear color in plane-polarized light. Extinction patterns in the quartz eye-shaped xenocrysts range from uniform to undulating. Undulose extinction is identified by white to yellow-orange first-order interference colors that sweep across the grain during rotation of the microscope stage. Extinction angles measured with respect to the c-crystallographic direction were used as identification characteristics for coarse grained silicate minerals.

Patches of fine-grained sericite occur throughout the groundmass and is more concentrated along stinger sulfide boundaries with grain sizes of quartz that are larger than surrounding groundmass (0.25 to 1.0 mm in diameter). Stringers are vein-like structures of opaque sulfide minerals within the host rock. Sample #029 contains stinger-style mineralization of sulfides 0.25 to 1 cm in diameter within the groundmass. Sulfide minerals are opaque in transmitted light. In mineralized zones, reflectance color of sulfide minerals have been used to identify them.

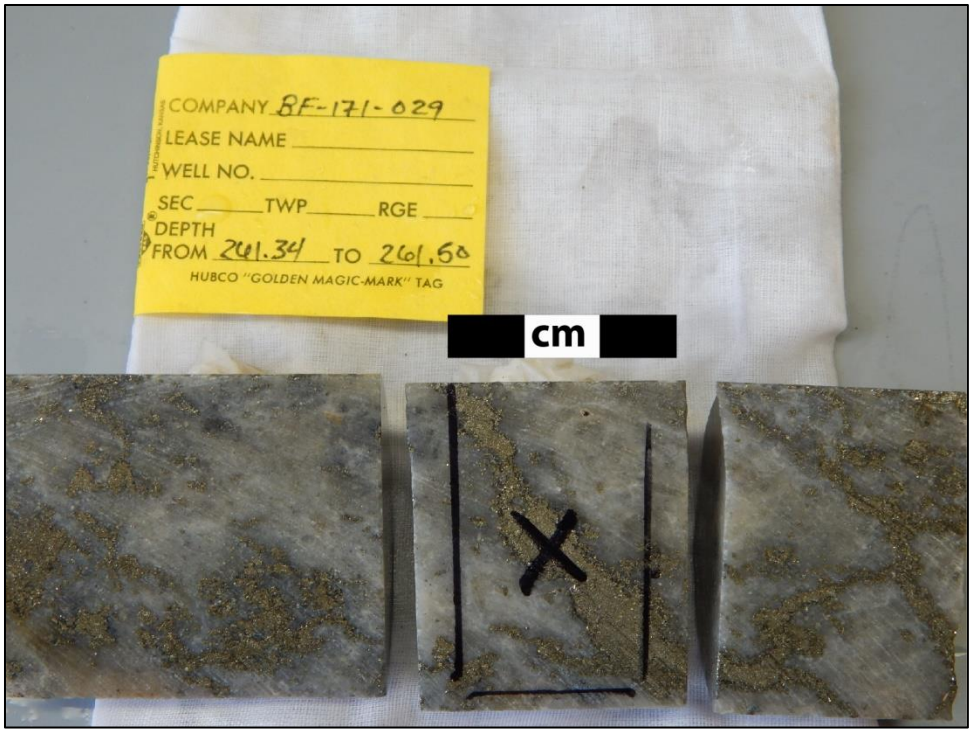

Figure 18: Hand sample, ID: LK–171– #029. Brassy-metallic pyrite within a groundmass of light colored quartz, altered alkali and plagioclase feldspar. Quartz eye-shaped xenocrysts occur throughout the groundmass.

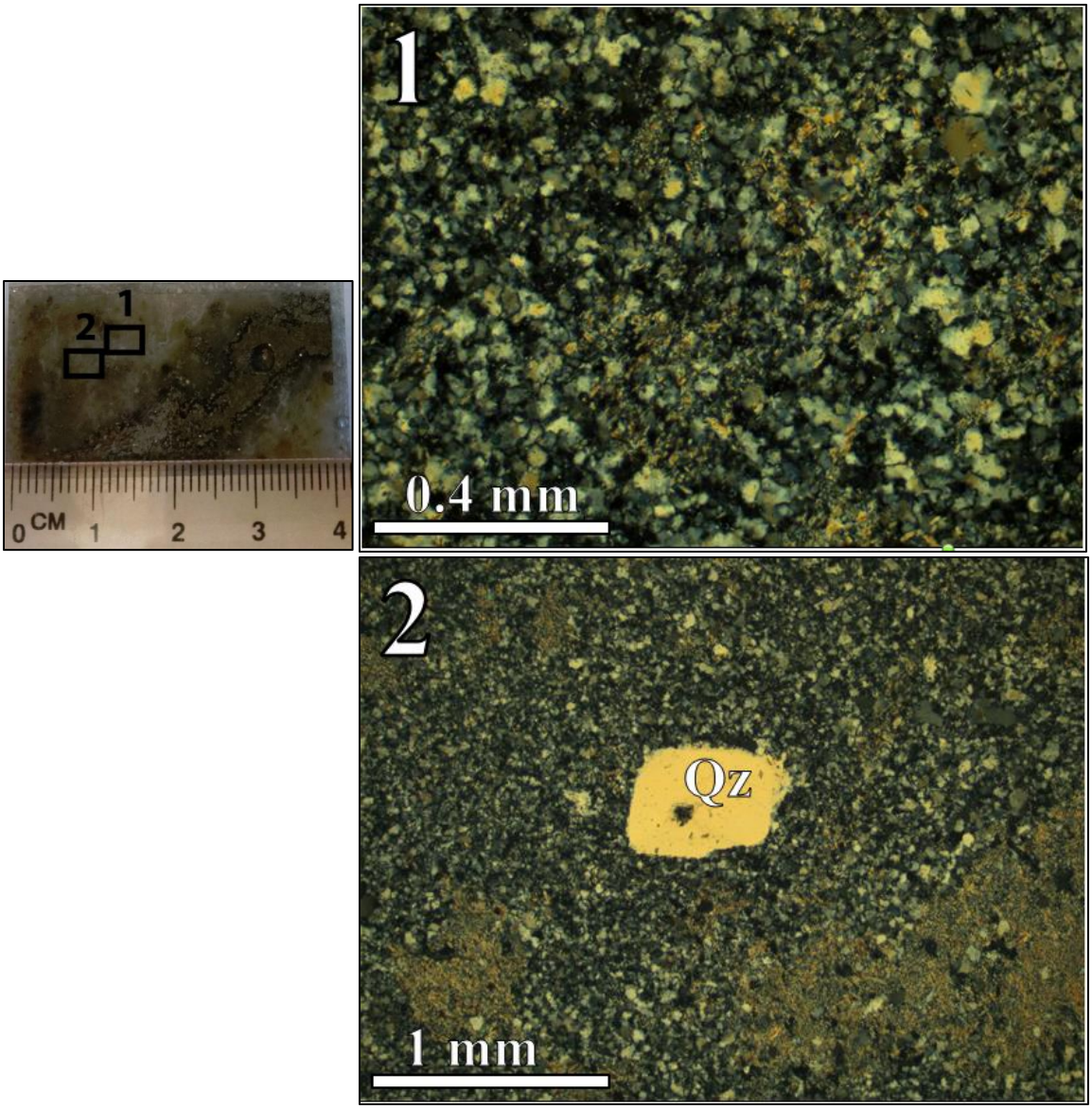

Figure 19: Photomicrographs, sample ID: LK–171– #029: [1] Light: plane-polarized, altered rhyolite groundmass of quartz, alkali and plagioclase feldspar. [2] Light: cross-polarized; quartz eye-shaped xenocrysts in a groundmass of quartz, alkali and plagioclase feldspar.

Sample ID: LK–171– #023
Zone: Rhyolite 1, Main Zone/Stinger Zone
Depth: 231.87-231.97 meters

Sample #023 is characterized by an altered rhyolite crystal tuff groundmass composed of quartz (~50%), alkali-feldspar altered to sericite (~45%), and plagioclase feldspar (~5%) indistinguishable from sample #029. Quartz eye-shaped xenocrysts (0.5 mm to 1 mm in diameter) are present throughout and exhibit extinction patterns indistinguishable to sample #029. Sericite occurs in patches, fine-grained masses more concentrated around sulfides. Quartz and calcite veins occur through the host rock. Calcite is identified by a cloudy appearance in transmitted light, third to forth-order interference color in crossed-polarized light, fine-grained texture, and a positive reaction to hydrochloric acid without needing a powdered surface. This calcite often encases quartz, sericite, and chlorite within spaces between sulfides. Sample #023 contains stinger-style mineralization of sulfides (0.25 to 1 cm in diameter) within the groundmass.

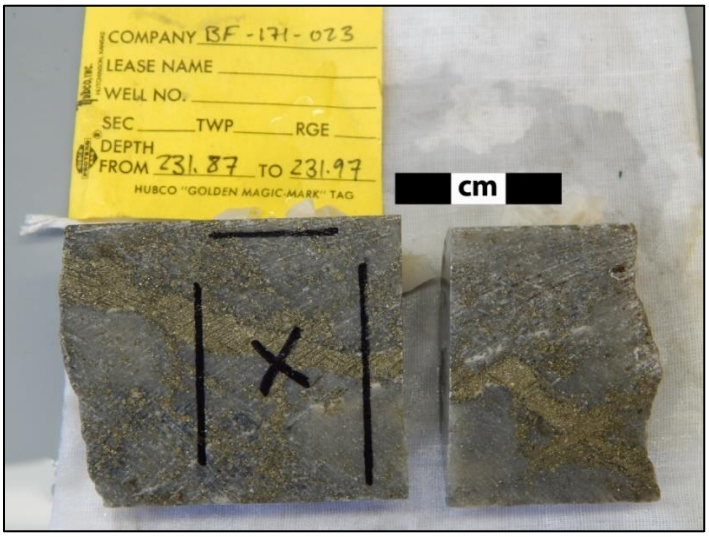

Figure 20: Hand sample, ID: LK–171– #023. Quartz and alkali-feldspar altered to sericite groundmass host brassy-yellow sulfide stringers (0.25 to 1 cm in diameter).

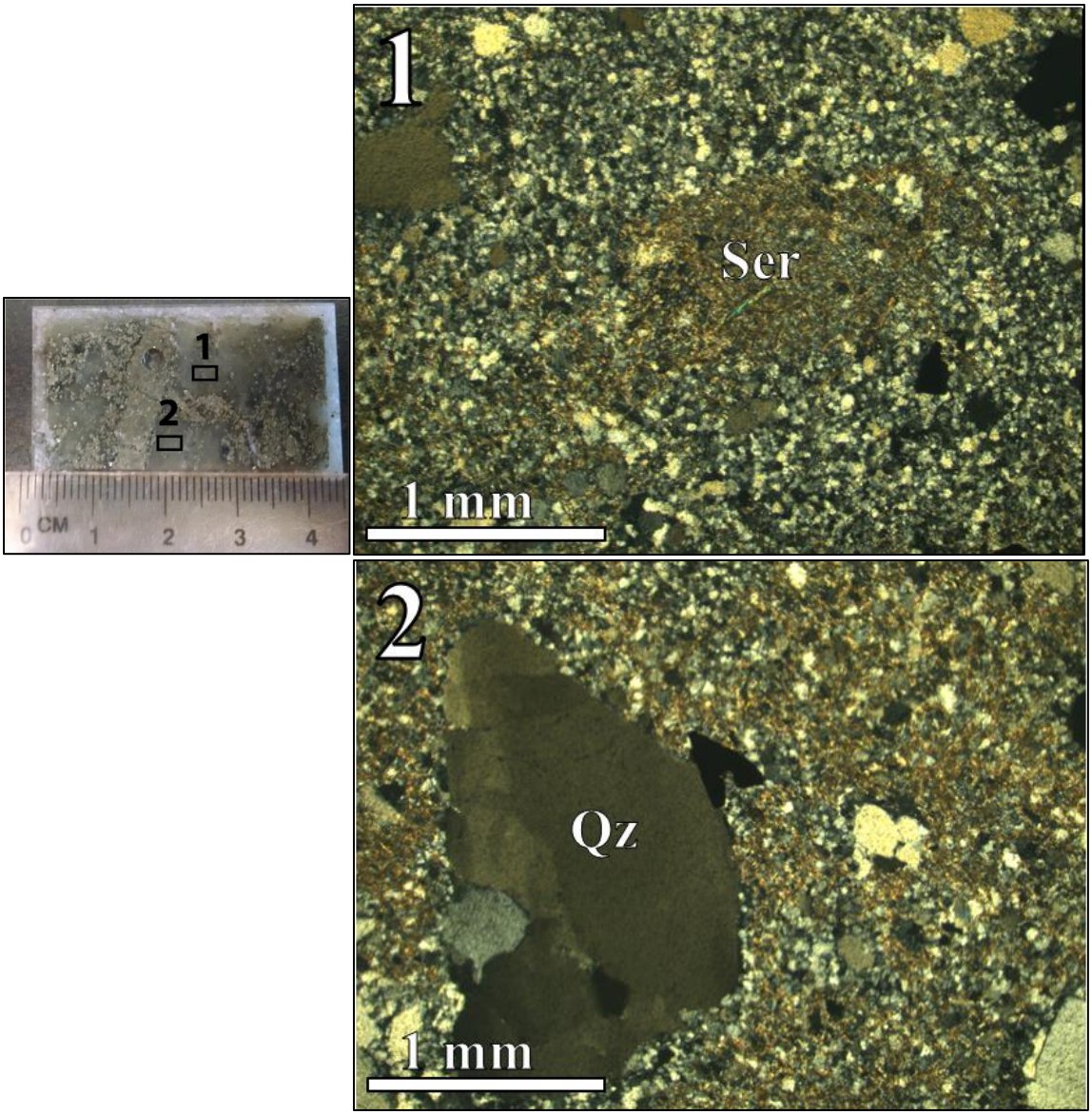

Figure 21: Photomicrographs, sample ID: LK–171– #023: [1 and 2] Light: crossed-polarized, altered rhyolite groundmass composed of quartz, alkali-feldspars altered to sericite, and quartz eye-shaped xenocrysts with undulose extinction.

Sample ID: LK–451– #106
Zone: Rhyolite 2 Crystal Tuff, Tuff Zone
Depth: 179.91 – 180.20 meters

Sample #106 contains groundmass mineralogy nearly indistinguishable to sample #029 from rhyolite 1 crystal tuff, composed of quartz (~50%), alkali (~45%) and plagioclase feldspar (~5%). Quartz eye-shaped xenocrysts (~ 0.5 mm in diameter) display extinction patterns and grain sizes indistinguishable from samples #029 and #023 from rhyolite 1crystal tuff. Chlorite occurs as platy colorless grains with moderate relief in plane-polarized light, and first-order grey inference colors in cross-polarized light. Cleavage is well developed in chlorite grains that are typically 0.5 to 1.5 mm in diameter. Patches of fine-grained sericite occur throughout the groundmass and is more concentrated along boundaries where grain sizes of quartz are larger than surrounding groundmass (0.25 to 1.0 mm in diameter), nearly indistinguishable from samples #029 and #023 from rhyolite 1crystal tuff. Sample #106 contains thin (0.25 to 0.50 cm in diameter) sulfide minerals within the rhyolite groundmass.

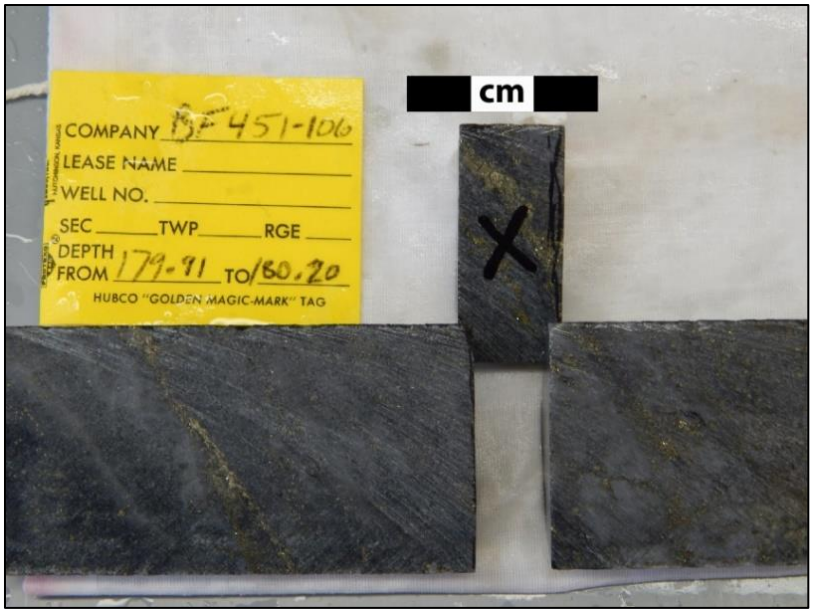

Figure 22: Hand sample, ID: LK–451– #106. Brassy-metallic pyrite layers within a grey colored groundmass of quartz, altered alkali and plagioclase feldspar, and chlorite. Quartz eye-shaped xenocrysts occur throughout the groundmass.

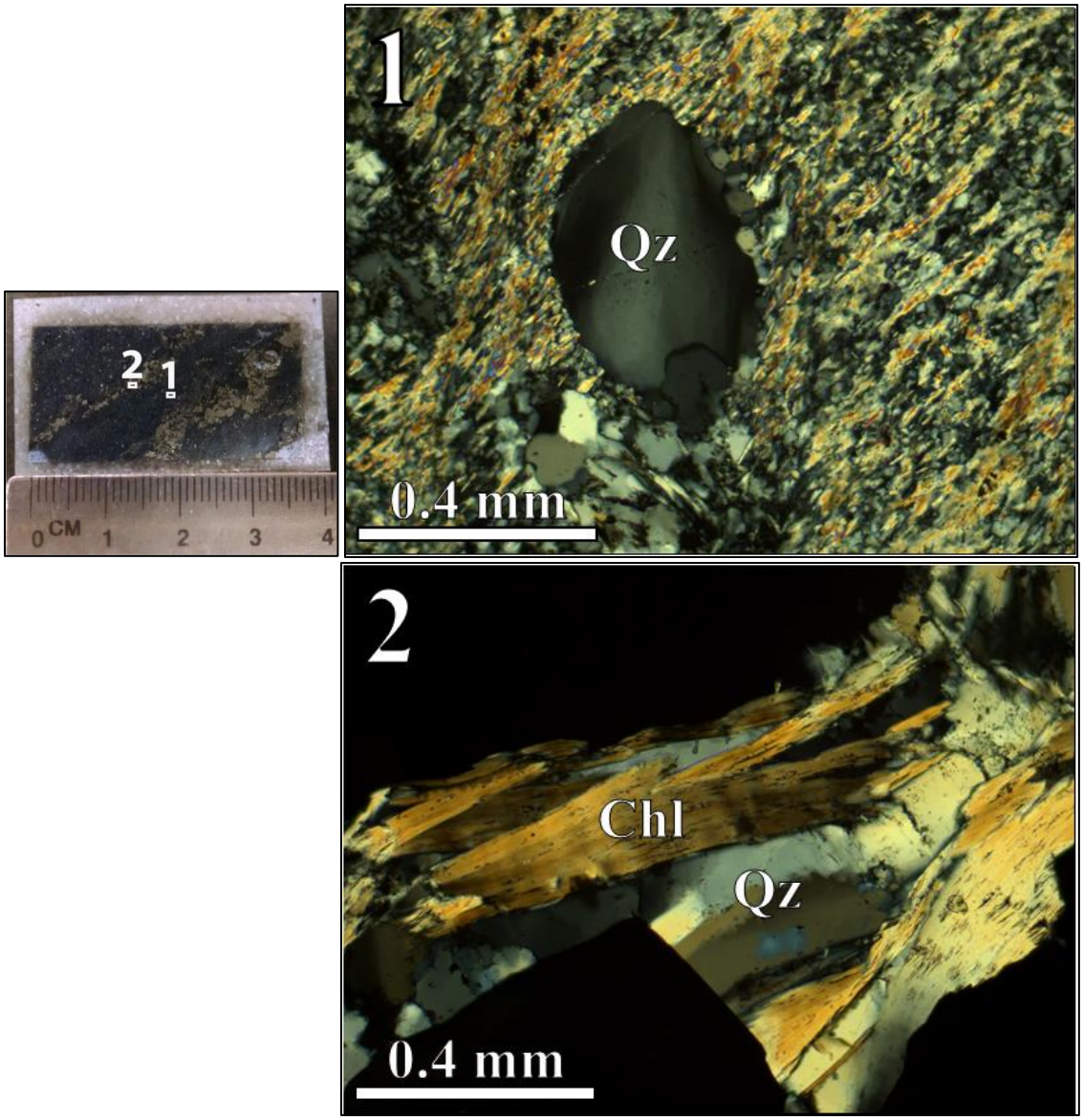

Figure 23: Photomicrographs, sample ID: LK–451– #106: [1] Light: cross-polarized, cross-polarized; quartz eye-shaped xenocrysts in a groundmass of quartz, alkali and plagioclase feldspar. [2] Light: crossed-polarized, platy chlorite and quartz adjacent to opaque sulfides.

Sample ID: LK–150– #060
Zone: Rhyolite 2 Crystal Tuff, Main Zone
Depth: 46.40 – 46.50 meters

Sample #060 contains groundmass mineralogy nearly indistinguishable to sample #106 from rhyolite 2 crystal tuff, composed of quartz (~50%), alkali (~45%) and plagioclase feldspar (~5%). Quartz eye-shaped xenocrysts (~ 0.5 mm in diameter) display extinction patterns and grain sizes indistinguishable from sample #029. Patches of fine-grained sericite occur throughout the groundmass and is more concentrated along boundaries where grain sizes of quartz are larger than surrounding groundmass (0.25 to 1.0 mm in diameter), nearly indistinguishable from samples #023 and #029 from rhyolite 1 crystal tuff.

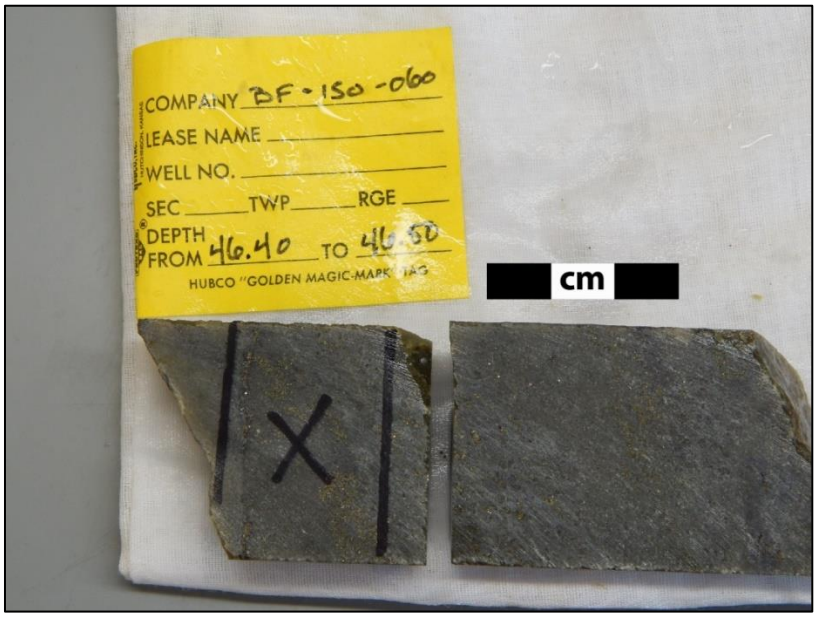

Figure 24: Hand sample, ID: LK–150– #060. Brassy-metallic disseminated sulfides within a grey colored groundmass of quartz, altered alkali and plagioclase feldspar. Quartz eye-shaped xenocrysts occur throughout the groundmass.

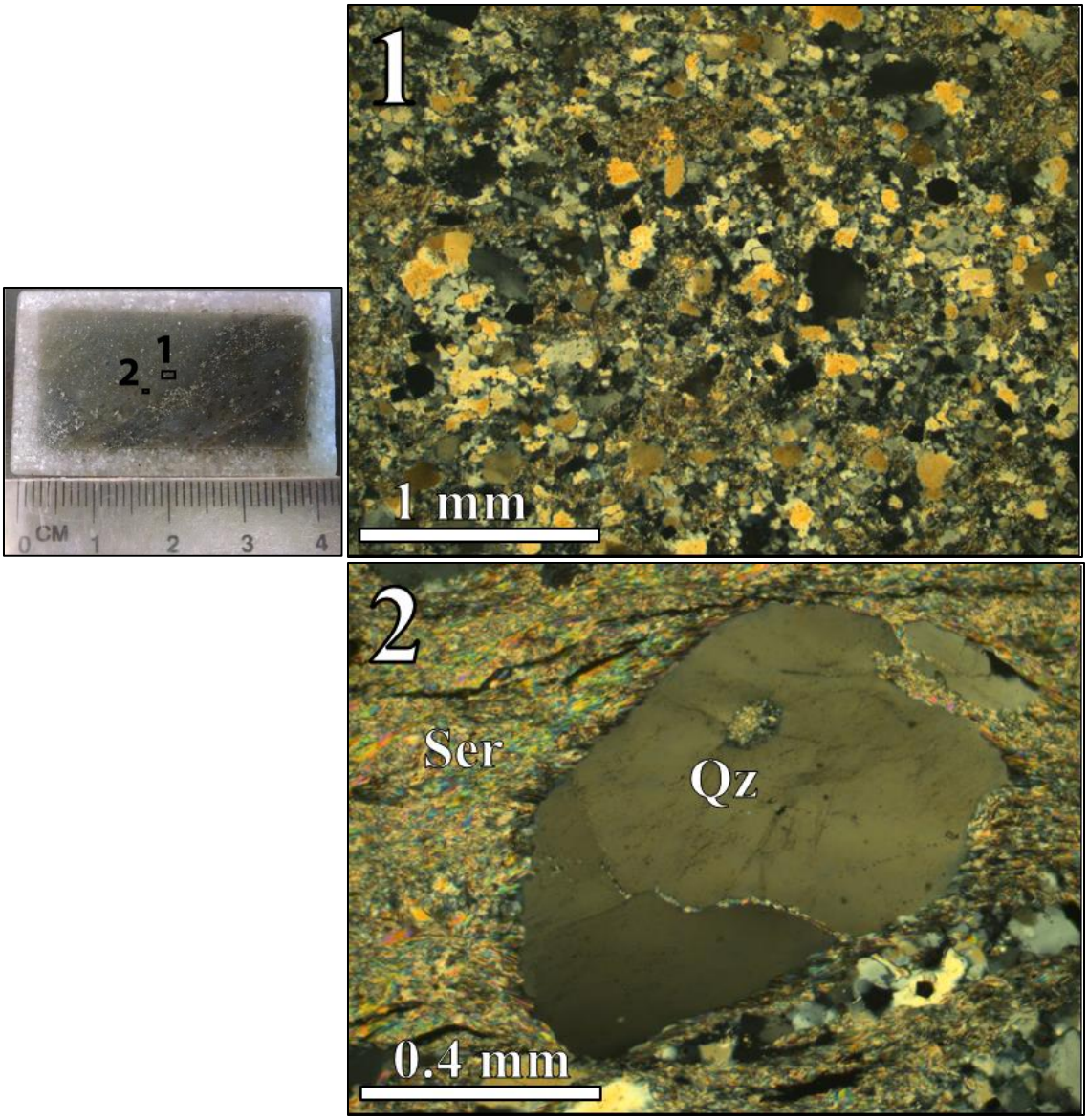

Figure 25: Photomicrographs, sample ID: LK–150– #060: [1 and 2] Light: crossed-polarized, altered rhyolite groundmass composed of quartz, alkali-feldspars altered to sericite, and quartz eye-shaped xenocrysts with undulose extinction.

Sample ID: LK–150– #055
Zone: Quartz-Feldspar Porphyry, Main Zone North
Depth: 10.19 – 10.33 meters

Sample #055 contains quartz eye-shaped xenocrysts (< 1 mm in diameter) in a groundmass of fine-grained hematite. Extinction patterns in some quartz eye-shaped xenocrysts are undulose, extinction patterns different than in sample #029 (Figure 12) and #106 by having a segmented appearance to the pattern extinction, from white to black first-order interference colors in cross-polarized light across the grain. Hematite occurs with a fine-grained habit and in irregular patches throughout the groundmass giving the sample a red color. Hematite occurs as opaque, deep red and fine-grained patches lacking crystal habit in plane-polarized and cross-polarized light. The hematite is very weak, unconsolidated and friable. Angular rock fragments are composed of fine-grained quartz and sericite, occurring within the groundmass (1 to 3 mm in diameter). Angular quartz grains (0.10 to 0.20 mm in diameter) accompany larger rock fragments.

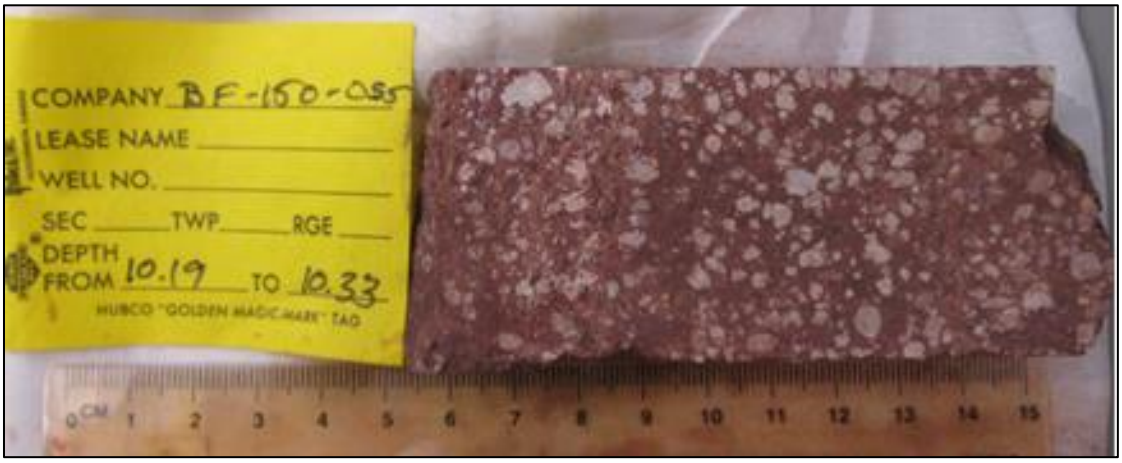

Figure 26: Hand sample, ID: LK–150– #055. Hematite produces the red color throughout the sample, near complete oxidation.

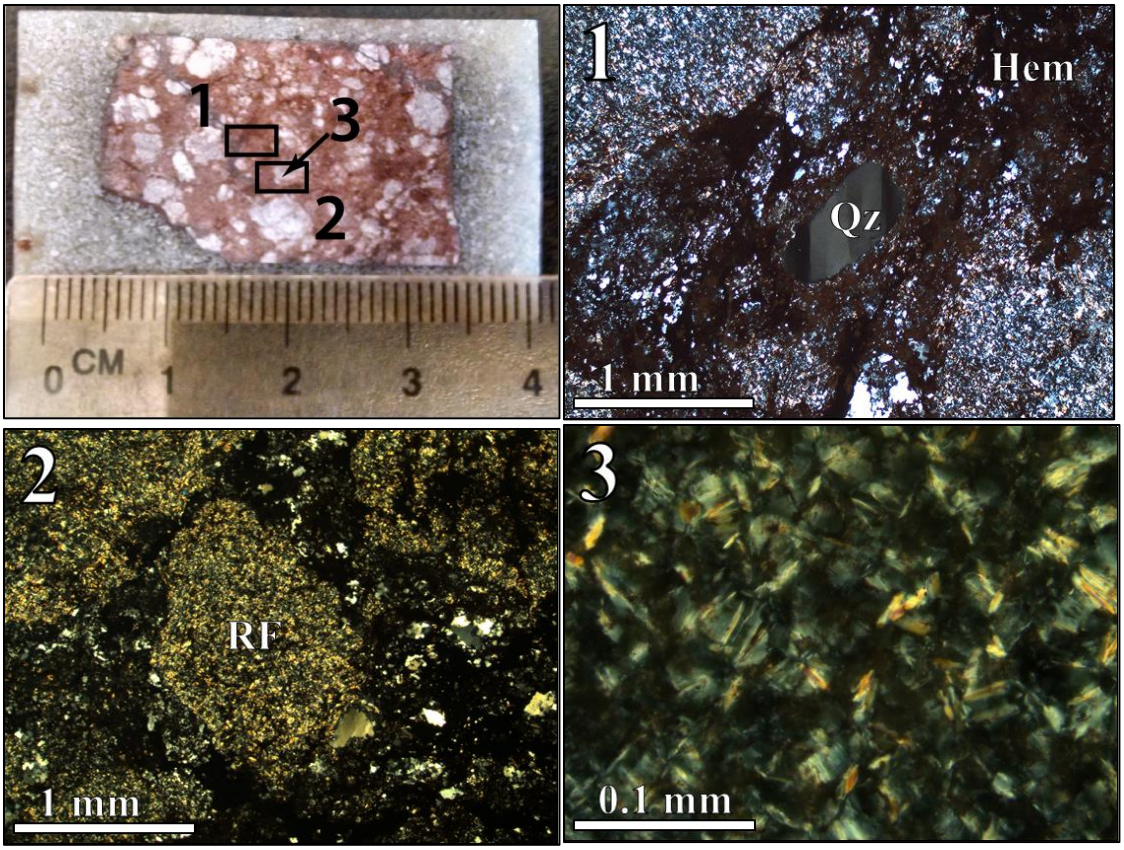

Figure 27: Photomicrographs, sample ID: LK–150– #055: [1] Light: cross-polarized, quartz eye-shaped xenocrysts in a groundmass of quartz, alkali and plagioclase feldspar with hematite formation. [2 and 3] Light: crossed-polarized, rock fragment (RF) composed of lath-like plagioclase grains and quartz.

Sample ID: LK–150– #058
Zone: Quartz-Feldspar Porphyry, Main Zone North
Depth: 42.10 – 42.24 meters

Sample #058 contains quartz eye-shaped xenocrysts (~0.5 mm in diameter) in a groundmass of quartz (quartz grains < 1mm in diameter). Unlike sample #055, chlorite occurs in irregular patches throughout 90% of groundmass. Chlorite displays weak pleochroism (light green to dark green) in plane-polarized light when the microscope stage is rotated, this is different than colorless chlorite in sample #106. Extinction patterns in quartz eye-shaped xenocrysts are nearly identical to the segmented pattern of white to black, first-order interference colors across the grain in sample #055. Hematite occurs with a fine-grained habit and in irregular patches along fractures. Angular rock fragments are composed of fine-grained quartz and sericite, occurring within the groundmass (1 to 3 mm in diameter) and identical material to those that occur in sample #055. Angular quartz grains (0.10 to 0.20 mm in diameter) accompany larger rock fragments identical to those that occur within sample #055.

Figure 28: Hand sample, ID: LK–150– #058. Rock fragments with a grey groundmass composed of quartz with irregular patches of chlorite.

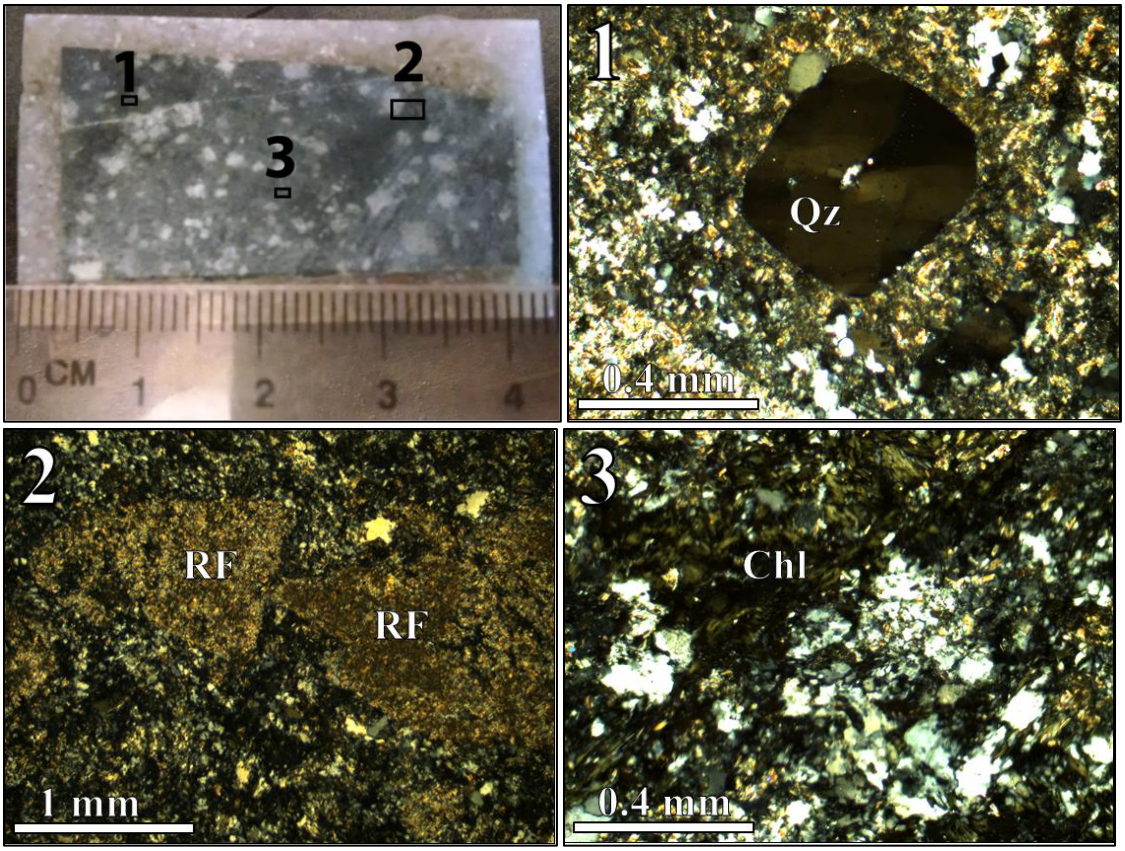

Figure 29: Photomicrographs, sample ID: LK–150– #058: [1] Light: cross-polarized, quartz eye-shaped xenocrysts. [2] Light: cross-polarized, rock fragments (RF). [3] Light: cross-polarized, chlorite patch in groundmass.

Sample ID: LK–150– #085
Zone: Quartz-Feldspar Porphyry, Main Zone South
Depth: 279.09 – 279.19 meters

Sample #085 is un-oxidized, contains quartz eye-shaped xenocrysts and veins of quartz, calcite, and green chlorite (weakly pleochroic similar to sample #058). Extinction patterns in quartz eye-shaped xenocrysts are nearly identical to the segmented pattern of white to black, first-order interference colors across the grain in sample #055 and #058.Plagioclase grains show first-order grey interference color, low relief, and albite twinning (deformed, i.e. offset of albite twining lamellae). These have often been altered to epidote which is identified by high relief, light green to dark green pleochroism, and third-order interference colors. Calcite veins consist of micro-crystalline calcite, highly fractured, exhibiting high-order interference colors in cross-polarized light, and low relief in plane-polarized light. These calcite veins effervesce when tested with hydrochloric acid. The sample reacts with hydrochloric acid without powdering of the sample surface. Quartz veins cross-cut calcite veins and contain the opaque sulfides. Angular quartz grains (0.10 to 0.20 mm in diameter) occur within the groundmass identical to those in samples #055 and #058.

Figure 30: Hand sample, ID: LK–150– #085. Calcite veins react with hydrochloric acid, and differentiated from quartz veins also by hardness. Chlorite tints the sample a pale green color.

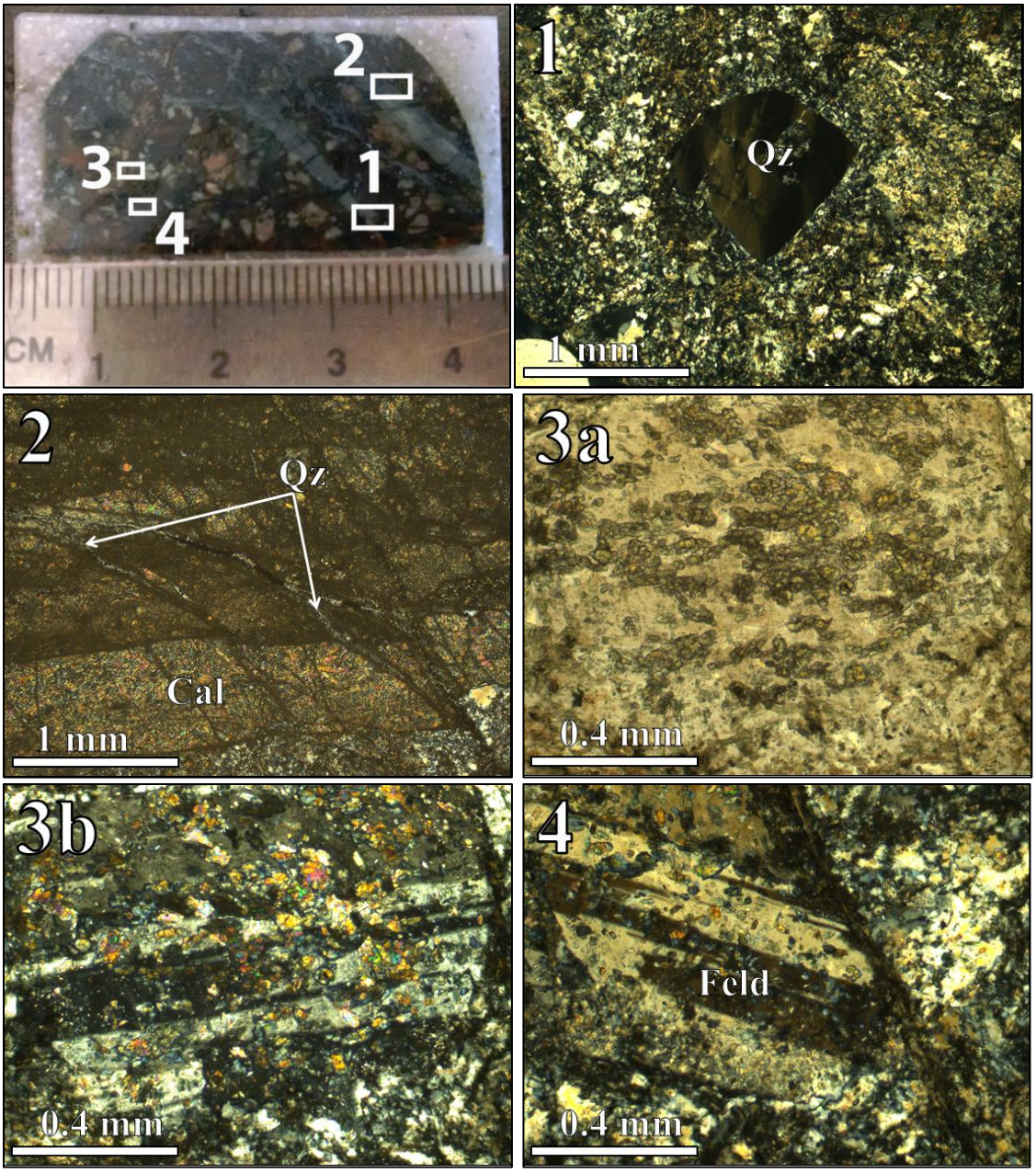

Figure 31: Photomicrographs, sample ID: LK–150– #085. [1] Light: cross-polarized, quartz eye-shaped xenocrysts in a groundmass of quartz and sericite. [2] Light: cross-polarized, calcite veins and cross-cutting quartz veins with sulfides. [3a]: Light: plane-polarized, fine-grained epidote with high relief and light green to dark green weak pleochroism. [3b and 4]: Light: crossed-polarized, third-order pink-yellow-green interference colors of epidote alteration atop first-order white-black plagioclase grains with albite twinning.

Sample ID: LK–451– #087
Zone: Quartz-Feldspar Porphyry, Tuff Zone
Depth: 20.60 – 20.75 meters

Alkali-feldspar and quartz xenocrysts occur within a groundmass of sericite, muscovite, and fine-grained quartz. Plagioclase feldspars are not present (the overall groundmass composition is ~40% quartz, ~56 altered alkali-feldspar, ~2% chlorite, and 2% muscovite). Alkali-feldspar xenocrysts are pink-red in color, highly altered to sericite with high relief in plane-polarized light, and fourth-order pink to green interference colors in cross-polarized light. Alkali feldspar grains are euhedral and they display simple twinning in most grains. Simple twinning is observed in cross-polarized light when two to three zones of the grain go extinct different positions as the microscope stage is rotated. In most cases, the grains contain only two zones and are even in size. Muscovite occurs as fine-grained, subhedral grains low in relief and lacking color in transmitted light. Under cross-polarized light, muscovite has fourth-order interference colors. Quartz xenocrysts are not eye-shaped and display only uniform extinction patterns, different from samples #055, #058, and #085.

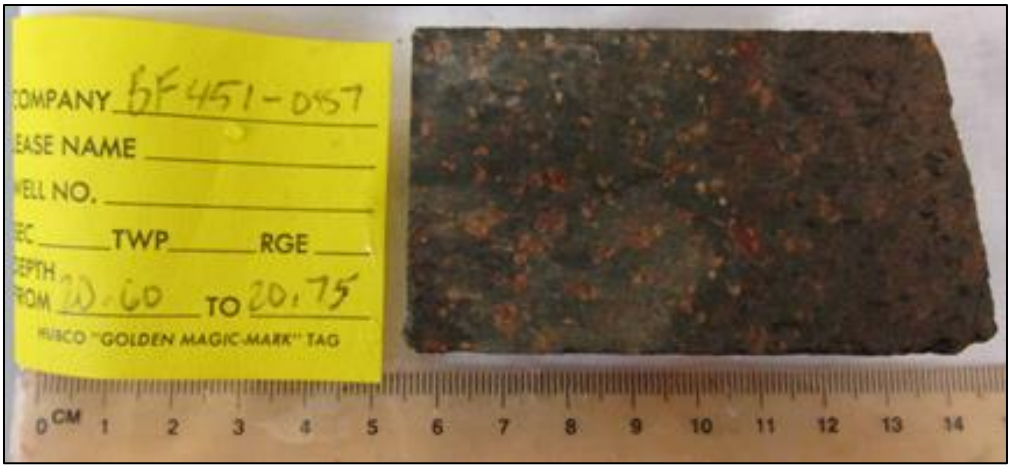

Figure 32: Hand sample, ID: LK–451– #087. Pink alkali-feldspar xenocrysts within a highly altered light grey groundmass

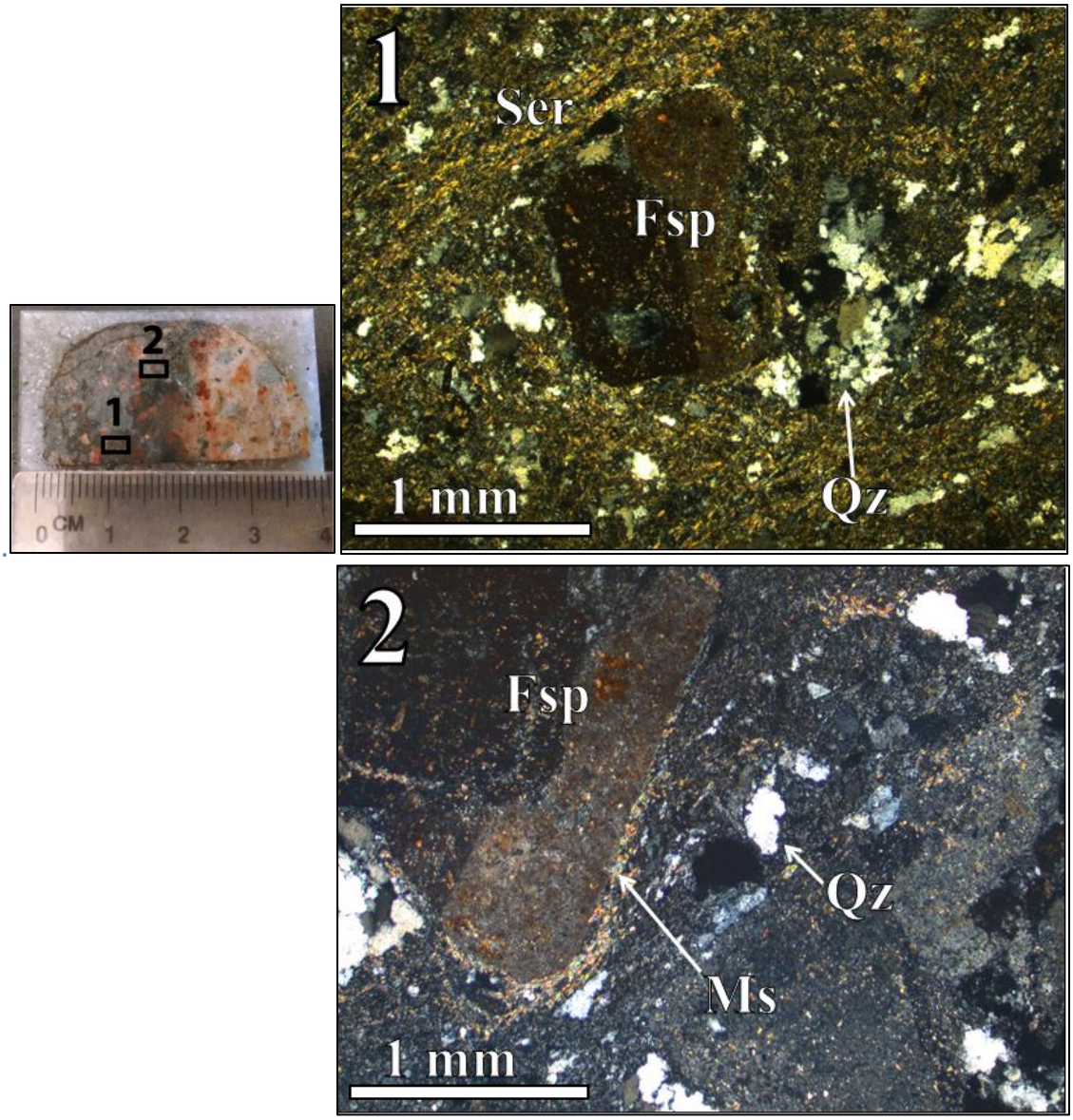

Figure 33: Photomicrographs, sample ID: LK–451– #087: [1] Light: cross-polarized, alkali-feldspar xenocryst, sericite, and quartz. [2] Light: cross-polarized, alkali feldspar exhibiting simple twinning surrounded by muscovite and quartz.

Sample ID: LK–171– #007
Zone: Tuff Sediments, Tuff Zone
Depth: 60.90 – 61.00 meters

Sample #007 is characterized by a groundmass of quartz (~60%), alkali feldspar altered to fine-grained sericite (~39%), and plagioclase feldspar (~1%) distinguished from the rhyolite crystal tuff (samples #029 and #106) by smaller grain sizes of quartz and a lack of quartz eye-shaped xenocrysts. Unlike the Quartz-Feldspar Porphyry samples, rock fragments are not present. Euhedral, platy muscovite grains (0.25 to 0.75 mm in length) occur with large patches of sericite along boundaries with sulfide minerals. In hand specimen, sample #007 has a layered appearance with alternating bands of silicate and sulfide minerals.

Figure 34: Hand sample, ID: LK–171– #007. This sample contains a layered appearance consisting of alternating bands of silicate and sulfide minerals.

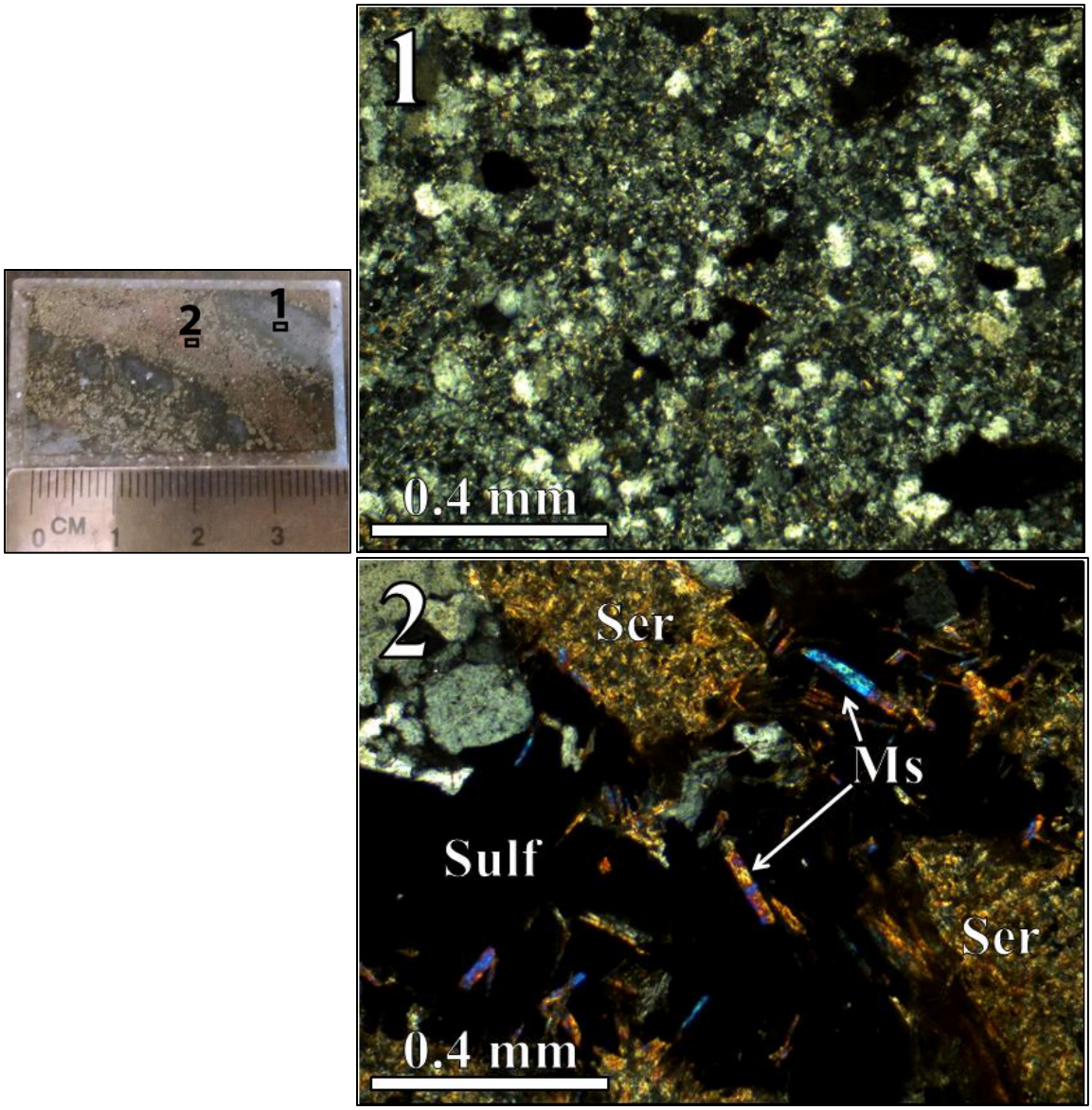

Figure 35: Photomicrographs, sample ID: LK–171– #007: [1] Light: cross-polarized, alkali-feldspar and quartz fine-grained groundmass. [2] Light: cross-polarized, sericite patches and euhedral muscovite grains surrounding opaque sulfides.

Sample ID: LK–451– #092
Zone: Tuff Sediment, Tuff Zone
Depth: 84.94 – 85.03 meters

Sample #092 contains chlorite, sericite, and muscovite within a groundmass of fine-grained quartz (~50%) and alkali-feldspar altered to fine-grained sericite (~50%). Sample #092 is very similar to sample #007, but with exception of sericite occurring in more irregular patches within the groundmass. Bands of chlorite are identified in transmitted light by a moderate relief, green color, and weakly pleochroic from light to dark green. In crossed-polarized light, the chlorite layers exhibit diagnostic anomalous blue interference colors. Muscovite occurs as fine-grained, subhedral grains low in relief and lacking color in transmitted light. Grain boundaries are indistinct due to intergrowth with chlorite. However, under crossed-polarized lighting, muscovite grains can be discerned amongst intergrowth by high-order pastel interference colors. Sulfide minerals are opaque. Alternating and thinly bedded layers of sulfides and alteration minerals (e.g. chlorite, sericite, and muscovite) occur within the groundmass.

Figure 36: Hand sample, ID: LK–451– #092. Thin layers of fine-grained chlorite, muscovite, and sulfides within a groundmass of fine-grained quartz and alkali-feldspar altered to sericite.

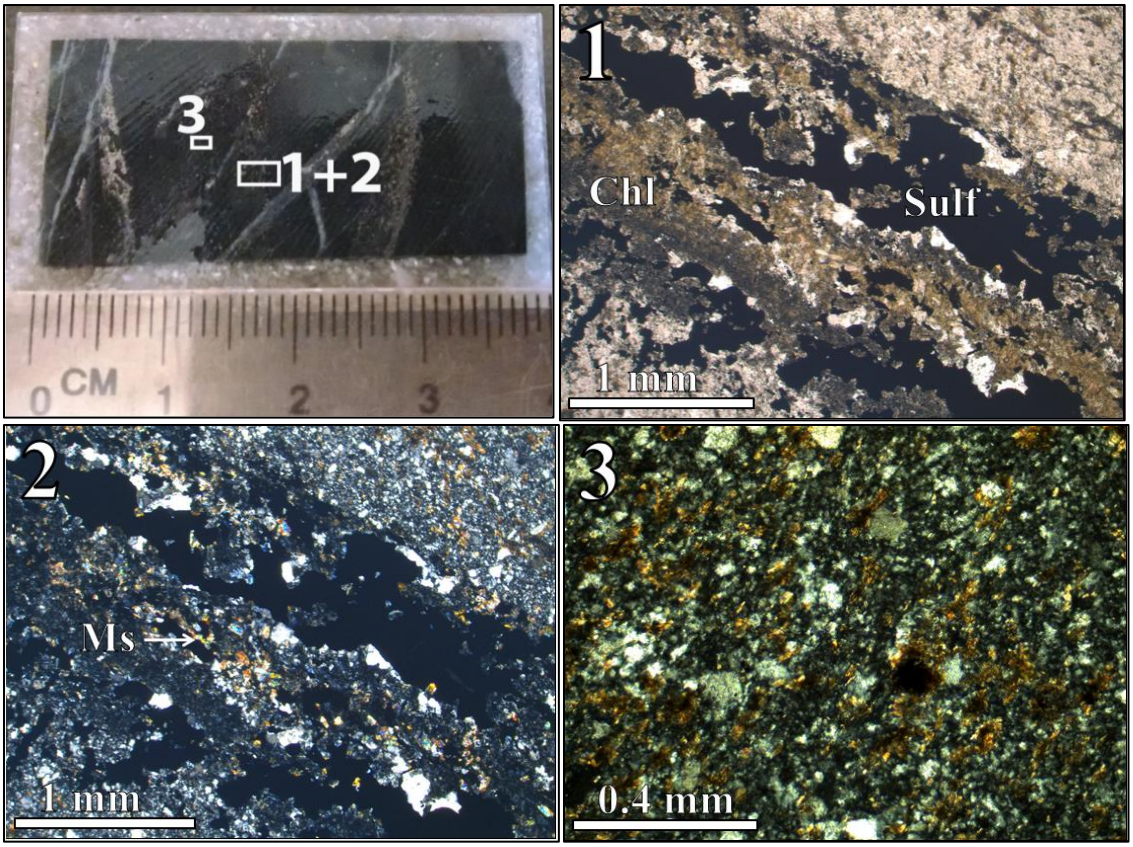

Figure 37: Photomicrographs, sample ID: LK–451– #092: [1] Light: transmitted, bands of anhedral opaque sulfides and green chlorite. [2] Light: cross-polarized, fine-grained muscovite intergrown with chlorite. [3] Light: cross-polarized, quartz and alkali-feldspar altered to sericite.

Sample ID: LK–166– #150
Zone: Tuff Sediment, Tuff Zone
Depth: 16.76 – 16.91 meters

Sample #150 consists of hematite and chert. Chert layers (0.25 to 1 cm thick) consist of microcrystalline quartz, containing fractures bearing hematite, and alternate with hematite layers. Chert is identified by patchy masses of microcrystalline quartz. The chert is low in relief and clear in color when viewed under plane-polarized light. In hand specimen, the chert is a milky-white dull color and is resistant to weathering. When viewed under crossed-polarized light, the chert exhibits first-order grey interference colors.

Figure 38: Hand sample, Sample ID: LK–166– #150.

Sample ID: LK–171– #038
Zone: Deep Zone
Depth: 324.74 – 324.94 meters

Sample #038 consists of a groundmass of quartz (~60%) plagioclase (~35%) and alkali-feldspar (~5%). Sulfide minerals fill multiple sets of fractures, lined by large grained quartz (0.25 to 0.50 mm in diameter) and green chlorite (0.25 to 0.75 mm in width). Chlorite des not display pleochroism. Unlike samples #007 and #092, this sample does not display layers consisting of alternating bands of sulfide, chlorite, quartz, and muscovite. Irregular patches of coarser-grained quartz-alkali feldspar masses occur within the finer-grained quartz-plagioclase feldspar groundmass.

Figure 39: Hand sample, ID: LK–171– #038. Fine-grained quartz and plagioclase groundmass with multiple sets of fracture confined sulfides.

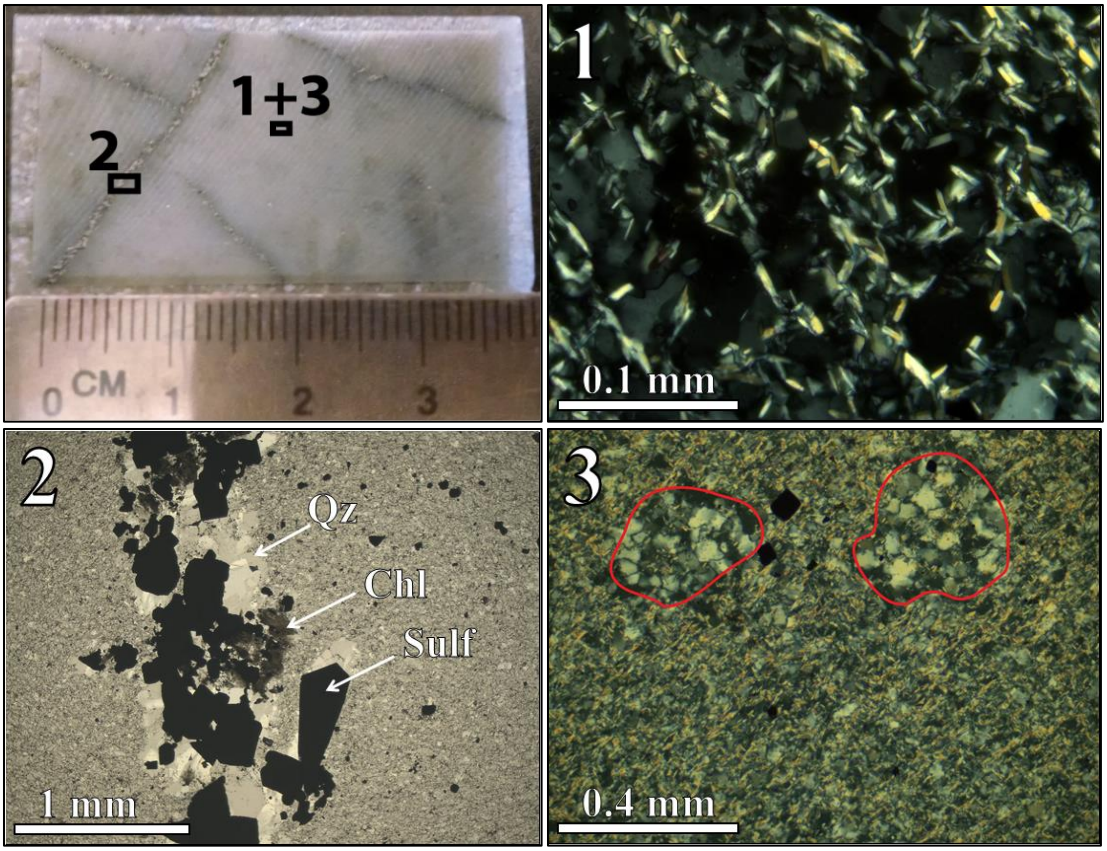

Figure 40 : Photomicrographs, sample ID: LK–171– #038: [1] Light: cross-polarized, quartz and lath-like plagioclase groundmass. [2] Light: cross-polarized, large grained quartz along sulfide boundaries with green chlorite. [3] Light: cross-polarized; coarser-grained quartz-alkali feldspar masses within finer-grained quartz-plagioclase feldspar groundmass.

Sulfide Mineralization

Sulfide mineralization consists of massive, semi-massive, disseminated, stringer textures, and gossan textures. With the exception of gossan samples, these textures are based on volumetric/modal abundances of sulfide minerals based on petrographic estimations. Massive sulfides contain >80% sulfides by volume, semi-massive 40 – 80%, and disseminated < 40%. Stringer textures are identified as distinct veins of sulfides through host rocks, resembling a branching network. Gossan textures are identified by complete oxidation and the presence of botryoidal textures.

Minerals and Properties

Pyrite

Pyrite is identified by having a pale-yellow, semi-brilliant metallic luster in reflected light when viewed under the microscope. Pyrite is opaque in transmitted light. Pyrite often displays a cubic habit. Pyrite and sphalerite are the two most abundant sulfide minerals in the deposit and these have been found within all units of the deposit and occur within all units of the deposit.

Sphalerite

Sphalerite is identified by a semi-opaque, deep red color in transmitted light when viewed under the microscope. In reflected light, sphalerite is a dull-grey sub-metallic luster. In all occurrences, sphalerite displays no distinct or identifiable crystal habit. Sphalerite commonly occurs with pyrite, within all units of the deposit.

Chalcopyrite

Chalcopyrite, like pyrite, is opaque in transmitted light when viewed under the microscope. Chalcopyrite is identified from pyrite by having a diagnostic, brilliant yellow-orange metallic luster in reflected light. Pyrite and chalcopyrite are primarily intergrown with one another in many occurrences. In few instances, chalcopyrite displays a euhedral crystal faces, however uncommon. In many instances, chalcopyrite displays tarnishing to a purple or blue color in small splotches. Chalcopyrite is minor in modal abundance within the deposit, but occurs within all units.

Galena

Galena is present exclusively in the Tuff Zone and occurs in grains larger than all other sulfides (1 – 5 mm in diameter), while minor in overall abundance even within the Tuff Zone. Galena is opaque in transmitted light when viewed under the microscope. In reflected light, galena has a brilliant metallic silver-grey luster. Galena is also the only sulfide to display a cubic cleavage habit. While cleavage is often well developed and easily identified, crystal faces are not present and the grain boundaries have a dissolved appearance to adjacent sulfides. Galena is a mineral exhibiting complex replacement patterns because it is late-crystalizing and affects pre-existing minerals which it often replaces as a result (Augustithis, 1995).

Marcasite

Marcasite is opaque in transmitted light when viewed under the microscope. Marcasite has a metallic golden or tarnished blue to purple luster when viewed in reflected light. The crystal habit of marcasite is the most distinguishing feature, with tabular, oval shaped grains and well-developed cleavage in one-direction. Overall, marcasite is rare in occurrence and it is found only where pyrrhotite is present in massive or semi-massive sulfide zones.

Pyrrhotite

Pyrrhotite is opaque in transmitted light when viewed under the microscope. Pyrrhotite has a metallic golden-brown luster when viewed in reflected light. Pyrrhotite is found only where another mineral is engulfing or replacing pyrrhotite. For this reason pyrrhotite is not seen to display any distinct crystal habit. Pyrrhotite occurrence is rare, and only found in massive or semi-massive sulfide zones.

Arsenopyrite

Arsenopyrite is opaque in transmitted light when viewed under the microscope. Arsenopyrite is distinguished from pyrite by a brilliant pearly-white metallic luster in reflected light. Arsenopyrite occurs as euhedral grains evenly distributed in massive, semi-massive, disseminated, and stringer sulfide-bearing assemblages.

Bornite

Bornite is opaque in transmitted light when viewed under the microscope. Bornite has an iridescent purple-red-green and brilliant metallic luster when viewed in hand-sample, and a purple-red-brown luster when viewed under reflected light with the microscope. Bornite displays no crystal habit and has been identified only in the Deep Zone.

Sample ID: LK–150– #065
Zone: Upper Main Zone North
Depth: 103.29 – 103.49 meters

Sample #065 contains >80% sulfides by volume at the upper portion of the Main Zone and is representative of a massive texture. Pyrite and sphalerite are in nearly equal occurrence (~45% pyrite, ~55% sphalerite) with trace arsenopyrite. Pyrite displays concave grain boundaries in a groundmass of sphalerite. Pyrite and chalcopyrite are intergrown with one another in layered seams. Overall, sulfides lack well-developed crystal edges.

Figure 41: Hand sample, ID: LK–150– #065. Scale: billet face (marked “x”) is 2.7 cm by 4.6 cm. Massive texture, >80% sulfides by volume, with pyrite (brassy color) and sphalerite (black).

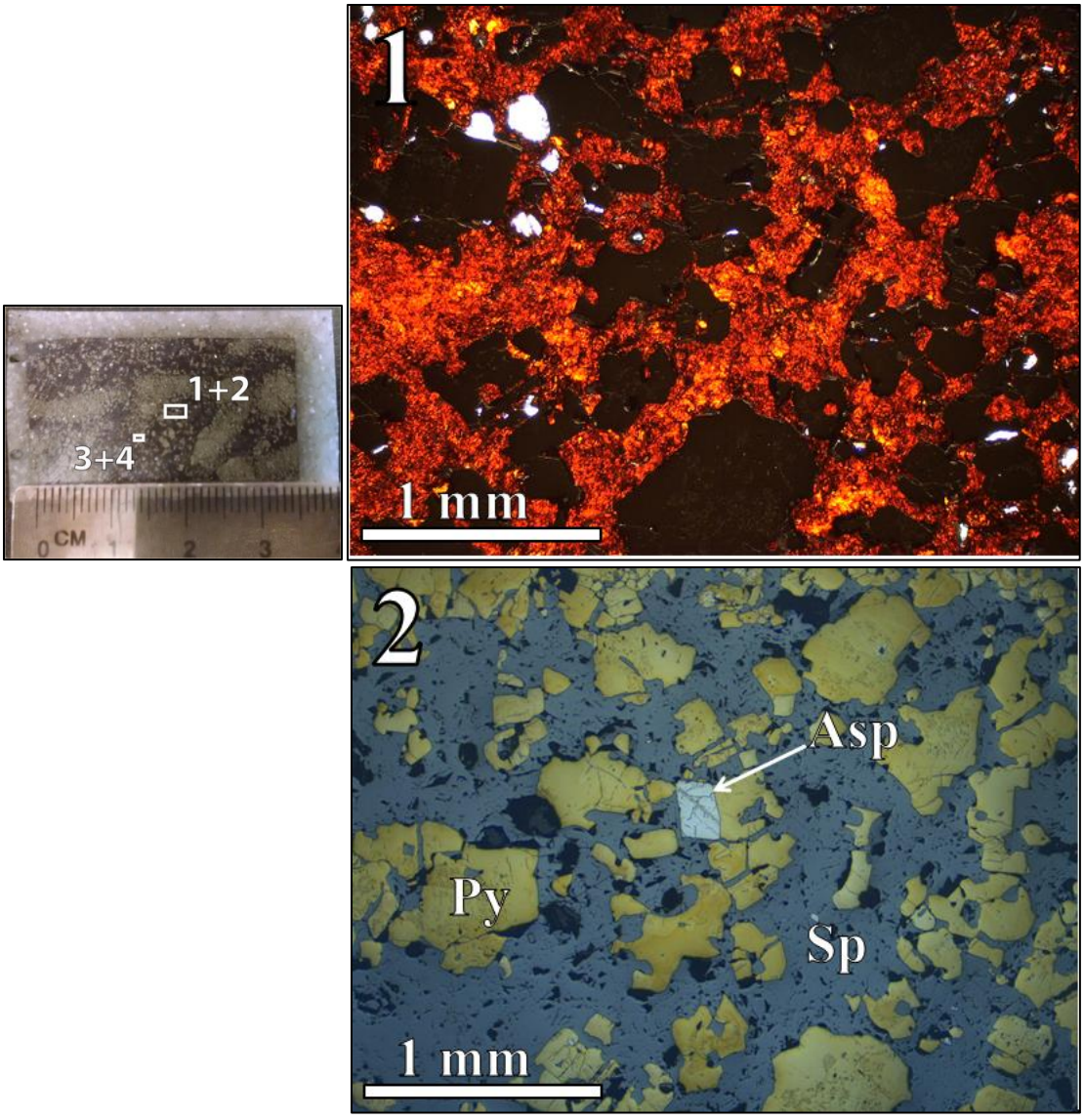

Figure 42: Photomicrographs, sample ID: LK–150– #065 [1] Light: plane-polarized, red sphalerite, black pyrite, and white non-sulfides. [2] Light: reflected, euhedral arsenopyrite, anhedral pyrite in a groundmass of grey sphalerite.

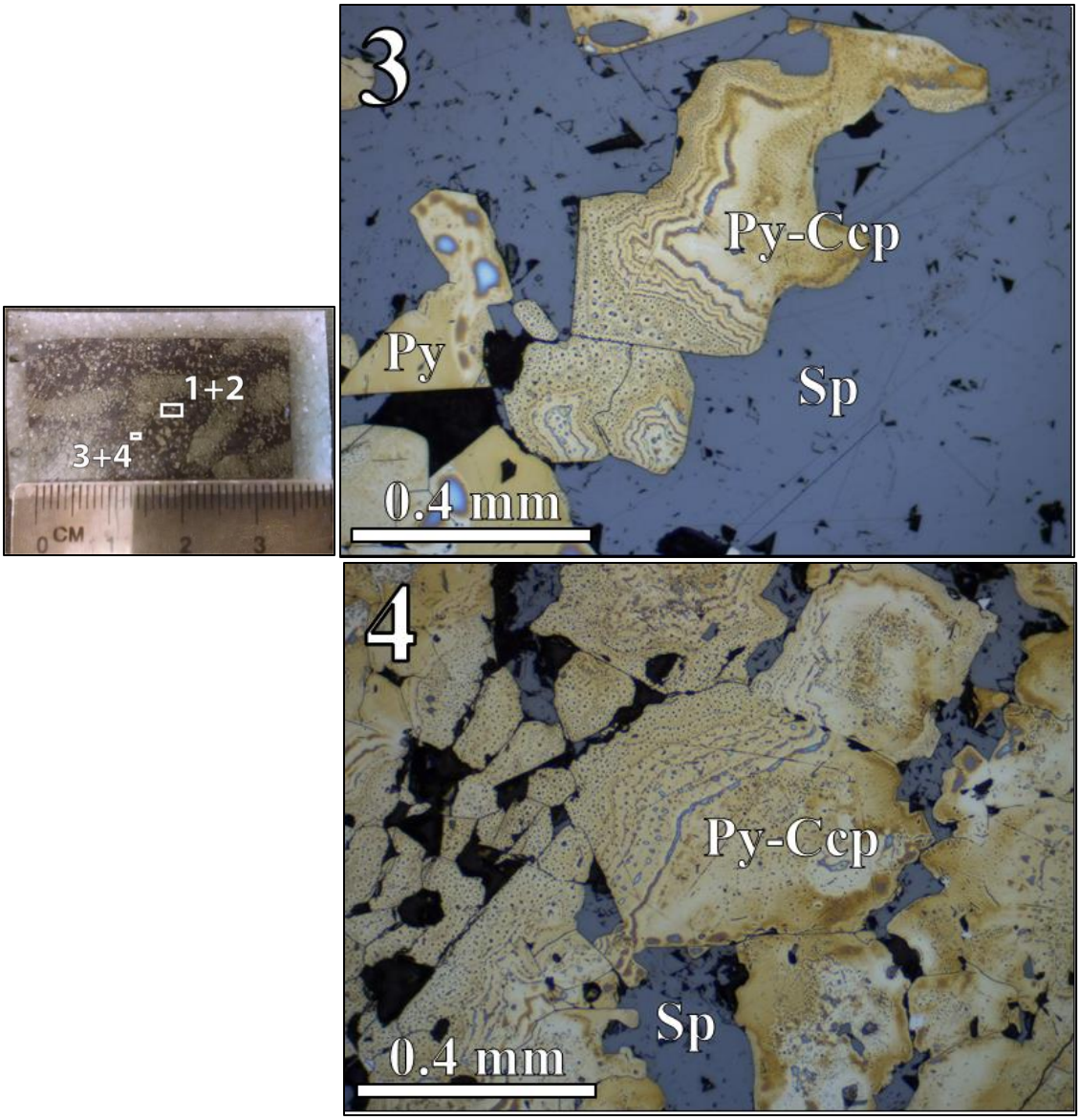

Figure 43: Photomicrographs, sample ID: LK–150– #065. [3 and 4] Light: reflected, pyrite and chalcopyrite intergrowth texture with purple-blue tarnishing.

Sample ID: LK–150– #068
Zone: Lower Main Zone North
Depth: 103.29 – 103.49 meters

Sample #068 contains >80% sulfides by volume at the upper portion of the Main Zone and is representative of a massive texture. Pyrite and sphalerite are in nearly equal occurrence (~50% pyrite, ~50% sphalerite) with trace pyrrhotite and marcasite. Pyrite occurs as euhedral to subhedral crystals in a groundmass of sphalerite. Pyrite and chalcopyrite are intergrown with one another in layered seams and tarnished similar to sample #065. Sphalerite and pyrite occur in respectively dominated horizons giving the sample a layered appearance. Chalcopyrite and sphalerite occur as interstitial grains to pyrite. Interstitial is a texture where mineral grains occur between two or more adjacent larger mineral crystal surfaces. Pyrrhotite occurs completely engulfed by marcasite. Overall, sulfides lack well-developed crystal edge.

Figure 44: Hand sample, ID: LK–150– #068. Layered appearance given by brassy-yellow pyrite and black sphalerite in a massive texture.

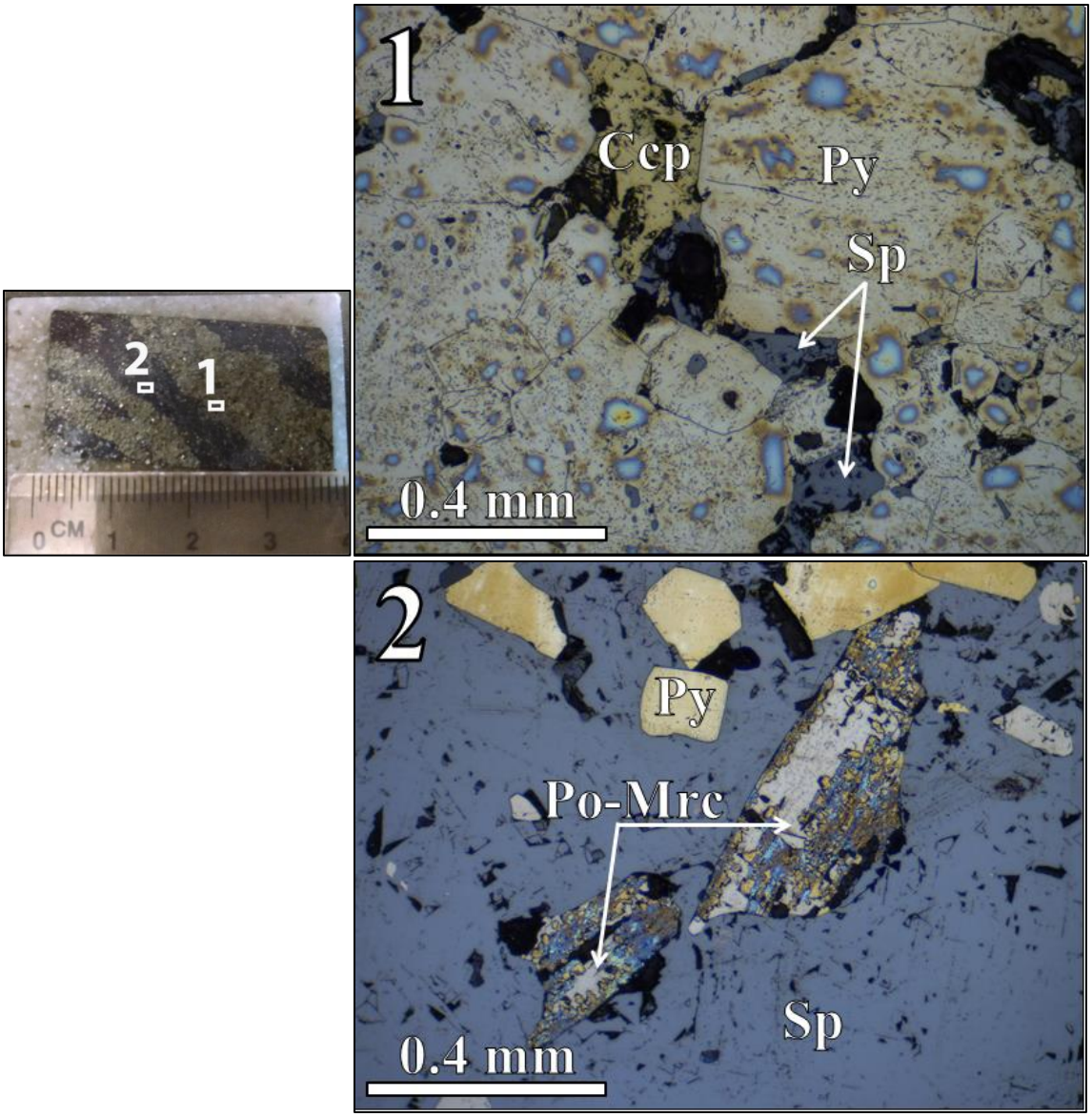

Figure 45: Photomicrographs, sample ID: LK–150– #068: [1] Light: reflected, interstitial chalcopyrite and sphalerite in tarnished pyrite. [2] Light: reflected, pyrrhotite replaced/engulfed by marcasite in a groundmass of sphalerite and adjacent euhedral pyrite.

Sample ID: LK–171– #016
Zone: Main Zone South
Depth: 163.45 – 163.52 meters

Sample #016 contains >80% sulfides by volume at the Main Zone and is representative of a massive texture. Pyrite comprises more than 95% of the sulfides present, with trace interstitial sphalerite, and trace chlorite occurring within quartz veins. Sulfide minerals occur as anhedral crystals.

Figure 46: Hand sample, ID: LK–171– #016. Brassy-yellow pyrite, quartz veins with chlorite, and trace interstitial, red-brown sphalerite in a sample of massive sulfide.

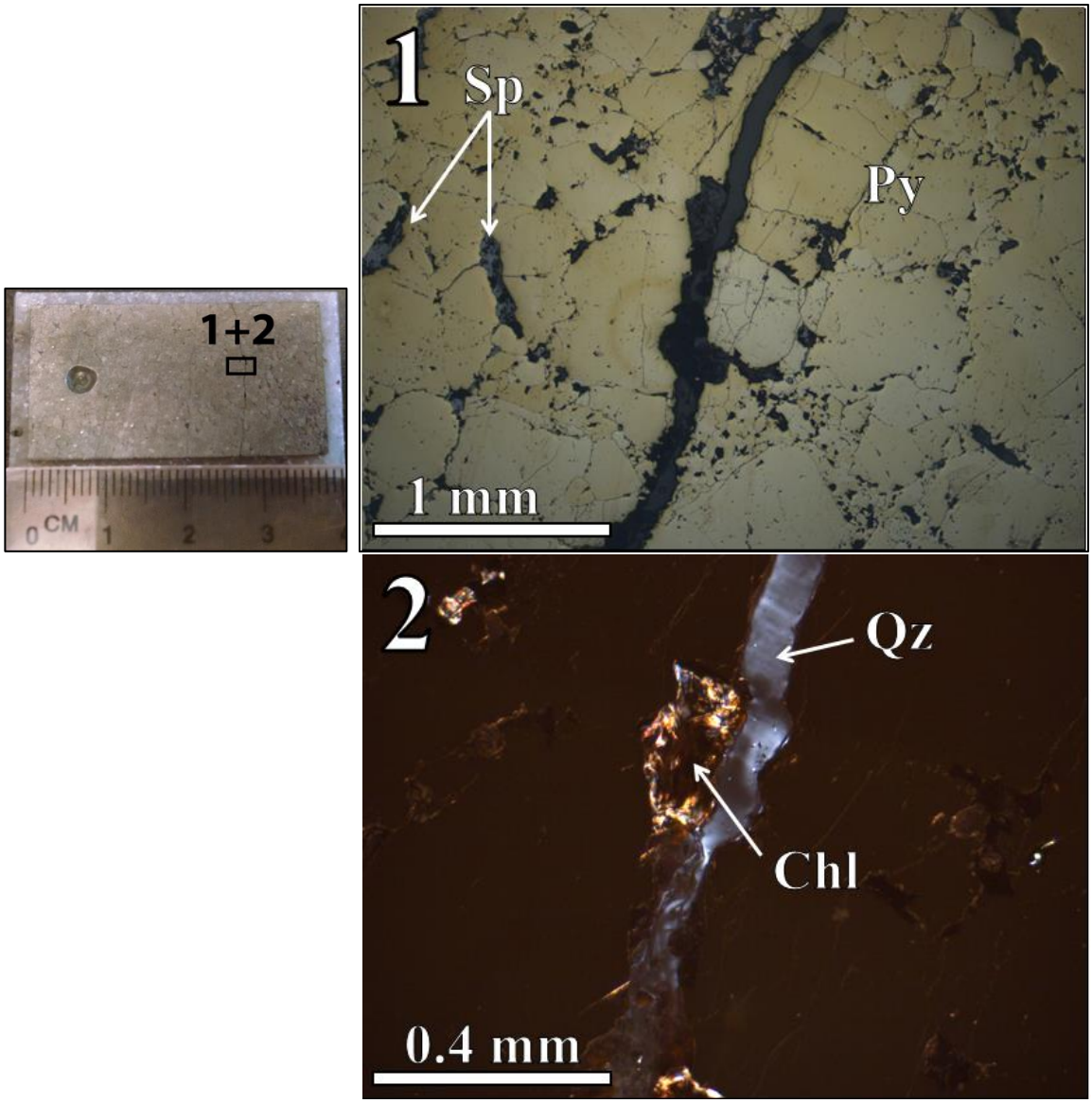

Figure 47: Photomicrographs, sample ID: LK–171– #016: [1] Light: reflected pyrite and interstitial sphalerite. [2] Light: cross-polarized, chlorite in quartz vein.

Sample ID: LK–171– #035
Zone: Deep Zone
Depth: 308.37 – 308.47 meters

Sample #035 contains >80% sulfides by volume in the Deep Zone and is representative of a massive texture. Pyrite comprises the majority of sulfides with trace interstitial sphalerite, chalcopyrite and bornite. Pyrite and chalcopyrite are intergrown with one another in layered seams and tarnished similar to samples #065 and #068. Sulfide mineral grains are anhedral. Muscovite occurs as euhedral, interstitial plate-like grains 0.3 to 0.8 mm in length.

Figure 48: Hand sample, ID: LK–171– #035. Massive texture in the deep zone is composed mostly of brassy-yellow pyrite, with interstitial sphalerite and trace chalcopyrite and bornite.

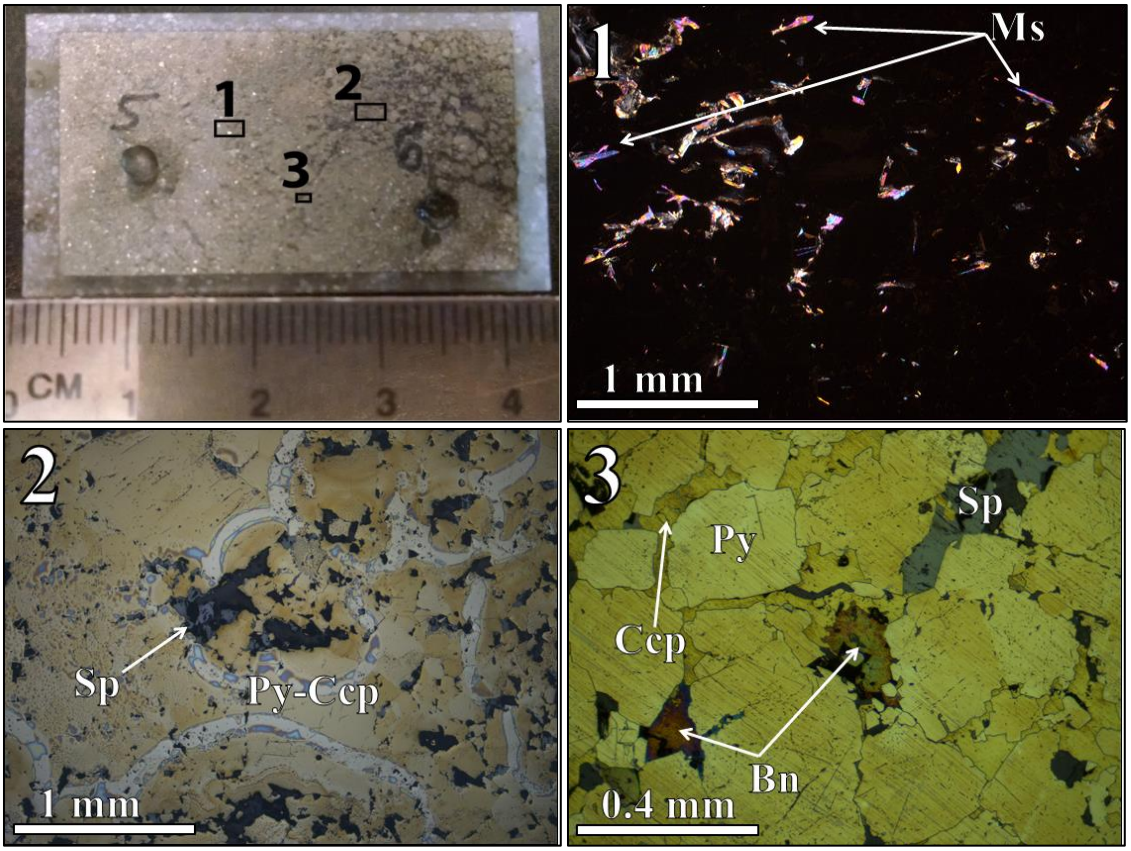

Figure 49: Photomicrographs, sample ID: LK–171– #035: [1] Light: crossed-polarized, euhedral muscovite with high-order inference colors. [2] Light: reflected, pyrite and chalcopyrite intergrowth with tarnishing and interstitial sphalerite. [3] Light: reflected, large grains of pyrite and interstitial sphalerite, chalcopyrite, and bornite.

Sample ID: LK–451– #103
Zone: Tuff Zone
Depth: 165.80 – 165.96 meters

Sample #103 contains >80% sulfides by volume at the Tuff Zone and is representative of a massive texture. Galena occurs as large grains compared to all other sulfides (3 – 5 mm in diameter), with well-developed cubic cleavage, and engulfing other adjacent minerals with a dissolved appearance to grain boundaries. Marcasite, sphalerite, and chalcopyrite occur ingrown with each other and galena. Pyrite occurs as relatively euhedral grains, with well-developed crystal edges. Overall, sulfides lack well-developed crystal edges.

Figure 50: Hand sample, ID: LK–451– #103. Galena occurs as much larger grains compared to other sulfides with a brilliant metallic silver-grey luster.

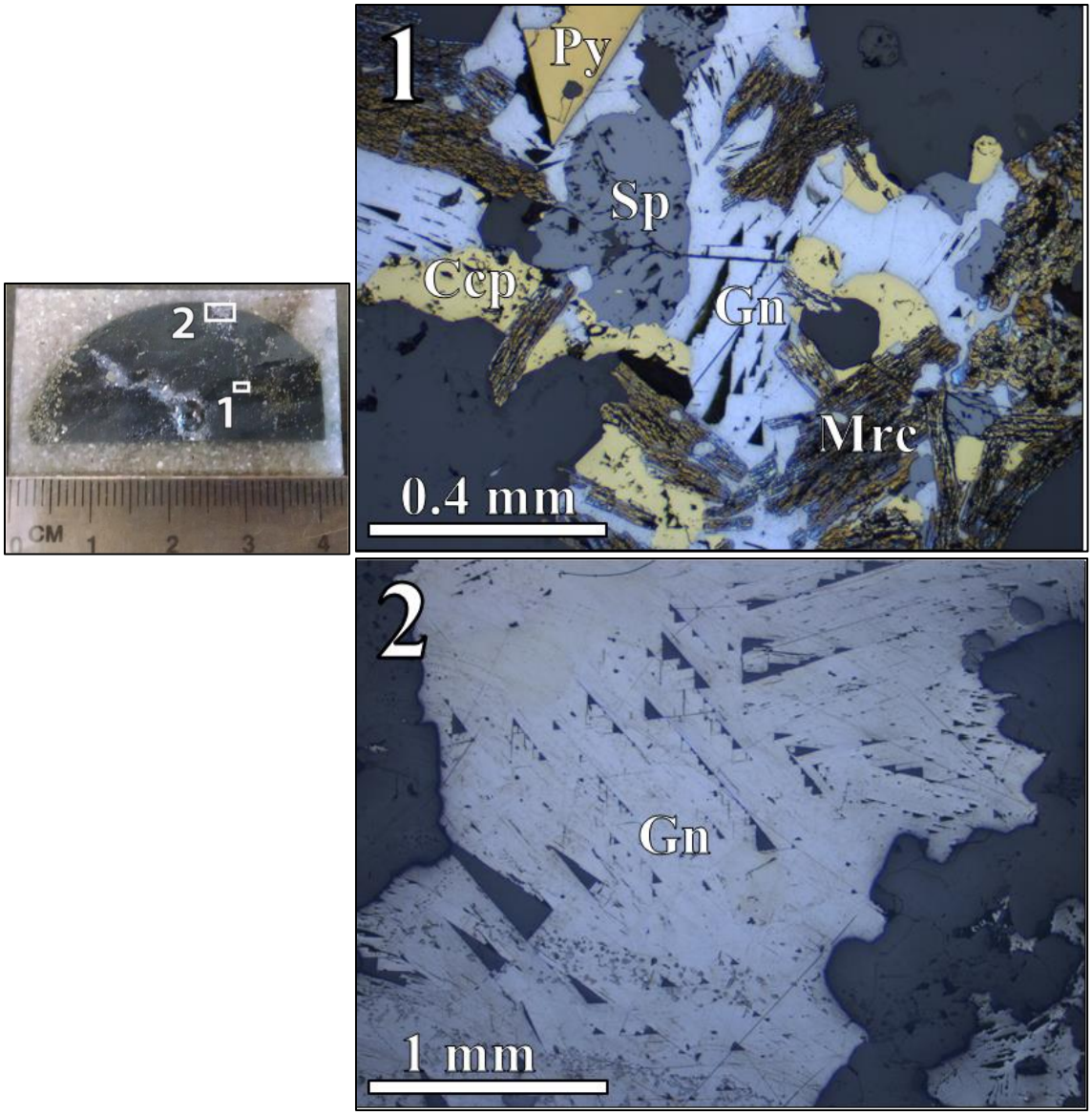

Figure 51: Photomicrographs, sample ID: LK–451– #103B: [1 and 2] Light: reflected, sphalerite, chalcopyrite, marcasite, and galena intergrown with one another while pyrite occurs as euhedral grains with no intergrowth texture to other sulfides.

Sample ID: LK–127– #045
Zone: Pinwheel Zone
Depth: 8.78 – 8.85 meters

Sample #103 contains >80% sulfides by volume in the Pinwheel Zone and is representative of a massive texture. Anhydrite occurs in small cracks (< 3 mm in width), displaying diagnostic twinning and fourth-order interference colors. This twinning is representative of well-developed cleavage in anhydrite. Native copper can is seen in hand-sample as fine-grained, oxidized masses with a diagnostic pale-green patina, or weathered surface. Chalcopyrite and pyrite occur as intergrowths in two forms: intergrowth texture identified by a three-dimensional repetitive structure, or as vein-like structures of chalcopyrite within tarnished pyrite. A dissolved appearance to grain boundaries is present along void spaces in the sample. Overall, sulfides lack well-developed crystal edges.

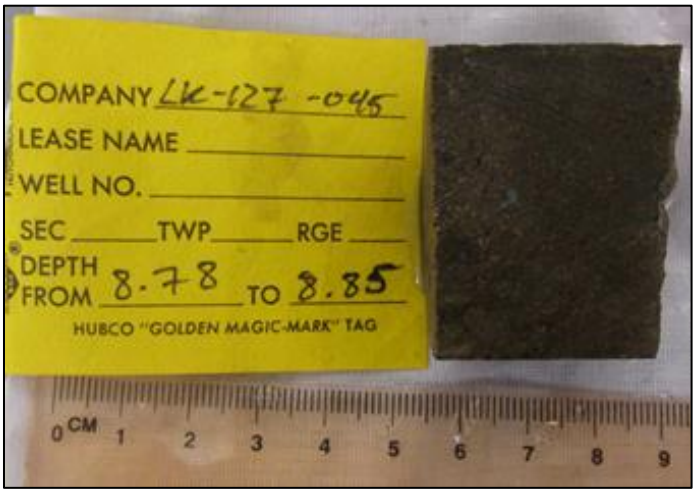

Figure 52: Hand sample, ID: LK–127– #045. Massive texture composed of pyrite and chalcopyrite with small cracks and void spaces (1 – 3 mm wide). Native copper occurs as pale-green fine-grained masses.

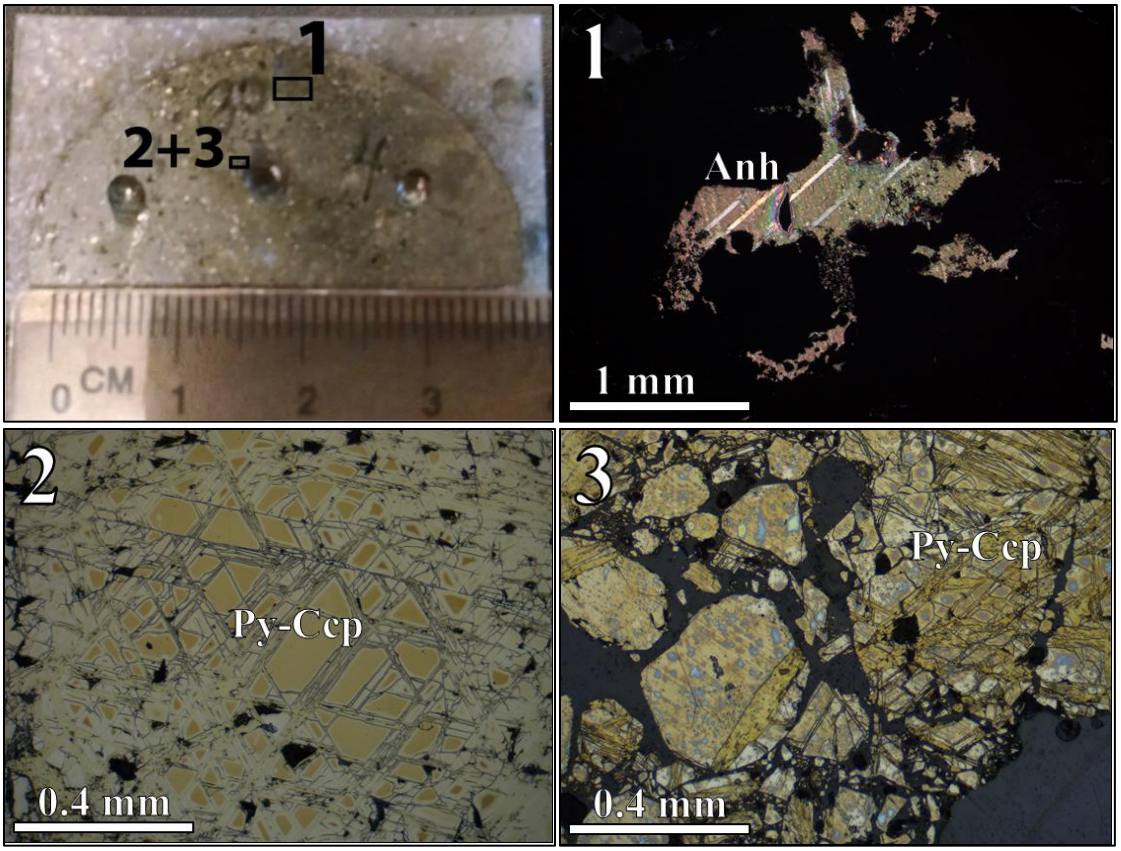

Figure 53: Photomicrograph, sample ID: LK–127– #045: [1] Light: crossed-polarized transmitted, anhydrite filling void space. [2] Light: reflected, three-dimensional repetitive structure of pyrite intergrown with chalcopyrite. [3] Light: reflected, vein-type intergrowth of chalcopyrite in tarnished pyrite.

Sample ID: LK–150– #069
Zone: Lower Main Zone North
Depth: 161.84 – 161.99 meters

Sample #069 contains approximately 50% sulfide by volume and is representative of semi-massive (40 – 80 % sulfides by volume) at the lower portion of the Main Zone. Pyrite and sphalerite are in sub-equal abundance, with approximately 2:1 ratio of pyrite to sphalerite. Pyrite occurs as euhedral grains. Sericite occurs as fine-grained patchy patches with euhedral muscovite (0.3 to 0.6 mm in length) interstitial or surrounding sulfides. Quartz grains are much larger along sulfide boundaries than host rhyolite grain size, as seen along stringer sulfide in samples #023, #029, #060, and #106. Overall, sulfide mineral grains are subhedral to euhedral.

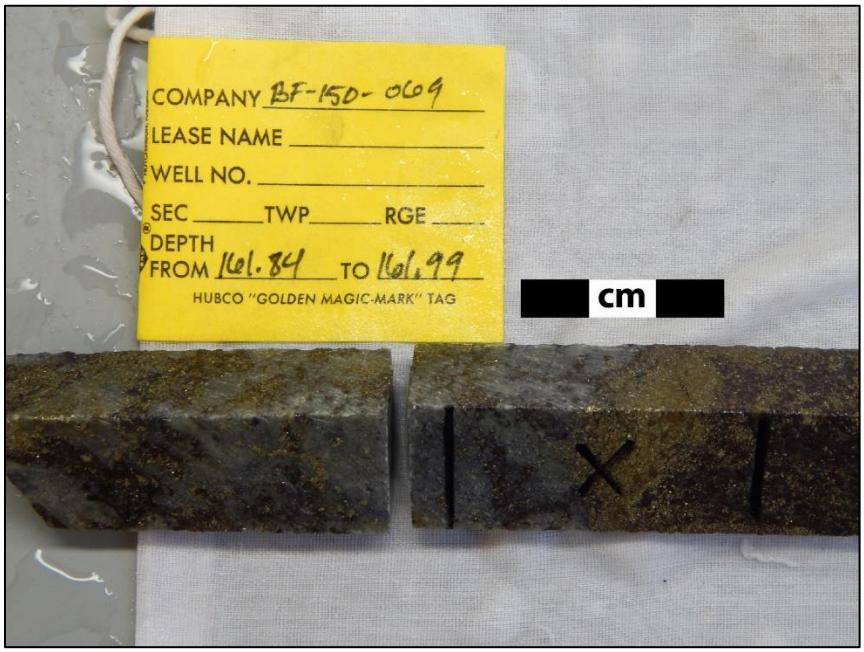

Figure 54: Hand sample, ID: LK–150– #069. Semi-massive texture at the lower contact of the Main Zone massive sulfide with rhyolite 1 crystal tuff. Brassy-yellow pyrite approximate 2:1 ratio to red-brown sphalerite.

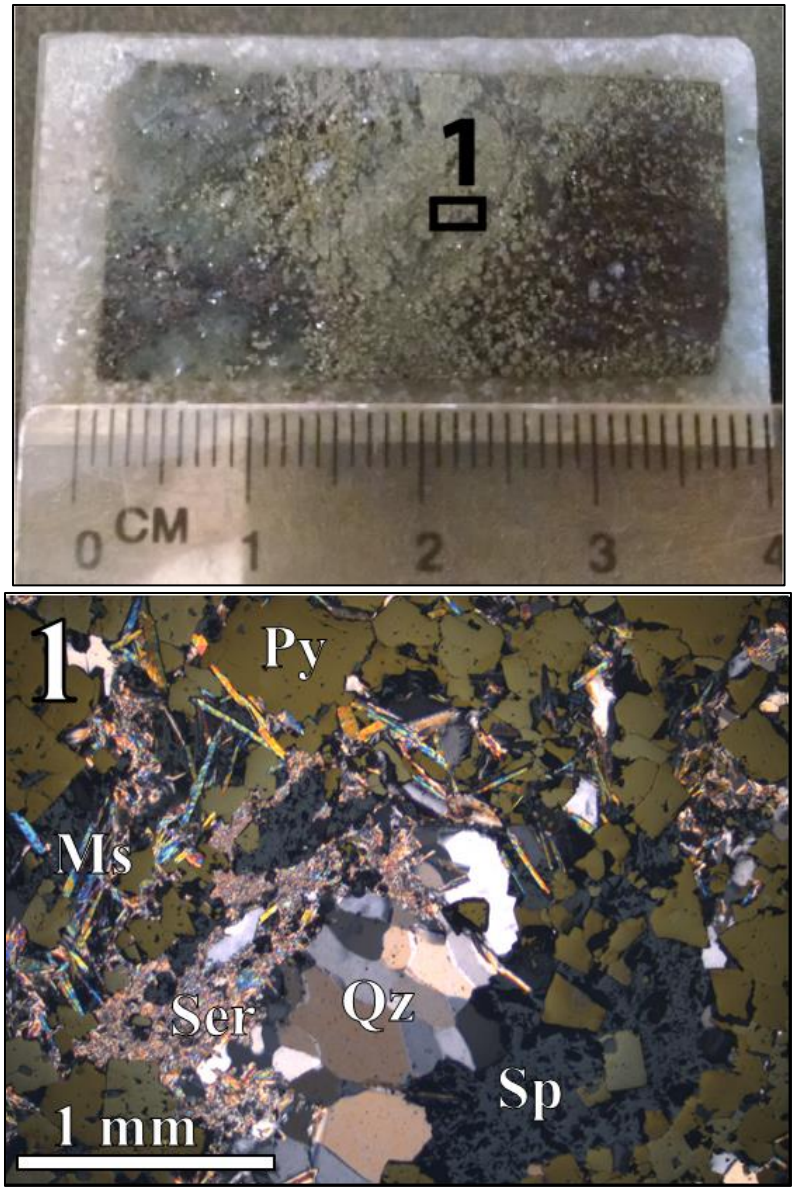

Figure 55: Photomicrographs, sample ID: LK–150– #069: [1] Light: reflected with cross-polarize, quartz, euhedral pyrite, sphalerite, and euhedral platy muscovite.

Sample ID: LK–150– #070
Zone: Lower Main Zone North
Depth: 164.83 – 164.98 meters

Sample #070 was taken approximately 3 meters below sample #069 and contains approximately 35% sulfide by volume, and is representative of a disseminated texture (< 40 % sulfides by volume) at the lower portion of the Main Zone. Pyrite and sphalerite are in relatively equal proportions. Sericite occurs as patchy patches with euhedral muscovite of subhedral. Where occurring, marcasite is found replacing and entirely engulfing pyrrhotite. Quartz grains are much larger along sulfide boundaries than host rhyolite grain size similar to #023, #029, #060, #069, and #106. Overall, sulfide minerals display clear crystal edges.

Figure 56: Hand sample, ID: LK–150– #070. Semi-massive texture at the lower contact of the Main Zone massive sulfide with rhyolite 1 crystal tuff. Brassy-yellow pyrite and red-brown sphalerite.

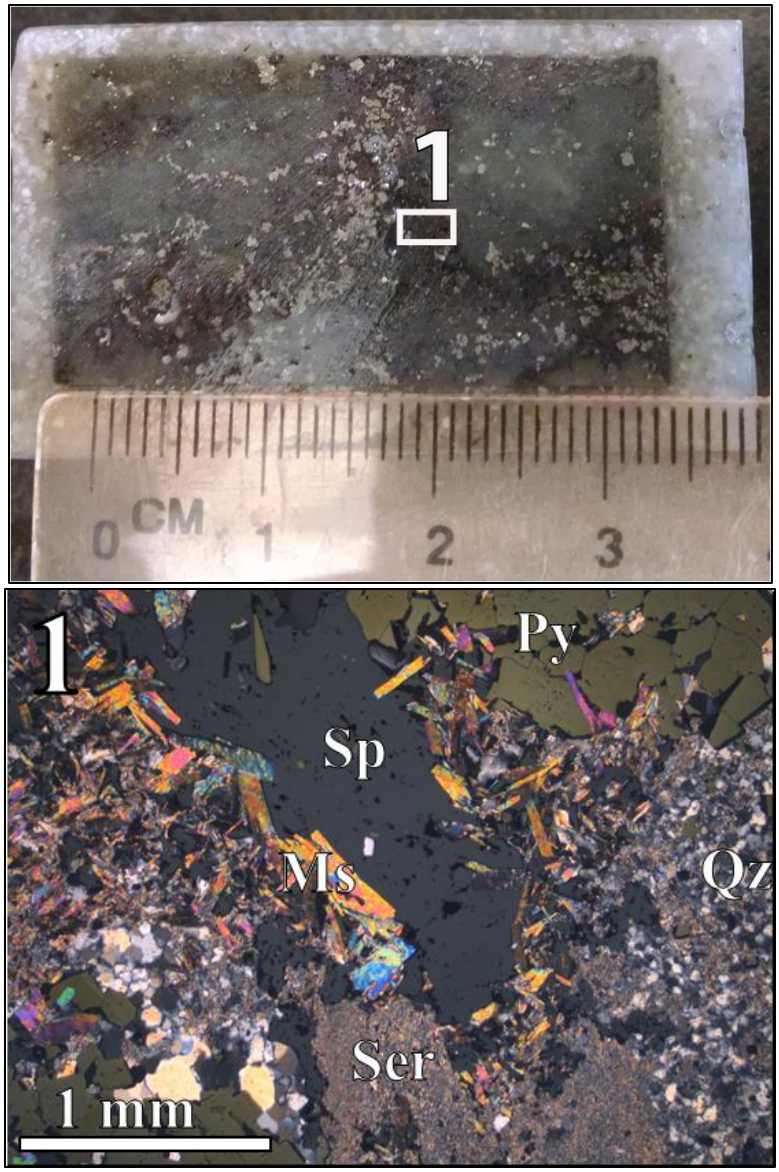

Figure 57: Photomicrographs, sample ID: LK–150– #070. [1] Light: reflected with cross-polarize, quartz, euhedral pyrite, sphalerite, and euhedral platy muscovite.

Sample ID: LK–171– #009
Zone: Tuff Zone
Depth: 83.72 – 83.92 meters

Sample #009 contains approximately 80% sulfide by volume and is representative of a massive texture (40 – 80 % sulfides by volume) at the Tuff Zone. Pyrite and sphalerite are in relatively unequal proportions, with pyrite dominated horizons (left end of the sample, figure below) grading into sphalerite dominated horizons (right end of sample). Sericite occurs as patchy patches with euhedral muscovite interstitial to sulfides. Overall, sulfides lack well-developed crystal edges.

Figure 58: Hand sample, ID: LK–171– #009. Left end of sample is pyrite-rich with the right end of the sample sphalerite-rich, total sulfide volume is approximately 70%.

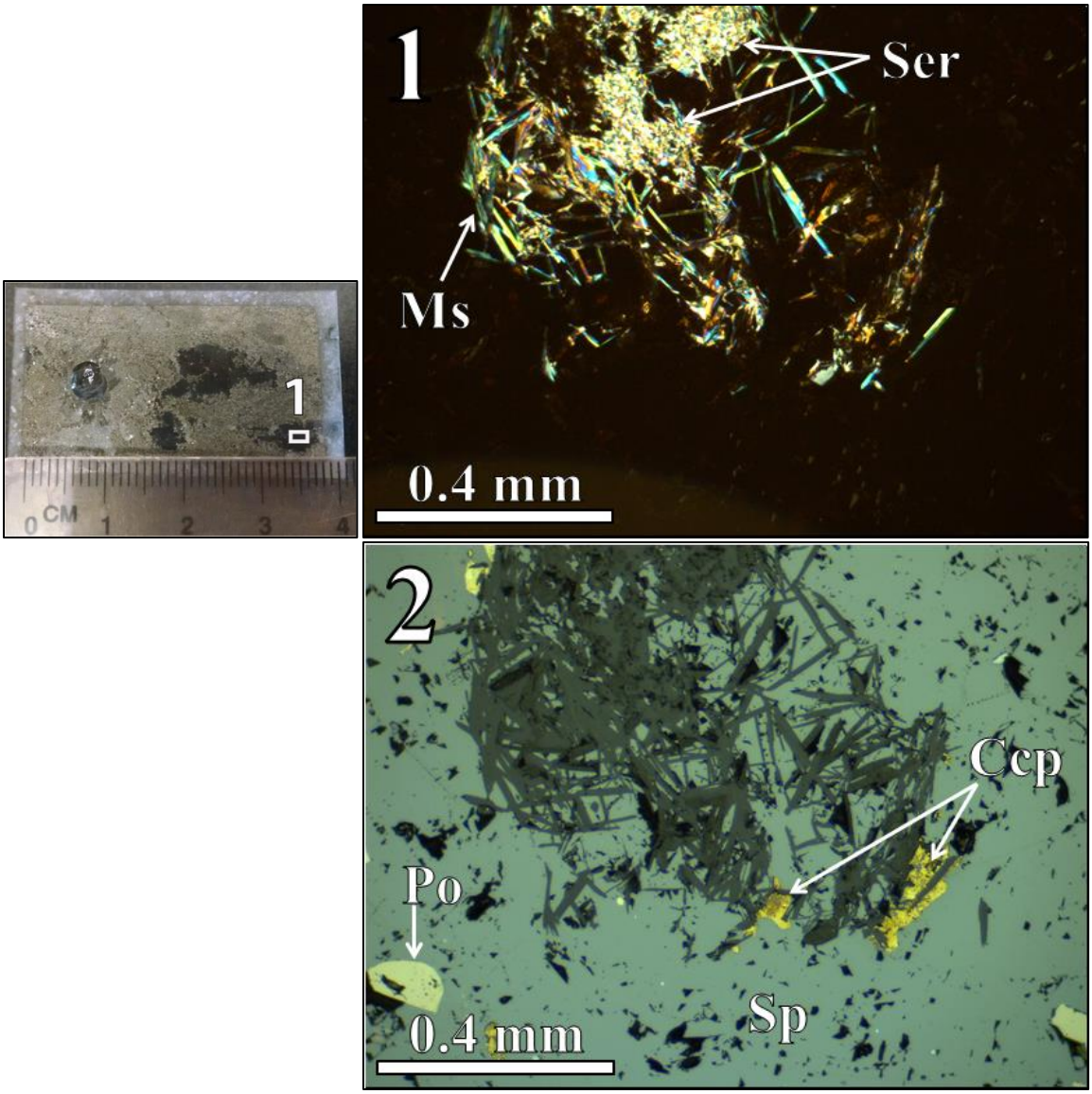

Figure 59: Photomicrograph, sample ID: LK–171– #009B; Zone: [1] Light: cross-polarized, euhedral muscovite and patchy fine-grained masses of sericite. [2] Light: reflected, sphalerite, chalcopyrite, and pyrrhotite.

Sample ID: LK–127– #043
Zone: Pinwheel Zone
Depth: 6.59 – 6.69 meters

Sample #043 contains little to no sulfide, and is completely oxidized with a botryoidal texture and represents the gossan texture. Hematite occurs as a minor constitute to the iron-oxide composition that is predominantly made of botryoidal goethite. The botryoidal habit of goethite has the appearance of a grape-like or bubble-shaped layered surface. These layers are rimmed by chlorite and silver. The space between the layers is filled completely with dolomite. The dolomite is identified by a positive reaction to hydrochloric acid only when the surface is powdered, diagnostic of dolomite.

Figure 60: Hand sample, ID: LK–127– #043. Brown-red botryoidal goethite with space filling dolomite can be observed in hand-sample. Amongst the layers of botryoidal goethite is silver, with a metallic light-grey luster.

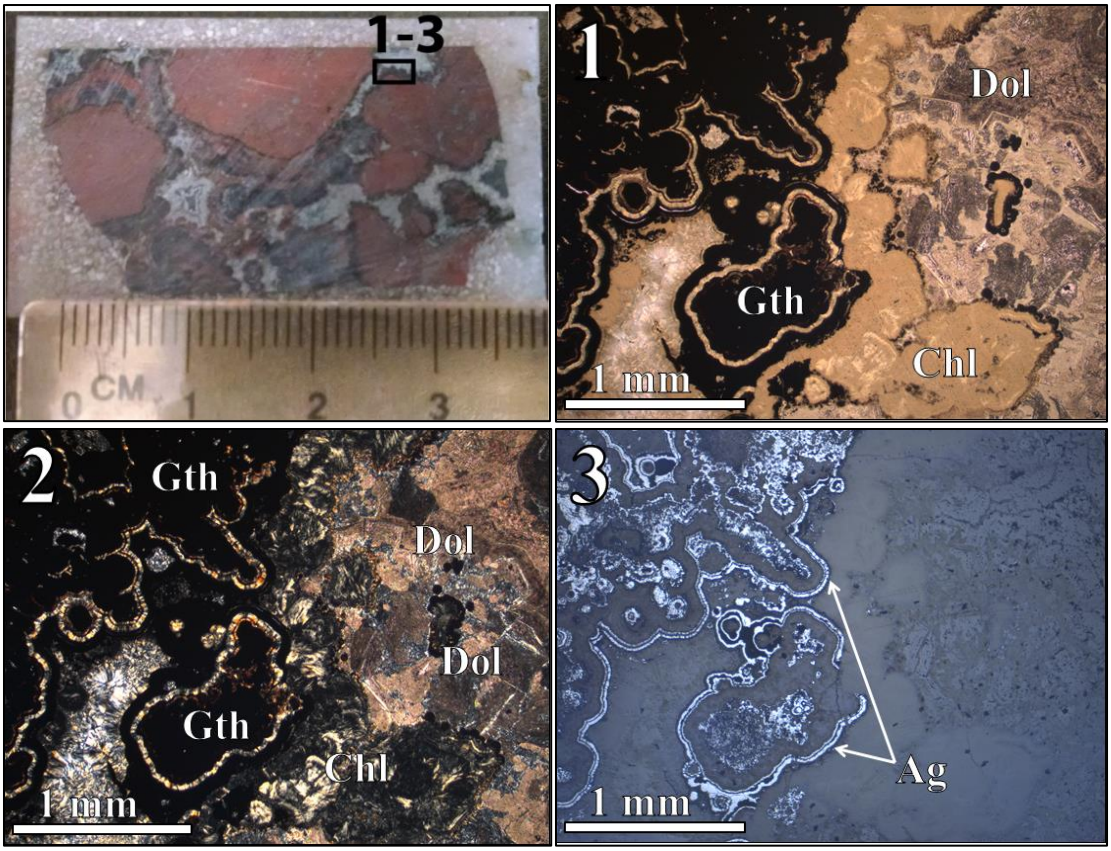

Figure 61: Photomicrographs, sample ID: LK–127– #043: [1] Light: transmitted, botryoidal goethite, chlorite, and zoned dolomite. [2] Light: cross-polarized, botryoidal goethite, chlorite, and zoned dolomite. [3] Light: reflected, silver (Ag) rimming the botryoidal goethite.

RESULTS, PART B:

GEOCHEMISTRY

Host Rocks

A small geochemical data set for the three rhyolites was provided by Aquila Resources for this study. This data has been used by this study for the purpose of identifying trace element concentrations of Zirconium (Zr) and Yttrium (Y) in these rhyolites in order to classify these rhyolites within a formal classification scheme for VMS hosting rhyolitic volcanic rock, developed by Lescher et al. (1983) and Barrie et al. (1993). The average Zr:Y ratio for 48 Rhyolite 1 data points is 6.96 with a standard deviation of ±1.60. The average Zr:Y for 82 Rhyolite 2 samples is 4.47 with a standard deviation of ±1.09. The average Zr:Y for 11Rhyolite 3 samples is 6.671 with a standard deviation of ±0.56. Under the classification scheme of Lescher et al. (1983) and Barrie et al. (1993), Rhyolite 1 data points cluster within the FII-type field and Rhyolite 3 within the FIIIa-type field, while Rhyolite 2 data points do not cluster within any field of the classification scheme (Figure 62).

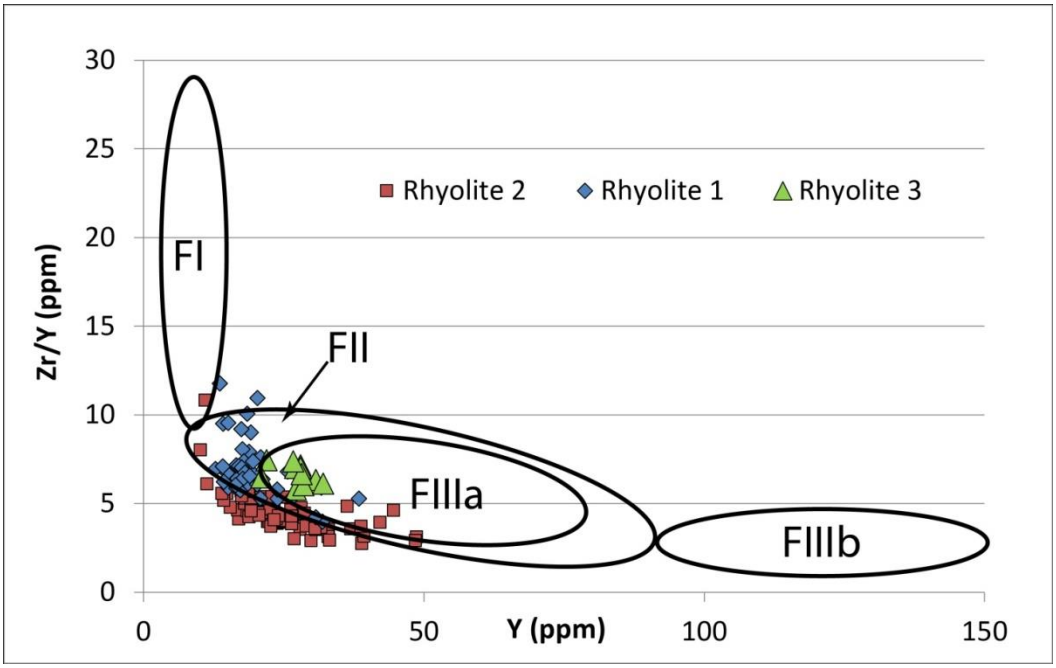

Figure 62: Rhyolite 1 data points for Zr/Y versus Y cluster within the FII-type field and Rhyolite 3 within the FIIIa-type field, Rhyolite 2 data points for Zr/Y versus Y do not cluster within any field in the classification scheme (after Lescher et al. 1983, and Barrie et al. 1993).

Mineralization

Sulfur isotope ($\delta^{34}S$) values obtained from twenty-seven sulfide minerals from the five major zones of sulfide mineralization in the Back Forty range from 0.76 to 5.06‰-VCDT, with an average of 3.07 ±1.08 (1 σ) (Table 5 and 6). Sulfur isotope measurements were carried out in two separate trials. Measured values (i.e. raw data) from samples and four internal lab standards (each owing to known values, relative to VCDT) were corrected to obtain values relative to VCDT by using a method consistent with the multiple-point linear normalization. The multiple-point linear normalization method produces negligible error (typically ≤ 0.01‰), superior to other methods, such as the single-point method, as described by a review of normalization methods of stable isotopic compositions by Paul et al., 2007.

Using this method, determining the calibration curve to compute the true (i.e. corrected) values of samples form a measured value yielded a correlation coefficient (R^2) greater than 0.9993 for both trials. The linear equations from the calibration curves were used to obtain the values relative to VCDT for the samples (Figure 63 and 64). In each equation, the measured value for each sample is represented as "y." Solving for "x," the corrected value was then obtained. Values for individual sulfides were plotted as a frequency histogram to present the distribution of sulfur isotope values between individual sulfides (Figure 65, Table 7).

Table 6: Batch 1.

Identifier	Mineral	Weight (mg)	Raw $\delta^{34}S‰$	$\delta^{34}S‰$-VCDT	Average Raw Value	True Value
EMR	Standard	0.17	-2.67	-0.11	-1.678	0.9
EMR	Standard	0.146	-1.392	1.18	^	^
EMR	Standard	0.166	-1.151	1.42	^	^
EMR	Standard	0.146	-1.499	1.07	^	^
ERE	Standard	0.452	-7.42	-4.90	-6.673	-4.7
ERE	Standard	0.397	-6.766	-4.24	^	^
ERE	Standard	0.444	-6.606	-4.08	^	^
ERE	Standard	0.432	-6.646	-4.12	^	^
PQM2	Standard	0.118	-17.587	-15.15	-17.585	-14.7
PQM2	Standard	0.114	-17.583	-15.15	^	^
PQB-D	Standard	0.426	37.113	40.00	37.508	40.5
PQB-D	Standard	0.404	37.902	40.80	^	^
171-039	Ccp	0.173	1.642	4.24	-	-
150-067	Sp	0.164	-0.744	1.83	-	-
150-67	Sp	0.154	-0.321	2.26	-	-
451-103	Gn	0.448	-1.356	1.22	-	-
150-67	Sp	0.182	0.368	2.95	-	-
171-039	Ccp	0.158	0.279	2.86	-	-
171-009B	Sp	0.176	0.434	3.02	-	-
451-103B	Gn	0.455	-1.085	1.49	-	-
451-103-2	Gn	0.387	-0.743	1.83	-	-
171-009B-2	Sp	0.176	0.454	3.04	-	-
150-067	Sp	0.165	0.292	2.88	-	-
150-067-2	Sp	0.162	0.274	2.86	-	-

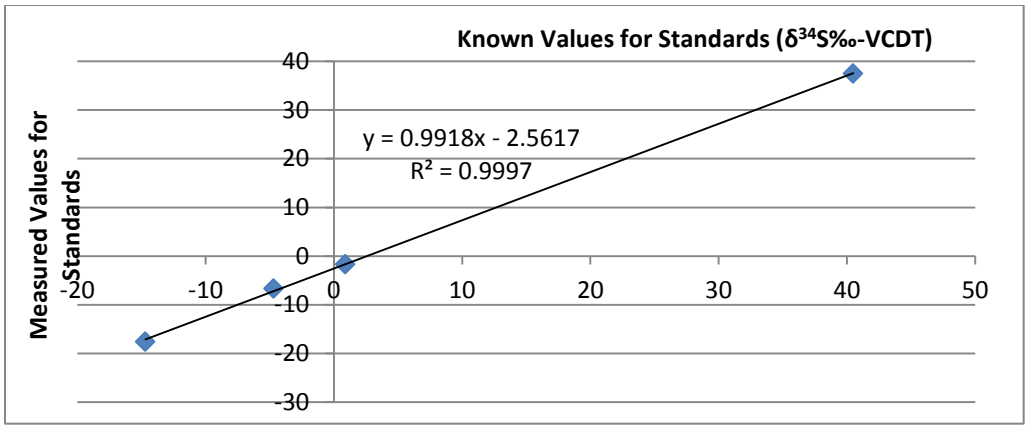

Figure 63: Batch 1

Table 7: Batch 2.

Identifier	Mineral	Weight (mg)	Raw $\delta^{34}S‰$	$\delta^{34}S‰$-VCDT	Average Raw Value	True Value
ERE	Standard	0.46	-7.505	-4.35	-7.145	-4.7
ERE	Standard	0.414	-6.785	-3.61	^	^
EMR	Standard	0.167	-1.275	2.05	-3.219	0.9
EMR	Standard	0.168	-5.337	-2.12	^	^
EMR	Standard	0.171	-3.046	0.23	^	^
PQM2	Standard	0.103	-17.549	-14.68	-17.549	-14.7
PQB-D	Standard	0.434	35.385	39.74	36.231	40.5
PQB-D	Standard	0.378	37.076	41.48	^	^
150-065	Py	0.083	-0.251	3.10	-	-
171-016	Py	0.105	-2.529	0.76	-	-
127-045	Ccp-Py	0.103	0.254	3.62	-	-
171-033	Py	0.105	0.504	3.88	-	-
127-045	Ccp-Py	0.119	0.565	3.94	-	-
171-035	Py	0.123	0.938	4.33	-	-
451-106	Py	0.094	-0.444	2.91	-	-
150-065	Py	0.115	0.172	3.54	-	-
171-025	Py	0.1	1.1	4.49	-	-
171-023	Py	0.101	0.906	4.29	-	-
171-035-2	Py	0.089	-0.044	3.32	-	-
171-029	Py	0.117	0.973	4.36	-	-
171-037	Ccp	0.167	1.653	5.06	-	-
171-039	Bn	0.21	-0.943	2.39	-	-
127-045-3	Ccp-Py	0.13	-1.025	2.31	-	-

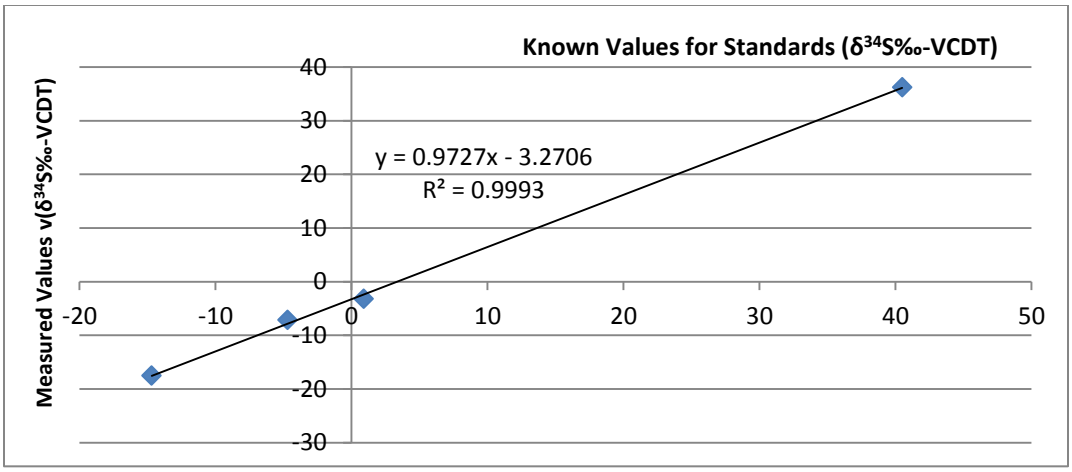

Figure 64: Batch 2

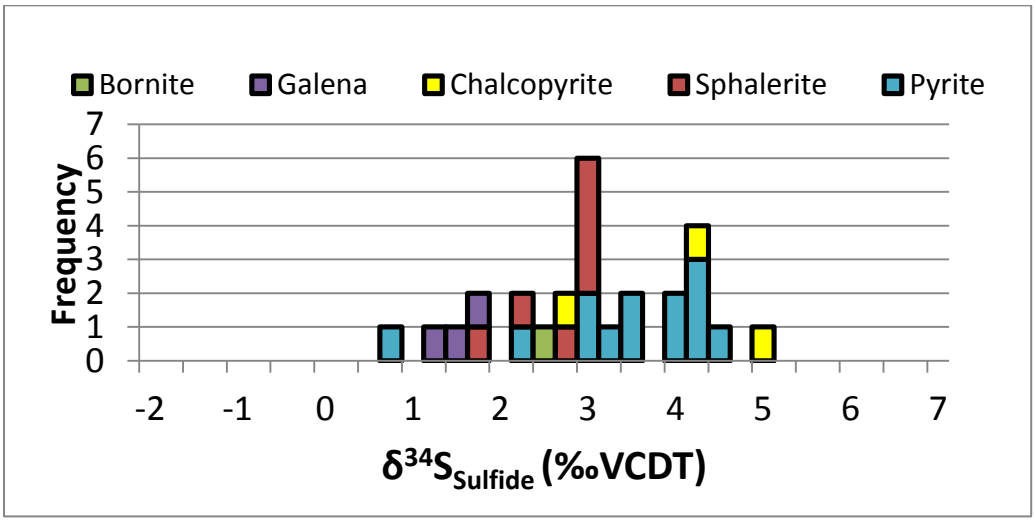

Figure 65: Frequency histogram of sulfur isotope values for five primary sulfide minerals in the Back Forty deposit.

Table 8: Values and standard deviations for each mineral measured for sulfur isotope composition.

Mineral Name	Pyrite	Sphalerite	Chalcopyrite	Galena	Bornite
Avg. $\delta^{34}S$ value	3.45 ± 1.03 (1 σ) (n = 13)	2.69 ± 0.46 (1 σ) (n = 7)	4.05 ± 1.11 (1 σ) (n = 3)	1.51 ± 0.31 (1 σ) (n = 3)	2.39 (n = 1)

CHAPTER IV

DISCUSSION

Host Rocks

The host rocks are composed of crystal tuff and lithic tuff. Tuffs are pyroclastic rocks composed of consolidated and subsequently lithified volcanic material, or tephra, ejected during volcanic eruptions. Tuffs can be classified as vitric tuffs, lithic tuffs, and crystal tuffs (Pettijohn, 1975; Schmid 1981)(Figure 66). These classifications are based on the composition of tuff as primarily glass, lithic, or crystal material, respectively.

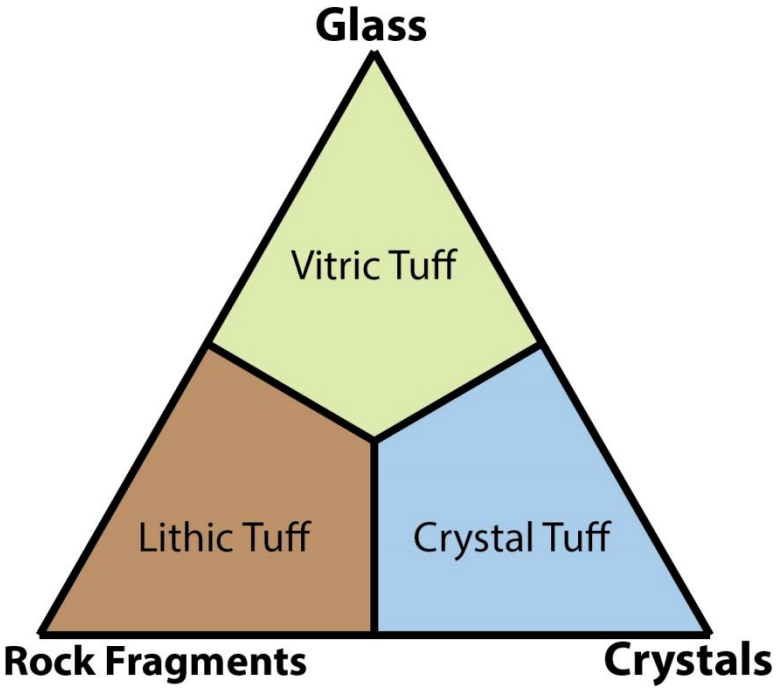

Figure 66: Ternary diagram used to determine rock types for tuffs based upon glass, rock fragments, and crystal relative compositions (after Pettijohn, 1975; Schmid 1981).

Grain-size is also used to further classify the tuffs as either lapilli-tuff (> 2mm), coarse-ash tuff (< 2 mm), and fine-ash tuff (< 0.064 mm) (Heiken and Wohletz, 1985) (Table 7). Three groups of tuffs have been identified in this study: coarse-ash crystal tuffs, fine-ash crystal tuff, and lapilli lithic tuff.

Table 9: Classification of pyroclastic rock types based on grain size.

Grain Size	Pyroclastic Rock Name
> 64 mm	Pyroclastic Breccia
< 64 mm	Lapilli-Tuff
< 2 mm	Coarse-Ash Tuff
< 0.064 mm	Fine-Ash Tuff

Crystal Tuffs

Coarse-Ash Crystal Tuffs

The coarse-ash crystal tuffs were identified by Aquila Resources as rhyolites based on SiO_2 versus Zr/TiO_2 (Thakurta and Quigley, 2013)(Figure 66), catalogued during sampling as either “Rhyolite 1” and “Rhyolite 2,” and underlie the Main Zone and Tuff Zone Massive Sulfide units, respectively (Figure 13 and 14). In this study, the two rhyolites are nearly indistinguishable based on petrographic inspection, yet demonstrate geochemical distinction based upon Zr/Y versus Y plots utilizing a geochemical dataset provided by Aquila Resources and a formal classification scheme for VMS hosting rhyolite volcanic rocks (Figure 62 and 63).

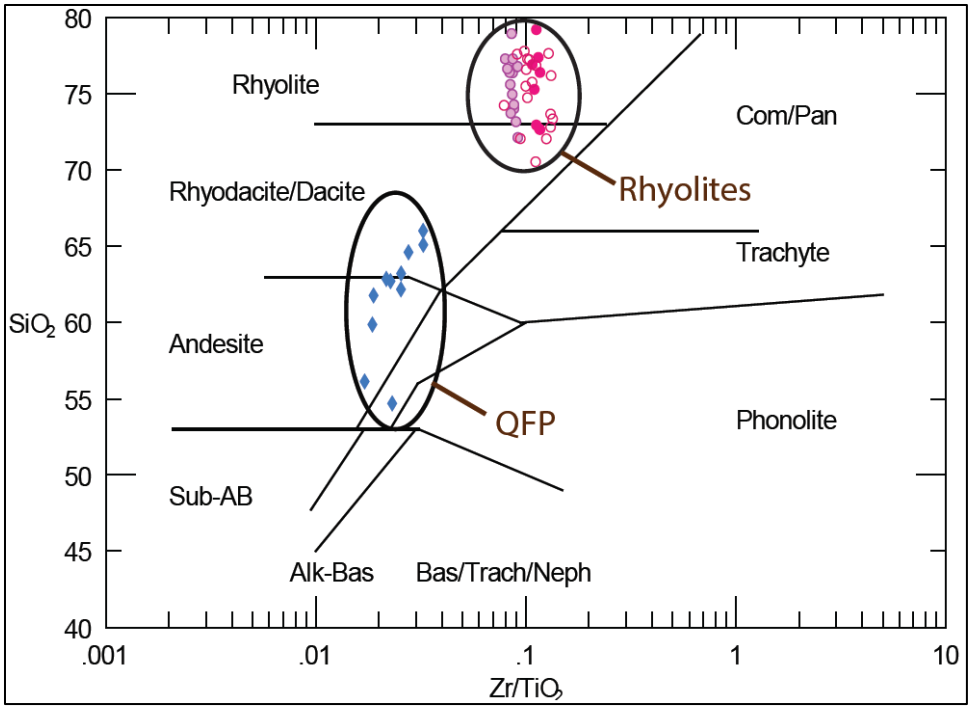

Figure 67: Rhyolite classification based on SiO_2 versus Zr/TiO_2. QFP samples identified by Aquila vary from rhyodacite/dacite to Andesite in composition (Thakurta and Quigley, 2013; Aquila Resources).

This study has renamed the two rhyolite units sampled based on petrographic descriptions of rock textures and xenocryst compositions. The coarse-ash crystal tuffs contain quartz eye-shaped xenocrysts within a crystal tuff groundmass of coarse ash-tuff (< 2 mm grain size) quartz crystals and sericite (Figure 25, Figure 23, Figure 21, and Figure 19). Quartz in the groundmass occurs as equant, rounded crystals surrounded by patchy, fine-grained sericite and disseminated or stringer sulfides. Two geochemically distinct varieties of coarse-ash crystal tuffs indicate that these units formed from two separate magmatic eruptions, but by similar eruption processes.

Fine-Ash Crystal Tuff

The fine-ash crystal tuff was catalogued during sampling as “Tuff Sediments”, based on Aquila Resources rock units, and renamed in this study based on petrographic descriptions of rock textures and xenocryst compositions. The fine-ash crystal tuff occurs overlying the Tuff Zone Massive Sulfide and underlie the Deep Zone Massive Sulfide (Figure 13 and 14 and consists of a non-layered to layered texture of alternating, thin to thick layers (1 mm to 15 mm) of chert, sulfides, chlorite, and muscovite within a groundmass of quartz and sericite (Figures 34 – 38). Layered sampled of fine-ash crystal tuff resemble banded iron formations, containing alternating layers of chert and hematite.

The fine-ash crystal tuff does not contain quartz eye-shaped xenocrysts within the crystal tuff groundmass of fine ash-tuff (< 0.064 mm grain size) which is dissimilar to the coarse-ash crystal tuffs. Quartz in the groundmass occurs as equant (rounded) crystals surrounded by patchy, fine-grained sericite and disseminated sulfides, similar to the coarse-ash crystal tuffs. Underlying the deep zone, the fine-ash crystal tuff contains fractures filled with sulfides. The fine-ash crystal tuff rarely contains patches of coarse-ash crystal tuff within the groundmass (Figure 40). It is unclear if these patches are xenoliths of coarse-ash crystal tuff.

Lapilli Lithic Tuff

The lapilli lithic tuff was catalogued during sampling as "Quartz-Feldspar Porphyry/Felsic Dikes," based on Aquila Resources rock units, and renamed in this study. The lapilli lithic tuff is interlayered with the fine-ash crystal tuffs, and are seen within the coarse-ash crystal tuff by as a dike structure (Figure 13 – 14). The lapilli lithic tuff consists of coarse ash-tuff sized angular quartz crystal fragments and angular lapilli size rock fragments composed of fine-ash tuff quartz and sericite within a groundmass of sericite (Figure 26 – 31). Quartz eye-shaped xenocrysts exhibit extinction patterns different from the coarse-ash crystal tuff, distinguished by segmented extinction patterns within the deformed xenocrysts (Figure 31, Figure 29, and Figure 27). The lapilli size rock fragments are texturally nearly identical to the groundmass of the fine-ash crystal tuffs, and are interpreted as xenoliths.

In some samples, the lapilli lithic tuff also consists of coarse ash-tuff sized angular quartz crystal fragments accompanied by large alkali and plagioclase feldspar xenocrysts within a groundmass of quartz and sericite (Figure 32 – 33) and lacking the angular lapilli size rock fragments as seen in others. The presence of alkali and plagioclase feldspar xenocrysts provides insight into the composition of a deeper magma system. The presence of alkali and plagioclase feldspar xenocrysts within the lithic tuff suggests a genetic and compositional link to the deeper granitic magmas within the Pembine Wausau Terrane, supplying heat and volcanic material to the formation of the Back Forty deposit.

Mineralization

Five major zones of sulfide mineralization are found within the Back Forty deposit: the Main Zone, Tuff Zone, Pinwheel Zone, Stringer Zone, and the Deep Zone (Figures 11 – 14). These zones contain sulfides in different textural modes of occurrence within the host rock. Textural relationships between sulfides and the sulfide minerals present also vary between different zones. The primary sulfide minerals in the deposit are pyrite (FeS_2), sphalerite ((Zn,Fe)S), and chalcopyrite ($CuFeS_2$). Minor sulfide minerals include galena (PbS), marcasite (FeS_2), pyrrhotite ($Fe_{1-x}S$), arsenopyrite (FeAsS), and bornite (Cu_5FeS_4).

Textural Occurrences

Massive and Semi-Massive

In this study, massive textures represent the greatest volumetric abundance of sulfides minerals within the host rock. Sulfide minerals in massive sulfide zones lack well-developed crystal outlines in thin-section (i.e. anhedral crystal shape)(Figure 42 – 43, Figure 45, Figure 47 , Figure 49, Figure 51, Figure 53, and Figure 59). Massive textures comprise the major ore zones identified by Aquila Resources as “Massive Sulfide” (Figure 13 – 14). This study distinguished sulfide-bearing zones into three groups based on the concentration of sulfides by volumetric (%) abundance within samples. Grading into the massive zones are semi-massive textures representing (40 – 80%) zones with less concentrated sulfides. Unlike massive textures, semi-massive sulfide display more developed crystal outlines in thin-section (Figure 55).

Disseminated and Stringer

Disseminated and stringer sulfides underlie massive and semi-massive sulfide-bearing zones. Disseminated sulfides are identified by < 40% volumetric abundance of sulfides. Stringer sulfides are vein-like structures of sulfide minerals within the host rocks, occurring as branching networks. This network of stringers represents faults and fractures through the host rocks, permeated by ore fluids. These fluids supplied sulfides to the overlying massive and semi-massive units. With lesser abundance of sulfides within the host rock, sulfide minerals display greater development of crystal edges, occurring with euhedral to subhedral crystal outlines as opposed to anhedral crystal outlines in massive and semi-massive textures. Increased quartz grain sizes, by as much as 10x the surface area, along stinger sulfide boundaries with the host rocks indicate that dissolved silica may have accompanied the dissolved sulfides in the ore-forming fluid or formed through alteration-recrystallization of the host rock along these boundaries (Figure 40). The vein structures formed by sulfides could have provided a pathway for later hydrothermal fluids supplying additional silica and sulfides, as evidenced by the variable size of vein structures. Larger quartz grain sizes are also seen along disseminated sulfide grain boundaries within the host rocks (Figure 35, Figure 55, and Figure 57).

Gossan

The "Gossan" Zone was defined by Aquila Resources as the upper portion of the Pinwheel Zone (Figure 13 – 14). The gossan texture is characterized by fine-grained and botryoidal iron-oxide (hematite and goethite), surrounded by silver, chlorite, and dolomite, respectively (Figure 60 – 61). Underlying the Gossan Zone is a Massive

Sulfide zone with an intergrowth pattern between pyrite and chalcopyrite that does not resemble any texture overserved in all other massive sulfide-bearing zones (Figure 53). This intergrowth texture occurs as repetitive three-dimensional structure composed of vein-like structures of chalcopyrite and pyrite. This zone is also characterized by an absence of sphalerite.

Aquila Resources identified this zone as an up-faulted portion of the Main Zone (Figure 13 – 14). The up-faulted massive sulfide unit of the main zone would have underwent oxidation at the surface, forming the gossan textures. Zoned dolomite and botryoidal iron-oxides indicate a period of continual growth through multiple periods of oxidation with dissolved minerals infiltrating into greater depths. The process of dissolving minerals is reflected by the void spaces that occur within the Pinwheel Zone massive sulfide (Figure 53). Within some of these void spaces anhydrite has formed. Native copper can also be identified in hand-sample (Figure 52). Native copper does not occur in samples from all other zones. The presence of zoned dolomite and iron-oxide minerals in the Gossan zone, with intergrowth textures (between pyrite and chalcopyrite) and native copper in the underlying massive unit represents a secondary process of mineralization that is has not occurred in the other major zones.

Sulfur Isotope Analysis

$\delta^{34}S_{Sulfide}$ values of the Back Forty are consistent with values that have been obtained from the four other major VMS deposits of the Penokean Volcanic Belt (PVB)(Figure 66). This indicates a similar source or process delivering sulfur to the ore forming fluids during the formation of the major VMS deposits of the PVB. While the

metal content of the deposits varies considerably (Table 3, Figure 6 – 7), the sulfur isotope values do not appear to vary with any degree of significance; it is unlikely that sulfur isotope values can be correlated with differences in metal content between the major deposits. The range in values at Back Forty, and others, is narrow and tightly clustered.

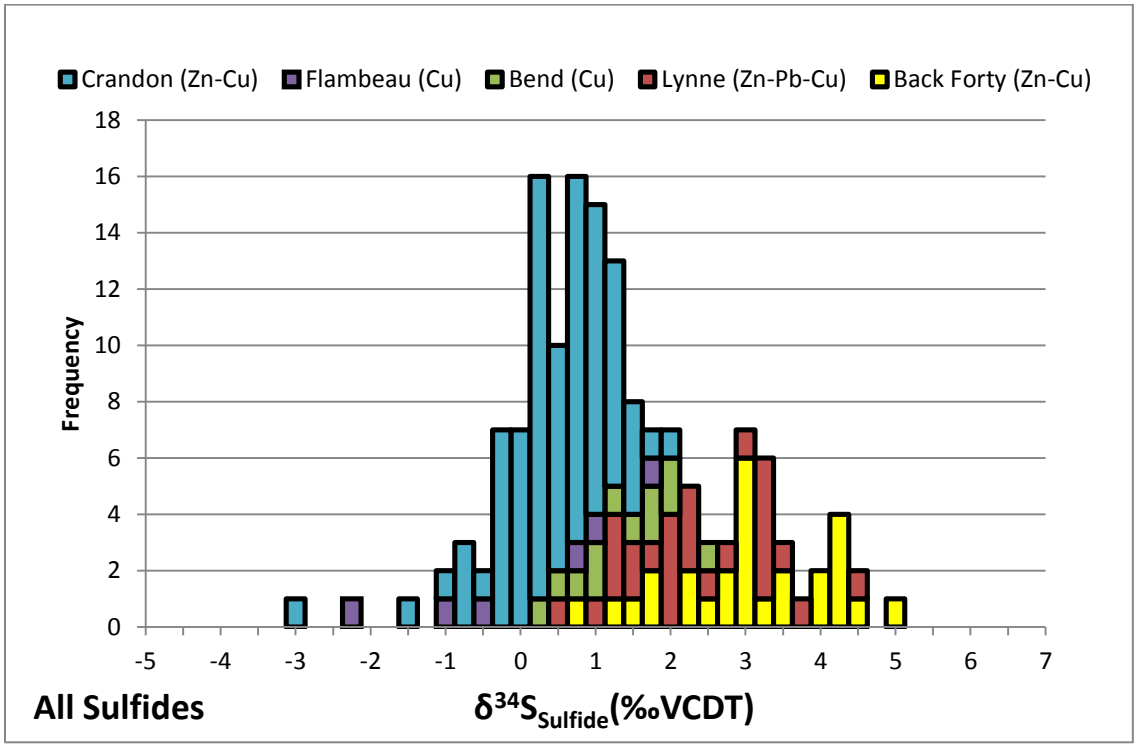

Figure 68: Frequency histogram of sulfur isotope values of the five major VMS deposits of the Penokean Volcanic Belt (Crandon Values: Lesley Myers, 1983; Bend, Lynne, and Flambeau values: Laurel Woodruff, USGS, written communication).

The sources of sulfur may be mantle rocks, biologically reduced seawater sulfate, or from seawater sulfate. Magmatic or mantle derived sulfur has $\delta^{34}S$ values of 0 ± 2‰-VCDT (Ripley and Li, 2003). However, the isotopic composition of non-biological magma-derived sulfides may range – 4 to +4 per mil of the mantle value (Schneider,

1970). Biologically derived sulfur would produce depletion in ^{34}S or negative $\delta^{34}S$ values, resulting locally from microbial reduction of seawater sulfate (Taylor et al., 2010). The sulfate-reducing bacteria more readily metabolize ^{32}S relative to ^{34}S (Seal, 2006). Sulfur derived from seawater sulfate would produce enrichment in ^{34}S or positive $\delta^{34}S$ values (Strauss and Schieber, 1990).

Large differences of up to 40 to 45 per mil between seawater sulfate and sedimentary sulfide are present through the Proterozoic 2.3 to 1.8 Ga (Canfield and Raiswell, 1999). The deposits within the PVB formed around 1.875 Ga. Ohmoto, 1996, identified sedimentary sulfides derived by bacterial (biologic) sulfate reduction as having produced depletion in ^{34}S by typically 45 ± 20‰. During the Paleoproterozoic, $\delta^{34}S$ values of seawater sulfate varied between +10 and +30 ‰ (Ohmoto, 1996). Therefore, biological reduction of seawater derived sulfur would produce highly variable and negative values in samples from the Back Forty if it were a factor in the composition of the ore-forming fluid.

Sulfur isotope values in the Back Forty deposit range from 0.76 – 5.06 ‰-VCDT. Negative values of sulfide samples from the Back Forty have not been found by this study. This indicates that biologically reduced seawater-derived sulfur was not a possible source for the sulfur in the ore-forming fluid. This is supported by the absence of sedimentary rocks within the Back Forty stratigraphy. The sulfur may then have been derived in two ways, producing a hydrothermal species of H_2S. One source may be the leaching of underlying volcanic rocks, producing a "Type 1" species of H_2S within the hydrothermal, ore-forming fluid with a $\delta^{34}S$ composition of ~ 0‰ (Ohmoto, 1996). A second source may be "Type 2" H_2S derived by non-biological reduction of seawater

sulfate through reaction with Fe^{2+}-bearing minerals and/or by organic carbons, producing H_2S with a $\delta^{34}S$ composition of –8 to +22‰ within the hydrothermal, ore-forming fluid (Ohmoto, 1996) (Equation 2: Woodruff and Shanks, 1988) (Equation 3: Seal, 2006).

$$8FeS + 10H^+ + SO_4^{2-} \rightarrow 4FeS_2 + H_2S + 4H_2O + Fe^{2+} \quad \textbf{(2)}$$

$$2CH_2O + SO_4^{2-} \rightarrow H_2S + 2HCO^{3-} \quad \textbf{(3)}$$

The narrow range in values of samples at Back Forty is between 0.76 and 5.06‰. This is consistent with mantle values of sulfur derived by leaching of underlying volcanic rocks as defined by Ripley and Li (2003), Schneider (1970), and Ohmoto (1996). The geologic time frame is also consistent with these findings. In Archean to Paleoproterozoic deposits, the bulk of the sulfur was derived by leaching rocks underlying the deposits with little contribution from seawater, resulting in uniform, near-zero per mil values of $\delta^{34}S_{Sulfide}$ (Huston et al., 2010).

Model of Formation

Starting around 1875 Ma, back-arc extension in the Pembine-Wausau Terrane began forming the PVB through thinning crust and upwelling of mantle magma and heat. The volcanic host rocks represent manifestations of the cycling of heat from deeper magmatic activity within the Pembine-Wausau Terrane. Quartz, alkali and plagioclase feldspar xenocrysts within lithic and crystal tuffs provide insight into the link between magmatic activity and subaqueous volcanic eruptions and hydrothermal activity.

Mineralization concordant to host rock formed as massive and semi-massive sulfides at seafloor venting zones. These venting sites were overlain by sequential

volcanic eruptions. Branching networks of stringers sulfides reflect the pathway of ore-forming fluids migrating toward seafloor venting zones.

Two geochemically distinct varieties of coarse-ash crystal tuffs indicate that these units formed from two separate magmatic eruptions, but by similar eruption processes. Mineralization of massive and semi-massive occurred above each of these units. Through the formation of the deposit, fine-ash crystal tuff interbedded with the lapilli lithic tuff formed between the second and third coarse-ash crystal tuff units (i.e. "Rhyolite 2 and 3"). Intruding through all units is a lapilli lithic tuff, dike-like structure which formed at the end of the sequence of volcanic events associated with the Back Forty deposit.

Folding and faulting of the deposit and host rocks led to the development of a south-west plunging anticline. The south limb of the deposit dips 65° and the north limb dipping 35° (Aquila Resources). Shearing is evident in the south limb of the anticline with the development of fractures filled by quartz (Figure 47). The upfaulted portion of the Main Zone Massive Sulfide to near-surface depths (0 – 50 m) represents the "Pinwheel Zone." Development of the modern erosional surface accompanied by oxidation of near surface sulfides produced secondary mineralization textures consisting of an intergrowth between pyrite and chalcopyrite. The process of secondary mineralization, overlying oxidation of sulfides and remobilization accompanies the enrichment in copper-bearing sulfide and the presence of native copper found only in the Pinwheel Zone.

Based on the stratigraphic relationship between each host rock unit and massive sulfide unit, accounting for deformation and the modern erosional surface, the sequence of events is illustrated in Figure 68. Underlying each massive sulfide zone, the host rock

contains stringer sulfides. These stringer sulfides developed during continued hydrothermal activity as multiple pyroclastic rock units were forming in the back-arc basin.

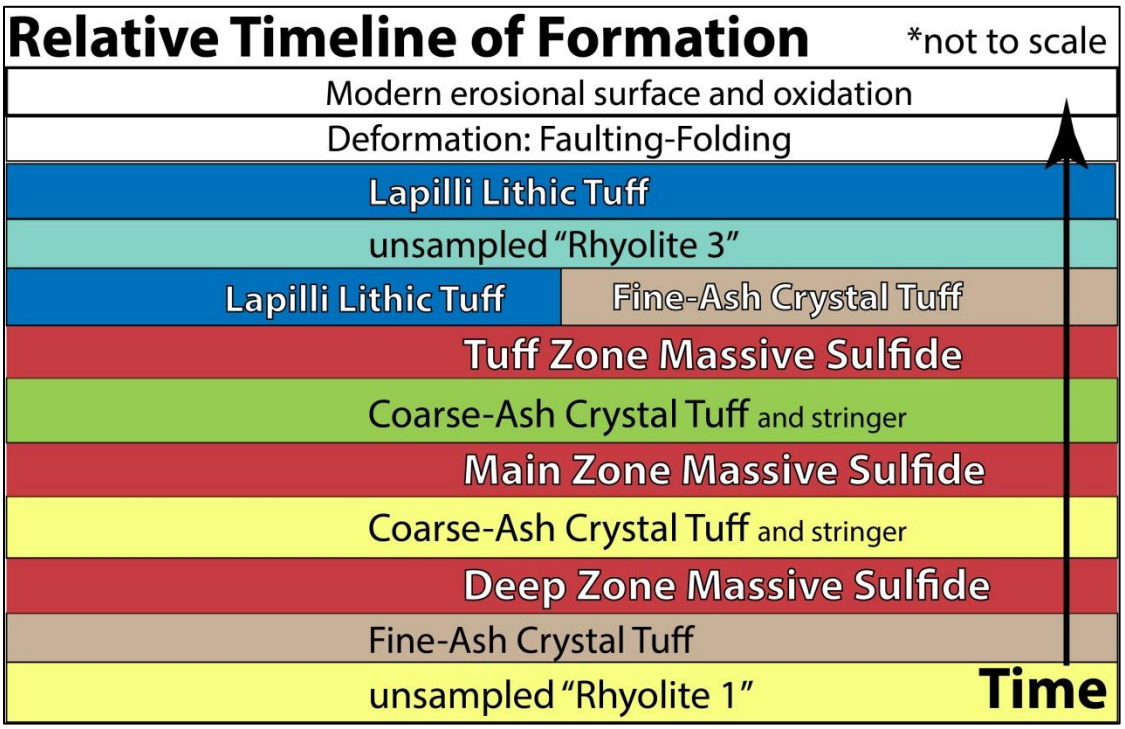

Figure 69: Relative timeline of volcanic and mineralization events.

REFERENCES

Allen, Rodney L., Fernando Tornos, and Jan M. Peter, 2011, "A Thematic Issue on the Geological Setting and Genesis of Volcanogenic Massive Sulfide (VMS) Deposits." *Mineral Deposita* 46:429-430.

Anders, E., and N. Grevesse, 1989, "Abundances of the elements: Meteoric and solar," *Geochemica et Cosmochimica Acta* 53:197-214.

Augustithis, S. S., 1995, "Atlas of the Textural Patterns of Ore Minerals and Metallogenic Processes," *Walter de Gruyter.*

Barrie, C.T., Ludden, J.N., and Green, T.H., 1993, "Geochemistry of Volcanic Rocks Associated with Cu-Zn and Ni-Cu Deposits in the Abitibi Subprovince," *Economic Geology*, 88: 1341-1358.

Bachmann, Oliver, and George W. Bergantz, 2008, "Rhyolites and their Source Mushes across Tectonic Settings," *Journal of Volcanology,* 49(12):169–198.

Baier, J., A. Audetat, and H. Keppler, 2008, "The origin of the negative niobium tantalum anomaly in subduction zone magmas," *Earth and Planetary Science Letters*, 267(1-2):290-300.

Barrett, T.J., and MacLean, W.H.,1999, "Volcanic sequences, lithogeochemistry, and hydrothermal alteration in some bimodal volcanic-associated massive sulfide systems," *Reviews in Economic Geology,* 8:101–131.

Barrett, T.J., and MacLean, W.H., 1994, "Chemostratigraphy and hydrothermal alteration in exploration for VHMS deposits in greenstones and younger volcanic rocks," *Geological Association of Canada Short Course Notes,* 11:433–467.

Barrie, C. T., and Hannington, M. D., 1999, "Volcanic-Associated Massive Sulfide Deposits: Processes and Examples in Modern and Ancient Settings," *Reviews in Economic Geology,* ed. Barrie, C. T., and Hannington, M. D. (8):1-11.

Barrie, C.T., 2007, "Petrography and Mineral Chemistry of the Back 40 VMS Deposit, Menominee County, Michigan: Initial Observations," *An interim report for Aquila Resources.*

Beard, J.S., Lofgren, G.E., 1991. "Dehydration melting and watersaturated melting of basaltic and andesitic greenstones and amphibolites at 1, 3 and 6.9 kb," *J. Petrol*. 32:365–401.

Boxleiter, A. R., Thakurta J.,, and Quigley, T.O., "Geochemical Investigation of the Origin of the Back Forty Volcanogenic Massive Sulfide Deposit in Menominee County, Michigan," Poster presentation: *ILSG 2014 Conference*, (May 2014) Hibbing, MN.

Briqueu, L., H. Bougault, and J. L. Joron, 1994, "Quantification of Nb, Ta, Ti and V anomalies in magmas associated with subduction zones' petrogenetic implications," *Earth and Planetary Science Letters* 68:297-308 *in Elsevier Science Publishers B.V., Amsterdam - Netherlands.*

Campbell, I.II., Coad, P., Franklin, J.M., Gorton, M.P., Scott, S.D., Sowa, J., and Thurston, P.C., 1982, "Rare Earth Elements in Volcanic Rocks Associated with Cu-Zn Massive Sulfide Mineralization," *A preliminary report: Canadian Journal of Earth Sciences,* 19:619-623.

Canfield, D. E. and Raiswell, R., 1999, "The Evolution of the Sulfur Cycle," *American Journal of Science,* 299:697–723.

Casey, W. H., and Taylor, B.E., 1982. "Oxygen, Hydrogen, and Sulfur Isotope Geochemistry of a portion of the West Shasta Cu-Zn District, California," in *Economic Geology,* 77:38–49.

Chen, T.T., Dutrizac, J.E., Owens, D.R. & Laflamme, J.H.G., 1980, "Accelerated Tarnishing of Some Chalcopyrite and Tennantite Specimens," *Can Mineral,* 18:173-180.

Costech Analytical Technologies Inc. "Elemental Combustion System CHNS-O."

Craig, J.R., David J. Vaughan, 1994, "Ore Microscopy and Ore Petrography 2nd Ed.," *John Wiley & Sons. Inc.,* pp. 434.

Deering, C.D., O. Bachmann, J. Dufek, and D.M. Gravely, 2011, "Rift-Related Transition from Andesite to Rhyolite Volcanism in the Taupo Volcanic Zone (New Zealand) Controlled by Crustal-melt Dynamics in Mush Zones with Variable Mineral Assembalges," *Journal of Petrology,* 52(11):2243-2263.

Encyclopædia Britannica, 2015, "Tuff,"*Encyclopædia Britannica Online.* Date Retrieved: Oct 5, 2015, http://www.britannica.com/science/tuff.

Ford, Mark T., Anita L. Grunder, and Robert A. Duncan, 2013, "Bimodal volcanism of the High Lava Plains and Northwestern Basin and Range of Oregon: Distribution and tectonic implications of age-progressive rhyolites," *Geochemistry, Geochemisty, Geosystems: AGU and Geochemical Society,* 14(8):2836-2856.

Foth Infrastructure & Environment, LLC, 2012. "Geochemical Investigation Report, Back Forty Joint Venture," *Prepared for HudBay Michigan, Inc.*

Franklin, J.M., H.L. Gibson, I.R. Jonasson, and A.G. Galley, 2005, "Volcanogenic Massive Sulfide Deposits," *Economic Geology 100th Anniversary Volume,* 523-560.

Frost, Ronald B., and Carol D. Frost, 2013, "Essentials of Igneous and Metamorphic Petrology," *Cambridge University Press,* 1-314.

Gaboury, D. and Pearson, V., 2008, "Rhyolite geochemical signatures and association with volcanogenic massive sulfide deposits: Examples from the Abitibi Belt, Canada,"*Economic Geology,* 103:1531-1562.

Galley, A.G., Hannington, M.D., and Jonasson, I.R., 2007, "Volcanogenic massive sulphide deposits," in Goodfellow, W.D., ed., Mineral Deposits of Canada: A Synthesis of Major Deposit-Types, District Metallogeny, the Evolution of Geological Provinces, and Exploration Methods," *Geological Association of Canada, Mineral Deposits Division, Special Publication,* 5:141-161.

Georgieva, S., A. Hikov, and E. Stefanova, 2012, "Mobility of major and trace elements during hydrothermal alteration of volcanic rocks from the Chelpech high-sulfidation epithermal Cu-Au deposit, Central Srednogorie, Bulgeria*," Bulgarian Geological Society, National Conference.*

Gibson, H.L. Watkinson, D.H., 1990, "Volcanogenic Massive sulfide deposits of Noranda cauldron and shield volcano, Quebec," *Canadian Institute of Mining and Metallurgy Special Volume,* 43:119-132.

Hart, T.R., Gibson, H.L. and Lesher, C.M., 2004, "Trace element geochemistry and petrogenesis of felsic volcanic rocks associated with volcanogenic massive Cu-Zn-Pb sulfide deposits," *Economic Geology,* 99:1003-1013.

Hannington, M.D., Jonasson, I.R., Herzig, P.M. and Peterson, S., 1995, "Physical and chemical processes of sea floor mineralization at mid-ocean ridges," *Geophysical Monograph,* 91:115-157.

Hannington, M.D., Poulson, K.H., Thompson, J.F.H., and Sillitoe, R.H., 1999b, "Volcanogenic gold in the massive sulfide environment," *Reviews in Economic Geology,* 8:325-356.

Hannington, M.D., J.W. Jamieson, B.A. Wing, and J. Farquhar. 2006. "Evaluating Isotopic Equilibrium Among Sulfide Mineral Pairs in Archean Ore Deposits: Case Study From the Kidd Creek VMS Deposit, Ontario, Canada," *Economic Geology* 101:1055-1061.

Heiken, G. and Wohletz, K., 1985, "Volcanic Ash," *University of California Press.*

Hikov, A., and L-A. Daieva, 2007, "Trace elements in hydrothermally altered rocks from Asarel porphyry copper deposit, Central Srednogorie," *GEOSCIENCES:*78-79.

Hildreth, Wes, 2004, "Volcanological perspectives on Long Valley, Mammoth Mountain, and Mono Craters: several contiguous but discrete systems," *Journal of Volcanology and Geothermal Research,* 136(3–4):169–198.

Hopwood, T.P., 1976, "'Quartz-Eye'-Bearing Porhyroidal Rocks and Volcanogenic Massive Sulfide Deposits," *Economic Geology* (71):589-612.

Huston, D. L., S. Pehrsson, B. M. Eglington, K. Zaw, 2010, "The Geology of Volcanic-Hosted Massive Sulfide Deposits: Variations through Geologic time with Tectonic Setting," *Economic Geology* 105:571-591.

Isomass Scientific Inc., "Stable Isotope Mass Spectrometer Operator Course," *Isomass Scientific Training Center, University of Ottawa, G.G. Hatch Isotope Laboratories, Ottawa, ON, Canada, December 3-5, 2014.*

Krouse, H.R., and Coplen, T.B., 1997, "Reporting of relative sulfur isotope ratio data," *Pure and Applied Chemistry,* 69:293-295.

Kearney, M.K., 2003, "Volcanic-Associated Massive Sulphide Deposits," *for Billiken Management Services. Toronto, Ontario. June 12.*

Large, R.R., Gemmell, J. B., Paulick, H., and Huston, D. L., 2001, "The alteration box plot: A simple approach to understanding the relationship between alteration mineralogy and lithogeochemistry associated with volcanic hosted massive sulfide deposits," *Economic Geology* 96:957–971.

Le Maitre (ed), R.W., A. Streckeisen, B. Zanettin, M. J. Le Bas, B. Bonin, P. Bateman, G. Bellieni, A. Dudek, S. Efremova, J. Keller, J. Lamere, P. A. Sabine, R. Schmid, H. Sorensen, and A. R. Woolley, 2002, "Igneous Rocks: A Classification and Glossary of Terms, Recommendations of the International Union of Geological Sciences, Subcommission of the Systematics of Igneous Rocks. *Cambridge University Press,* 2002.

Lentz, D.R., 1998, "Petrogenetic evolution of felsic volcanic sequences associated with Phanerozoic volcanic-hosted massive sulphide systems: the role of extensional geodynamics," *Ore Geology Reviews,* 12:289-327.

Lesher, C.M. Goodwin, A.M., Campbell, I.H., and Gorton, M.P., 1986, "Trace-element geochemistry of ore-associated and barren, felsic metavolcanic rocks in the Superior province," *Canadian Journal of Earth Sciences,* 23:222-237.

Ling, Q-C., and C-Q. Liu, 2002, "Behavior of the REEs and other trace elements during fluid-rock interaction related to ore-forming processes of the Yinshan transitional deposit in China," *Geochemical Journal*, (36):443-463.

Lister, C.R.B., 1976, "On the penetration of water into hot rocks," *Journal of the Royal Astronomical Society*, 39:465-509.

Macnmara J., Thode H.G., 1950, "Comparison of the isotopic of terrestrial and meteoritic Sulphur," *Phys Rev* 78:307 – 308.

McDonough, W., Albarede, F., Staudigel, H. and White, B. (1996). "Geoscientists unite to develop Earth Reference Model," *Eos, Transactions American Geophysical Union*.

Mcdonough, W.F. & Sun, S.-S., 1995, "The composition of the Earth," *Chemical Geology*, 120:228.

Myers, L. L., 1983, "Geochemistry of the Crandon Massive Sulfide Deposit, Wisconsin: Sulfur Isotope and Fluid Inclusion Data," *M.S. Thesis–UW-Madison.*

Nicholson, S. W., Schulz, K. J., and Woodruff, L. G., 2001, "Transitional epithermal - to – typical volcanogenic massive sulfide deposits in the Early Proterozoic Penokean Orogen, Northern Wisconsin," (abstract), *GSA Annual meeting* paper 76-0.

Nielsen H., Pilot J., Grinenko L.N., Grinenko V.A., Lein A.Y., Smith J.W., Pankina R.G., 1991, "Lithospheric sources of Sulphur," *In*: Stable Isotopes in the Assessment of Natural and Anthropogenic Sulphur in the Environment. Krouse HR, Grinenko VA (*eds*) *SCOPE* 43, *J Wiley and Sons* 65 – 132.

Ohmoto, H., 1996, "Formation of volcanogenic massive sulfide deposits: The Kuroko perspective," *Ore Geology Reviews* 10:135 – 177.

Ohmoto, H., and Rye, R.O., 1979, "Isotopes of sulfur and carbon," *in* Barnes, H.L., ed., "Geochemistry of hydrothermal ore deposits," second edition: *New York, John Wiley and Sons*, p. 509–567.

Pandarinath K., Dulski P., Torres Alvarado I.S. & Verma S.P., 2008, "Element mobility during the hydrothermal alteration of rhyolitic rocks of the Los Azufres geothermal field, Mexico," *Geothermics,* 37:53-72.

Paul, D., Skrzypek, G. and Forizs, I., 2007, "Normalization of measured stable isotopic compositions to isotope reference scales – a review," *Rapid Commun. Mass Spectrom,* 21:3006-3014.

Pettijohn, F.J., 1975. "Sedimentary Rocks," *Harper and Row Limited*. pp.628.

Quigley, T., Mahin, B., and Aquila Field Office Geologic Staff, 2008, "Back Forty Geology and Mineralization," *54th Annual Institute on Lake Superior Geology*, Field Trip #3.

Rapp, R.P., 1995, "Amphibole-out phase boundary in partially melted metabasalt, its control over liquid fraction and composition, and source permeability," *J. Geophys,* 100:15601– 15610.

Rapp, R.P., Watson, E.B., 1995, "Dehydration melting of metabasalt at 8–32 kbar: Implications for continental growth and crust– mantle recycling," *J. Petrol.* 36: 891–931.

Rapp, R.P., Watson, E.B., Miller, C.F., 1991, "Partial melting of amphibolitereclogite and the origin of Archean trondhjemites and tonalities," *Precombrian* 51:1–25.

Reed, Mark H., and James Palandri. 2006. "Sulfide Mineral Precipitation from Hydrothermal Fluids" *in* Sulfide Mineralogy and Geochemistry. *Reviews in Mineralogy and Geochemistry*. ed. David J. Vaughn. Series ed. Jodi J. Rosso, *Geochemical Society Mineralogical Society of America*, 61:609-630.

Ripley, Edward M. and Chusi Li, 2003, "Sulfur Isotope Exchange and Metal Enrichment in the Formation of Magmatic Cu-Ni-(PGE) Deposits," *Economic Geology* 98:365-641.

Ross, C., Hudak, G., Morton, R., Quigley, T. and Mahin, R., 2011, "Preliminary stratigraphy and physical volcanology associated with the Paleoproterozoic Back Forty VMS deposit, Menominee County, Michigan," *Institute of Lake Superior Geology poster abstract.*

Rushmer, T., 1991, "Partial melting of two amphibolites: contrasting experimental results under fluid-absent conditions," *Contrib. Mineral. Petrol*. 107:41–59.

Schneider, A., 1970, "The Sulfur isotope composition of basaltic rocks," *Contributions to Mineralogy and Petrology*, 25: 95–124.

Schieber, J., 2004, "Marcasite in Sediments and Sedimentary Rocks - Conundrum and Opportunity," *American Geophysical Union*, Fall Meeting 2004, abstract #OS14A-05.

Schoonen, M.A.A., H. L. Barnes, 1991, "Mechanisms of pyrite and marcasite formation from solution: III. Hydrothermal processes," *The Pennsylvania State University Ore Deposits Research Section.*

Schmid, R., 1981. "Descriptive nomenclature and classification of pyroclastic deposits and fragments: Recommendations of the IUGS Subcommission on the Systematics of Igneous Rocks," *Geology* 9:41-43.

Schulz, K.J. and Cannon, W.F., 2007, "The Penokean Orogeny in the Lake Superior Region, *Precambrian Research,*" 157:4-25.

Schulz, K.J.(USGS),"Sulfide Deposits and Associated Geology in Michigan and Wisconsin," *Special Presentation,* U.S. Geological Survey.

Schwartz, G.M., 1931. "Textures due to unmissing solid solutions," *Econ. Geol*., 26:730-763.

Schwartz, G. M., 1942. "Progress in the study of ex-solutions in ore minerals," *Econ, Geol*., 37:345-364.

Seal, R.R., 2006, "Sulfur Isotope Geochemistry of Sulfide Minerals," *Reviews in Mineralogy & Geochemistry* 61:633 – 677.

Shanks, W.C. Pat, III and Thurston, Roland, 2010 "Volcanogenic massive sulfide occurrence model: Chapter C," *Mineral deposit models for resource assessment. USGS Scientific Investigations Report*: 2010-5070-C.

Shanks, W.C. Pat, III, and Thurston, Roland, eds., 2012, "Volcanogenic massive sulfide occurrence model," *U.S. Geological Survey Scientific Investigations Report* 2010–5070–C, 345 p.

Shinjo, Ryuichi and Kato, Yuzo, 2000, "Geochemical constraints on the origin of bimodal magmatism at Okinawa Trough, an incipient back-arc basin," *Elsevier, Lithos* 54:117-137.

Staudigel, H, Albarede F, Blichert-Toft J, Edmond J, McDonough B, Jacobsen SB, Keeling R, Langmuir CH, Nielsen RL, Plank T, Rudnick R, Shaw HF, Shirey S, Veizer J, White W, 1998, "Geochemical Earth Reference Model (GERM): description of the initiative," *Chemical Geology,* 145:153-159.

Strauss, H., & Schieber, J. (1990). "A sulfur isotope study of pyrite genesis: the Mid-Proterozoic Newland Formation, Belt Supergroup, Montana," *Geochimica et Cosmochimica Acta*, 54(1):197-204.

Sturchio N.C., Muehlenbchs K. & Meitz M, 1986, "Element redistribution during hydrothermal alteration of rhyolite in an active geothermal system: Yellowstone drill cores Y-7 and Y- 8," *Geochimica et Cosmochimica Acta*, 50:1619-1631.

Sun, S.S., McDonough, W.F., 1989, "Chemical and isotopic systematics of oceanic basalts: implications for mantle composition and processes," *in*: Saunders, A.D., Norry, M.J. Eds., Magmatism in Ocean Basins. *Geol. Soc. Spec. Publ*., pp. 313–345.

Taylor, Cliff D., Robert A. Zierenberg, Richard J. Goldfarb, James E. Kilburn, Robert R. Seal II, and M. Dean Kleinkopf, 1995, "Volcanic-Associated Massive Sulfide Deposits (Models 24a-b, 28a; Singer, 9186a,b; Cox, 1986)." USGS Publication *in "*Preliminary Compilation of Descriptive Geoenvironmental Mineral Deposit Models." Ed. Edward A. du Bray, June 1996. Chapter 16:137-144.

Taylor, C.D. and Craig A. Johnson 2010, Editors. *U.S. Geological Survey Professional Paper* 1763, 429 Pp., 7 plates on CD. ISBN 978-1-4113-2622-4.

Terakado Y. & Fujitani T.,1998, "Behavior of the rare earth elements and other trace elements during interactions between acidic hydrothermal solutions and silicic volcanic rocks, southwestern Japan. *Geochimica et Cosmochimica Acta*, 62: 1903-1998.

Tetra Tech, 2014. Report to: Aquila Resources Inc. "Preliminary Economic Assessment of the Back Forty Project, Michigan, USA," *PEA Document No. 1495140100-REP-R0001-02.*

Theart, H.F.J., R. Ghavami-Rabi, H. Mouri, P. Graser, 2011, "Applying the box plot to the recognition of footwall alteration zones related to VMS deposits in a high-grade metamorphic terrain, South Africa, a lithogeochemical application," *Chemie der Erde,* 71:143-154.

Tivey, M.G.. December 1, 1998, "How to Build a Black Smoker Chimney: The formation of mineral deposits at mid-ocean ridges," *Oceanus,* 41(2).

Tivey, M.G. March 2007. "Generation of Seafloor Hydrothermal Vent Fluids and Associated Mineral Deposits," *Oceanography* 20:50-65.

Thurston, P.C., 1981, "Economic evaluation of Archean felsic volcanic rocks using REE geochemistry," *Geological Society of Australia Special Publication,* 7:439-450.

Thakurta, J. and Quigley, T.O., 2013. "Geochemical Characterization of the Back Forty Volcanogenic Massive Sulfide Deposit in Minominee County, MI" *Western Michigan University; Kalamazoo, MI.*

Thorpe, R.I. ,1967, "Controls of Hypogene Sulphide Zoning," Rossland, British Columbia. *Ph.D. thesis, Univ. Wisconsin, Madison.*

Thurston P.C., 1982, "Rare earth elements in volcanic rocks associated with Cu-Zn massive sulfide mineralization: A preliminary report," *Canadian Journal of Earth Sciences*, 19:619-623.

Whitney, D.L., and Evans, B.W. 2010. "Abbreviations for names of rock-forming minerals," *American Mineralogist* 95:185-187.

Winter, J.D., 2001, "An Introduction to Igneous and Metamorphic Petrology*," Prentice Hall*, 697 pages.

Woodruff, L.G. (USGS), "Flambeau, Bend, and Lynne Sulfur Isotope Values," *Written Communication*. June 2, 2014.

Woodruff L.G., Shanks W.C. III (1988) sulfur isotope study of chimney mienrals and ven fluids from 21 degrees N East Pacific rise: hydrothermal sulfur sources and disequilibrium sulfate reduction, *J. Geophys. Res* 93:4562-4572.

Wolf, M.B., Wyllie, P.J., 1991, "Dehydration-melting of solid amphibolite at 10 kbar: textural development, liquid interconnectivity and applications to the segregation of magmas. *Mineral. Petrol.* 44:151–179.

APPENDIX A

SAMPLING LOG

Table 1—Sampling Log

Table 1 **Drill Hole_Sample #**	**Unit**	**Core Box #**	**Depth Interval (meters)**	**Thin-Section**
LK-171_001	CSS	1	10.41-10.46	No
LK-171_002	FLDK/QFP	1	14.40-14.46	No
LK-171_003	TFSD	3	20.63-20.68	No
LK-171_004	TFSD	7	36.30-36.42	No
LK-171_005	TFSD	8	41.84-41.90	No
LK-171_006	TFSD	11	52.66-52.73	No
LK-171_007	TFSD	13	60.90-61.00	Yes
LK-171_008	TFSD	15	70.34-70.48	No
LK-171_009	MASU	18	83.72-83.92	Yes
LK-171_010	MASU	20	92.10-92.20	No
LK-171_011	CHTF	18	88.35-88.40	No
LK-171_012	CHTF	27	120.74-120.89	No
LK-171_013	CHTF	25	104.20-104.35	No
LK-171_014	R2	32	140.75-140.89	No
LK-171_015	MASU	36	158.9-159.00	No
LK-171_016	MASU	38	163.45-163.52	Yes
LK-171_017	MASU	39	172.66-172.84	No
LK-171_018	QFP	43	191.93-192.02	No
LK-171_019	IMDK/QFP	46	201.00-201.20	No
LK-171_020	QFP	46	204.40-204.47	No
LK-171_021	IMDK/QFP	47	206.70-206.80	No
LK-171_022	QFP	48	209.90-210.00	No
LK-171_023	R1	53	231.87-231.97	Yes
LK-171_024	R1	53	235.35-235.43	No
LK-171_025	R1	54	235.57-235.67	Yes
LK-171_026	R1	56	245.64-245.73	No
LK-171_027	R1	56	245.97-246.08	No
LK-171_028	R1	57	251.53-251.59	No
LK-171_029	R1	59	261.34-261.50	Yes
LK-171_030	R1	63	278.60-278.71	No
LK-171_031	MASU	64	279.50-279.65	No
LK-171_032	MASU	64	280.35-280.44	No
LK-171_033	MASU	64	281.30-281.32	No
LK-171_034	IMDK/QFP	65	284.73-284.81	No
LK-171_035	MASU	71	308.37-308.47	Yes

Table 1-Continued Drill Hole_Sample ID	Unit	Core Box #	Depth Interval (meters)	Thin-Section
LK-171_036	TFSD	72	314.17-314.29	No
LK-171_037	MASU	72	315.77-315.82	No
LK-171_038	TFSD	75	324.74-324.94	Yes
LK-171_039	TFSD/MASU	75	326.15-326.38	No
LK-171_040	RATF	76	329.15-329.25	No
LK-171_041	SMAS	76	331.38-331.49	No
LK-171_042	R1	79	338.08-338.28	No
LK-127_043	GOSS	1	6.59-6.69	Yes
LK-127_044	GOSS	1	7.00-7.17	No
LK-127_045	MASU	2	8.78-8.85	Yes
LK-127_046	MASU	6	26.32-26.38	No
LK-127_047	R1	6	28.08-28.13	No
LK-127_048	R1	6	28.37-28.39	No
LK-127_049	R1	6	28.75-28.82	No
LK-127_050	R1	7	31.90-32.08	No
LK-127_051	R1	8	35.36-35.49	No
LK-127_052	R1	8	36.28-36.43	No
LK-127_053	R1	11	46.07-46.15	No
LK-127_054	R1	13	55.44-55.54	No
LK-150_055	QFP	3	10.19-10.33	Yes
LK-150_056	QFP	5	20.60-20.70	No
LK-150_057	QFP	11	43.14-43.25	No
LK-150_058	QFP	10	42.10-42.24	Yes
LK-150_059	QFP	9	36.73-36.81	No
LK-150_060	R2	11	46.40-46.50	Yes
LK-150_061	R2	18	75.5-75.60	No
LK-150_062	R2	22	94.00-94.20	No
LK-150_063	RATF	23	98.20-98.38	Yes
LK-150_064	MASU	24	99.64-99.72	No
LK-150_065	MASU	24	103.29-103.49	Yes
LK-150_066	MASU	31	133.73-133.82	No
LK-150_067	MASU	33	143.24-143.42	No
LK-150_068	MASU	36	153.07-153.15	Yes
LK-150_069	MASU	38	161.84-161.99	Yes
LK-150_070	R1-SZ/SFST	39	164.83-164.98	Yes
LK-150_071	R1-SZ/SFST	40	172.90-173.00	No
LK-150_072	MASU	39	168.37-168.47	No
LK-150_073	R1-SZ/SFST	44	186.27-186.38	No
LK-150_074	FLDK/QFP	47	200.30-200.43	No

Table 1-Continued Drill Hole_Sample ID	Unit	Core Box #	Depth Interval (meters)	Thin-Section
LK-150_075	R1	48	203.50-203.70	No
LK-150_076	FLDK/QFP	49	209.24-209.46	No
LK-150_077	QFP	52	224.73-224.98	No
LK-150_078	QFP	59	252.24-252.37	No
LK-150_079	FLDK/QFP	59	254.38-254.47	No
LK-150_080	R1	61	263.31-263.47	No
LK-150_081	QFP	62	267.85-267.96	No
LK-150_082	SMAS	63	271.35-271.50	Yes
LK-150_083	SMAS	64	273.87-273.92	No
LK-150_084	QFP	69	292.71-292.91	No
LK-150_085	QFP	65	279.09-279.19	Yes
LK-451_086	SS	1	9.08-9.13	No
LK-451_087	QFP	5	20.60-20.75	Yes
LK-451_088	QFP	5	22.78-22.90	No
LK-451_089	IMDK/QFP	8	30.90-30.98	No
LK-451_090	QFP	8	32.75-32.85	No
LK-451_091	QFP	21	77.83-77.96	No
LK-451_092	TFSD	23	84.94-85.03	Yes
LK-451_093	QFP	28	99.72-99.88	No
LK-451_094	TFSD	28	102.60-102.78	No
LK-451_095	QFP	32	112.94-113.06	No
LK-451_096	TFSD	32	116.00-116.11	No
LK-451_097	QFP	36	128.36-128.48	No
LK-451_098	IMDK/QFP	36	128.60-128.73	No
LK-451_099	QFP	38	134.18-134.26	No
LK-451_100	QFP	38	133.30-133.40	No
LK-451_101	TFSD	46	136.15-136.26	No
LK-451_102	TFSD	46	164.05-164.22	No
LK-451_103	MASU	46	164.80-165.96	Yes
LK-451_104	TFSD	46	166.40-166.48	No
LK-451_105	TFSD	50	177.23-177.35	No
LK-451_106	CHTF	50	179.91-180.20	Yes
LK-451_107	CHTF	52	184.88-184.95	No
LK-166_150	TFSD	3	16.76-16.91	No
LK-166_151	TFSD	5	22.38-22.51	No
LK-166_152	TFSD	6	27.20-27.29	No
LK-166_153	TFSD	8	34.66-34.88	No
LK-166_154	TFSD	10	42.62-42.80	No
LK-166_155	MASU	12	53.89-54.01	No

Table 1-Continued Drill Hole_Sample ID	Unit	Core Box #	Depth Interval (meters)	Thin-Section
LK-166_156	CHTF	13	55.18-55.26	No
LK-166_157	CHTF	13	57.01-57.21	No
LK-166_158	CHTF	15	65.20-65.80	No
LK-166_159	CHTF	16	70.85-70.99	No
LK-166_160	CHTF	18	78.13-78.32	No
LK-166_161	SMAS	18	76.24-76.53	No
LK-166_162	CHTF	21	90.45-90.66	No
LK-166_163	CHTF	22	94-94.9	No
LK-166_164	CHTF	23	100.7-100.77	No
LK-166_165	RCTF	24	103.28-103.49	No
LK-166_166	RCTF	27	117.73-117.87	No
LK-166_167	QFP	30	130.86-131.02	No
LK-166_168	QFP	36	154.51-154.75	No
LK-166_169	MASU/FPDK	38	162.1-162.24	No
LK-166_170	MASU	38	164.32-164.47	No
LK-166_171	MASU	38	164.39-164.54	No
LK-166_172	SFST	42	179.47-179.59	No
LK-166_173	SFST	42	181.63-181.83	No
LK-166_174	SFST	49	208.6-208.8	No
LK-166_175	SFST/MASU	50	213.05-213.26	No
LK-166_176	MASU	50	214.59-214.64	No
LK-166_177	IMDK	50	216.84-216.99	No
LK-166_178	SFST	57	241.63-241.84	No
LK-166_179	RCTF	60	259.22-259.41	No
LK-166_180	RCTF	64	273.31-273.42	No
LK-166_181	RCTF	67	286.36-286.69	No
LK-166_182	SFST	70	300.64-300.74	No
LK-166_183	SFST	71	304.84-304.95	No
LK-166_184	IMDK	75	321.54-321.79	No
LK-166_185	RCTF	89	382.04-382.15	No
LK-166_186	RCTF	93	398.25-398.41	No
LK-166_187	RCTF	101	431.71-431.84	No
LK-166_188	RCTF	104	444.26-444.09	No
LK-166_189	RCTF	108	462.37-462.54	No

APPENDIX B

TRACE ELEMENT GEOCHEMICAL DATA

Table 1 — Rhyolite 1

Table 1: ***Rhyolite 1***						
Drill Hole ID	**Sample#**	**Depth Start**	**Depth End**	**Zr**	**Y**	**Zr/Y**
-	**-**	**meters**	**meters**	**ppm**	**ppm**	**ppm**
108402	FX377072	88.39	89.92	107	16.7	6.407
108417	517261	25	26.5	203	38.4	5.286
108421	FX806640	149	150.5	118	16.5	7.152
108441	517252	35.05	36.55	126	23.9	5.272
108462	517271	165.5	168	134	21.1	6.351
LK-108E	133730	100.5	102	100	14.9	6.711
LK-118E	157208	29.3	30.8	175	25.7	6.809
LK-119P	157237	36	37.5	172	19.1	9.005
LK-122E	157314	17	18.5	135	14.2	9.507
LK-124E	157390	48.5	50	89	15.1	5.894
LK-127P	157454	50	51.5	127	17.5	7.257
LK-130P	157584	30.5	32	222	20.3	10.936
LK-131P	157566	56	57.5	129	19.1	6.754
LK-132P	517275	9	10.5	186	18.5	10.054
LK-133P	157610	43.7	45.2	123	17.5	7.029
LK-134P	158185	29	30.46	159	20.9	7.608
LK-146	517277	156	157.5	149	18.8	7.926
LK-167	164957	233.5	235	97	16.5	5.879
LK-171	171045	230	231.5	89	12.8	6.953
LK-174PE	171465	24	25.5	122	19	6.421
LK-178PE	171877	45.85	47.35	127	31.9	3.981
LK-180	517278	99.5	101	142	17.6	8.068
LK-181PE	172711	38	39.5	144	26.7	5.393
LK-185PE	170903	46.5	48	144	15.1	9.536
LK-190	255807	13.5	15	132	17.9	7.374
LK-197	256979	187	188.5	99	17.2	5.756
LK-203	517255	86	87.5	135	21.2	6.368
LK-220	336647	26.5	28	187	31.7	5.899
LK-249	355806	16.5	18	160	17.4	9.195
LK-253	356169	174.04	175.5	100	14.1	7.092
LK-257	356685	184.5	186	114	18.6	6.129
LK-312	417357	27	28.5	130	30.7	4.235

Table 1: Continued *Rhyolite 1*						
Drill Hole ID	**Sample#**	**Depth Start**	**Depth End**	**Zr**	**Y**	**Zr/Y**
-	**-**	**meters**	**meters**	**ppm**	**ppm**	**ppm**
LK-315	417498	30.5	32	89	14.3	6.224
LK-336	420119	156.5	158	121	17	7.118
LK-348	420604	17	18.5	138	23.8	5.798
LK-348	420669	176	177.5	110	20.8	5.288
LK-348	420746	293	294.5	123	17.5	7.029
LK-352	515529	40	41.5	123	20.2	6.089
LK-353	515733	85.5	87	122	18.1	6.740
LK-353	515744	118	119.5	131	19.6	6.684
LK-406	596810	46.5	48	113	17.7	6.384
LK-406	596817	57	58.5	144	19.5	7.385
LK-423	627173	161.45	163	99	16.4	6.037
LK-76	253987	50.5	52	124	18.9	6.561
LK-86	517273	8	9.5	160	13.6	11.765

Table 2 — Rhyolite 2

Table 2: *Rhyolite 2*						
Drill Hole ID	**Sample#**	**Depth Start**	**Depth End**	**Zr**	**Y**	**Zr/Y**
-	**-**	**meters**	**meters**	**ppm**	**ppm**	**ppm**
108401	517259	5	6.5	70	1.68	6.667
108407	FX806706	19.5	20	206	44.6	4.619
108409	FX808099	182	183.5	78	16.8	4.643
108416	FX808583	68.5	70	99	17.4	5.690
108418	FX806915	147.5	149	85	18.5	4.595
108423	FX806756	60.5	62	96	22.7	4.229
108423	FX806756-DUP	60.5	62	101	22.8	4.430
108433	FX809734	17	18.5	101	21.1	4.787
LK-116P	157161	54.5	55.6	120	27.3	4.396
LK-125P	158039	16	17.5	119	11	10.818
LK-126P	158085	63	64.5	99	24.1	4.108
LK-132P	158138	128	129.5	100	21.2	4.717
LK-140P	517276	123.9	125.4	176	36.3	4.848
LK-148	158428	14.5	16	83	14.9	5.570
LK-149	158623	114	115.5	166	42.2	3.934

Table 2: Continued *Rhyolite 2*						
Drill Hole ID	**Sample#**	**Depth Start**	**Depth End**	**Zr**	**Y**	**Zr/Y**
		meters	**meters**	**ppm**	**ppm**	**ppm**
LK-151	158831	88.5	90	99	27.9	3.548
LK-162	164072	32.5	34	74	15.5	4.774
LK-163	164230	66	67.5	90	18	5.000
LK-165	164268	24.9	26.4	88	22.1	3.982
LK-168	165053	114.5	116	134	28.1	4.769
LK-176	171626	127.5	129	96	19.7	4.873
LK-182PE	172886	76	77.5	87	29.9	2.910
LK-186	255353	89.5	91	117	33	3.545
LK-192	256373	120.5	122	117	30.8	3.799
LK-193	256531	41	42.5	116	30.4	3.816
LK-207	334334	60.5	62	104	20.7	5.024
LK-209	334834	70	71.5	95	23.4	4.060
LK-214	335843	42	43.5	113	21	5.381
LK-220	356377	26.5	28	93	23.8	3.908
LK-222	336845	36	37.5	108	30.7	3.518
LK-226	337559	82.5	84	152	48.7	3.121
LK-227	337589	35.5	37	111	22.2	5.000
LK-229	337871	27.5	29	100	19.6	5.102
LK-232	338075	18	19.5	122	26.3	4.639
LK-241	355156	14.5	16	103	32.9	3.131
LK-243	355454	72	73.5	141	48.5	2.907
LK-244	355532	84	85.5	80	18.8	4.255
LK-247	517256	25	26.5	108	29	3.724
LK-248	355700	66.5	68	99	19.7	5.025
LK-249	355891	148	149.5	111	26.1	4.253
LK-249	355904	179.01	180.5	110	21.2	5.189
LK-250	355954	49	50.5	102	23.3	4.378
LK-255	356372	88.5	90	92	23.8	3.866
LK-256	356554	105.5	107	94	20.9	4.498
LK-257	356571	22.18	23.5	102	23.6	4.322
LK-257	356620	93	94.5	89	22.4	3.973
LK-259	356789	8	9.5	115	31.6	3.639
LK-259	356800	43.5	45	96	18.1	5.304
LK-261	357040	110.5	112	114	26.6	4.286
LK-262	357130	123.5	120	23.3	34.2	5.150
LK-263	517258	33	98	19.2	33.7	5.104

Table 2: Continued *Rhyolite2*						
BH-ID	**Sample#**	**Depth Start**	**Depth End**	**Zr**	**Y**	**Zr/Y**
		meters	**meters**	**ppm**	**ppm**	**ppm**
LK-267	357603	29	30.5	96	24.4	3.934
LK-283	359483	141.5	143	98	24.9	3.936
LK-298	415805	11.59	13	107	38.9	2.751
LK-302	416387	13	14.5	124	39.3	3.155
LK-307	416892	50.5	52	106	18.7	5.668
LK-309	417076	20	21.5	100	25.1	3.984
LK-318	417664	9.5	11	100	24.7	4.049
LK-318	417665	11	12.5	136	25.4	5.354
LK-319	417735	18.5	20	81	10.1	8.020
LK-320	417816	45	46.5	128	28.7	4.460
LK-323	418081	16.5	17.99	74	14.3	5.175
LK-325	418251	19.5	21	95	17.5	5.429
LK-329	418421	25	26.5	78	14	5.571
LK-330	419818	61.5	63	104	24	4.333
LK-332	418554	126	127.5	89	22.8	3.904
LK-333	419893	85.5	87	97	33.2	2.922
LK-335	419942	75.5	77	98	23.7	4.135
LK-336	420027	12	13.5	102	26.4	3.864
LK-339	418743	28	29.5	94	21	4.476
LK-341	418812	26.5	28	84	22.7	3.700
LK-344	418881	40.5	42	113	26.4	4.280
LK-344	517281	140.5	142	106	22.6	4.690
LK-346	419058	90.5	91.73	104	24.1	4.315
LK-347	420570	33.5	35	81	26.9	3.011
LK-351	421320	55.5	57	89	20.6	4.320
LK-408	605830	120	121.5	89	19.2	4.635
LK-416	520393	55.2	57.62	88	19.2	4.583
LK-460	665132	21.53	23	69	11.3	6.106
LK-471	665799	18.5	20	132	37	3.568
LK-74	253947	57	58.5	144	38.8	3.711
LK-83	517284	131.5	133	113	21.5	5.256
LK-183	172943	25.5	27	110	30.6	3.595
108415	FX784840	41.5	43	123	22.9	5.371
108419	FX808921	56.5	58	95	23.3	4.077

Table 3 — Rhyolite 3

Table 3: ***Rhyolite 3***						
BH-ID	**Sample#**	**Depth Start**	**Depth End**	**Zr**	**Y**	**Zr/Y**
		meters	**meters**	**ppm**	**ppm**	**ppm**
LK-82	88869	91.5	93	194	30.7	6.319
LK-212	335577	57	58.5	157	27.1	5.793
LK-286	359791	49.5	51	163	21.9	7.443
LK-286	359808	81	82.5	200	28	7.143
108455	517263	27.4	28.9	136	21	6.476
108460	517265	12	13.5	172	28.5	6.035
LK-417	626549	41.5	43	196	28	7.000
LK-470	665721	109.5	110.97	189	27	7.000
LK-82	88869-DUP	91.5	93	196	32	6.125
108445	FX776108	36.5	38	188	28.2	6.667
108446	FX776317	60.5	62	197	26.7	7.378

Data provided by Aquila Resources Inc.

APPENDIX C

SULFUR ISOTOPE VALUES
(BEND, LYNNE, AND FLAMBEAU)

Data provided by Laurel Woodruff, U.S. Geological Survey
(written communication; 2014)

Table 1 – Mineral Abbreviations

Mineral Abbreviations
sp = sphalerite
po = pyrrhotite
ga = galena
py = pyrite
bn = bornite

Table 2 – Samples

Sample Name	Mineral	Deposit	$\delta^{34}S$
90-18,355	sp	Lynne	2.7
90-12, 175	sp	Lynne	1.5
90-16, 431	sp	Lynne	1.5
90-16, 321	sp	Lynne	3.1
90-18, 529	sp	Lynne	2.0
90-12, 85.5	sp	Lynne	2.3
90-16, 472.5	sp	Lynne	2.2
90-16, 342	po	Lynne	1.4
90-40, 540	po	Lynne	3.3
90-16, 456	sp	Lynne	3.4
90-7, 250	sp	Lynne	2.2
90-7, 388	sp	Lynne	3.4
90-7, 447	sp	Lynne	2.4
90-40, 575	sp	Lynne	3.8
90-40, 575	po	Lynne	3.6
90-16,375	po	Lynne	2.8
90-16, 367	po	Lynne	1.5
90-40, 613	po	Lynne	3.4
90-7, 399	sp	Lynne	1.7
90-7, 374	sp	Lynne	2.3
90-18, 366	sp	Lynne	2.0
90-12, 90	sp	Lynne	2.2
90-12, 87	po	Lynne	3.4
90-18, 577	ga	Lynne	0.7
90-40, 725	ga	Lynne	1.1
90-28, 171.5	po	Lynne	4.5
FLAMBEAU-1	bn	Flambeau	-0.8
FLAMBEAU-2	py	Flambeau	-0.3
22-9, 317	py	Flambeau	1.9
22-9, 973.5	py	Flambeau	0.9
22-9, 99.6	py	Flambeau	1.1
22-9, 104.5	py	Flambeau	-2.2
95-10, 200	py	Bend	0.8
94-172, 693.5	py	Bend	0.5
95-20, 164	py	Bend	1.0
95-20, 159	py	Bend	0.6
91-9, 142.9	py	Bend	2.1
95-21,112.2	py	Bend	1.7
95-20,188	py	Bend	1.4
95-21, 139	py	Bend	1.1
95-17, 625.5	py	Bend	1.9
91-9, 145.1	py	Bend	2.5
B-10, 1312	py	Bend	2.2
B-6, 961.5	py	Bend	1.8